Assemblies of Polyoxometalates

Universiteit Utrecht

Cover picture by A.A. Verhoeff. Model of a Keplerate type POM.

ISBN 978-90-393-5152-9
Subject headings: Polyoxometalates/POM-shells/self-assembly/crystallization/supramolecular chemistry/charge regulation/extended structures.

Assemblies of Polyoxometalates

Organisatie van Polyoxometalaten

(met een samenvatting in het Nederlands)

Proefschrift

ter verkrijging van de graad van doctor aan de
Universiteit Utrecht op gezag van de rector magnificus,
prof. dr. J.C. Stoof, ingevolge het besluit van het
college voor promoties in het openbaar te verdedigen
op 30 September 2009 des middags te 2.30 uur

door

Sandra Joyce Veen

geboren op 2 oktober 1981 te Vianen

Promotor: Prof. dr. W.K. Kegel

Het in dit proefschrift beschreven onderzoek werd gefinancierd door het gebied chemische wetenschappen (CW) van de Nederlandse Organisatie voor Wetenschappelijk Onderzoek (NWO).

"Science is built of facts the way a house is built of bricks; but an accumulation of facts is no more science than a pile of bricks is a house."
- Henri Poincaré

Contents

1

General Introduction

1.1. Polyoxometalates

Polyoxometalates, or POMs for short, come in a variety of shapes and sizes. Some of them are among the largest inorganic molecules known today. These molecules can be highly symmetrical and, as the name already implies, consist of (mainly) metal (molybdenum, tungsten, vanadium, iron, etc) and oxygen atoms in the form of metal oxide polyhedrons. The POMs that are central to this thesis are mostly polyoxomolybdates, meaning that the metal is mostly molybdenum.

The history of polyoxomolybdates dates back centuries ago with the famous blue waters observed by Native Americans near today's Idaho Springs in the Valley of the Ten Thousand Smokes [**1, 2**]. The blue color was a result of a solution of natural soluble molybdenum blue formed by partial oxidation of molybdenite, MoS_2. MoS_2 is a natural source of molybdenum and is mined in order to yield the pure metal. By partial oxidation it forms the mineral ilsemannite (with the approximate formula $Mo_3O_8 * nH_2O$)). The first attempt to resolve the structure of the species present in solution was made by Jöns Jakob Berzelius in 1826. He reported the first formula for the blue powder isolated from blue water solutions [**3**]. Though many thereafter reported slightly different compositions of this mysterious molybdenum blue, it would take until the end of the 20th century until it was fully resolved. In 1995 Müller et al. reported the first successful attempt to gain pure crystals from molybdenum blue solutions [**4**]. It took however more then two years after this first preliminary data was published for the exact formula of the crystalline compound to be determined [**5**]. Their findings showed that molybdenum blue consists of large wheel shaped molecules of approximately 3.6 nm in diameter, consisting of polyhedrals of molybdenum oxide linked together by sharing of the oxygen atoms.

Due to the novel synthesis route discovered by the attempt to crystallize molybdenum blue, the route to the synthesis of other polyoxomolybdates and -metalates was opened. Today polyoxomolybdates come in a wide variety of shapes and sizes. From the giant wheel shaped molybdenum blue, to hollow spherical- and "hedgehog"-shaped clusters (Figure 1.1). With the discovery of this new class of molecules, also came a new field of interest. POMs in general and POMs containing molybdenum in particular have received attention in the fields of material science [**6**], catalysis [**7, 8**] and medicine [**9**].

1.2. Assemblies of Polyoxometalates

Although the crystalline structure of molybdenum blue was no longer a mystery (partially resolved in 1995 [**4**]), one issue still remained to be resolved. The crystalline structure obtained from solution consists of the wheel shaped clusters of approximately 3.6 nm in diameter. Light-scattering experiments however, revealed colloidal sized species in solution ranging in size from 20 to 100 nm in radius. Molybdenum blue has

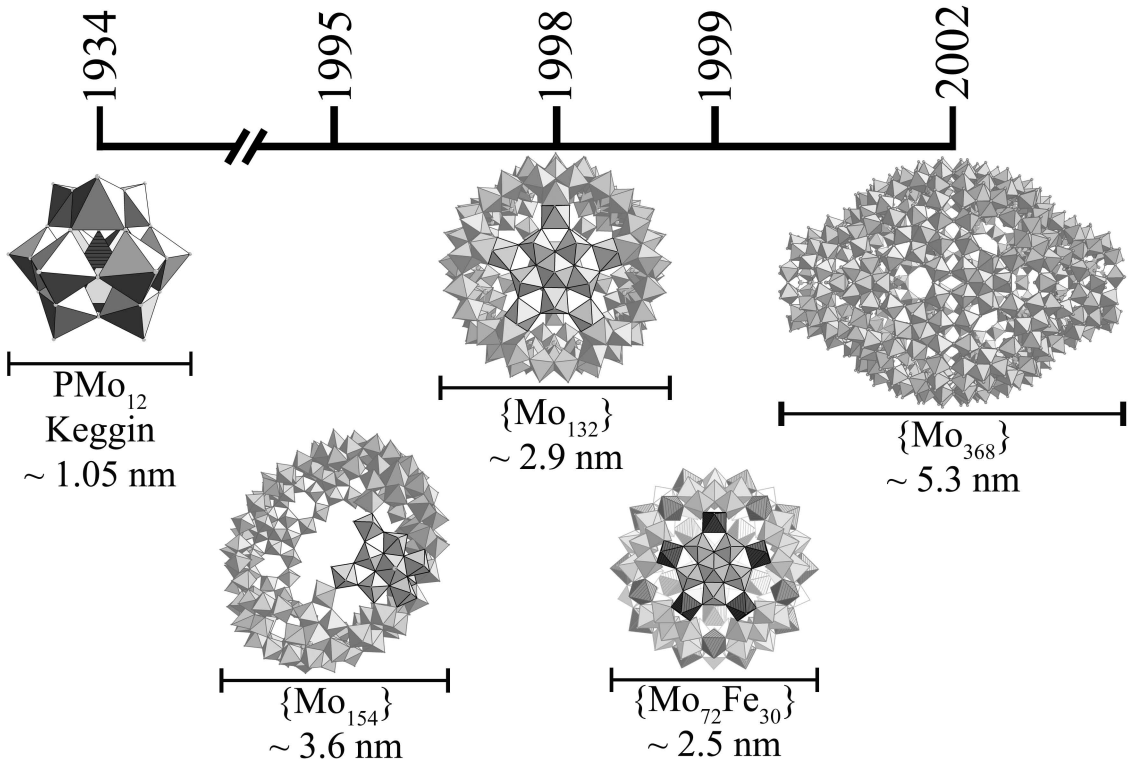

FIGURE 1.1. History of Polyoxomolybdates. From the determination of the Keggin structure by J. F. Keggin in 1934 [**10**], via the resolved structure of the wheel shaped molybdenum blue (1995) to the creation of novel Keplerate type polyoxomolybdates (1998 and 1999) and the protein sized Hedgehog structure (2002). All molecules are given in polyhedral representation. In this representation the oxygen atoms are located at the tips of the polyhedrals and the metal atoms (in most cases molybdenum) in the center.

always been known for its high solubility in water and a wide range of polar solvent. Moreover, the "aggregates" that were formed did not show any tendency to grow and precipitate as would be the case for less soluble species. This peculiar behavior was investigated by Müller [**11**] and Liu [**12**] and explained by the presence of large hollow, spherical superstructures consisting of a monolayer of over a hundred individual wheels. These type of shell-like superstructures or POM-shells seemed to form spontaneously in solutions. Further research showed that this type of behavior was not limited to the wheel shaped molybdenum blue only, but seemed to be a characteristic trade for a wide variety of POMs [**13**].

1.3. KEPLERATES

One such class of POMs that has been shown to spontaneously form POM-shells in solution are Keplerates. Keplerates are highly symmetric, hollow, spherically shaped

POMs. They consist of 12 five-fold building blocks or pentagons which are linked together to form a sphere in much the same way as a soccer ball.

The name Keplerate was first introduced by Müller et al.[**14**]. The term comes from Johannes Kepler, a 17^{th} century mathematician, astronomer and astrologer. In his opus *Mysterium Cosmographicum* he described his vision of planetary motion [**15**]. He suggested a theory for the distances between the orbits of the planets in our solar system based on the five Platonic solids [**14**]. Platonic solids are three dimensional geometrical objects of which the faces, edges and angles are all the same. As is the case for, for instance, a cube or a tetrahedron. Around each of the platonic solids, a sphere can be placed which touches every corner of the structure. In a similar manner a sphere can be placed inside a platonic solid, which will then touch the center of the structures edges. By ordering the solids by way of octahedron, icosahedron, dodecahedron, tetrahedron and cube, Kepler found that the spheres around and within these solids could be placed at intervals corresponding to the relative sizes of each planet's path, assuming the planets circle the sun (Figure 1.2).

The subclass of polyoxometalates named after Kepler can also be seen as being constructed of a sphere around a platonic solid. Examples of this type of POM are show in Figure 1.1. For instance in the POMs abbreviated as $\{Mo_{132}\}$ and $\{Mo_{72}Fe_{30}\}$ an icosahedron can be recognized inside the spherical shell of the 132 outermost (terminal) oxygen atoms. The 12 corners of the icosahedron are defined by the 12 central molybdenum atoms of the 12 pentagons. Müller suggested to name these molecules Keplerates since "the systematic nomenclature would be far too unwieldy".

1.4. This Thesis

Most of the work done in this thesis was performed on POM-shells of a Keplerate type polyoxometalate. Putting aside the intriguing question as to why Keplerates form shell-like superstructures, much can already be deduced from the behavior of these POM-shells in solution. In **Chapter 2** of this thesis a stabilization mechanism for the POM-shells is presented based on charge regulation. The experimentally determined variation in equilibrium size of these POM-shells as a function of the dielectric constant of the solvent will be compared to predictions made by a charge regulation model. Moreover, estimates will be made of the cohesive bond energies involved in the formation of the POM-shells and compared to model independent calculations.

The charge regulation model can also be used in order to describe a new type of structural instability of the POM-shells. In **Chapter 3** an instability based on a structural change in the POM-shells themselves will be demonstrated. Evidence as well as a theoretical explanation of the new experimental stability limit will be presented for a system of POM-shells of a Keplerate type POM.

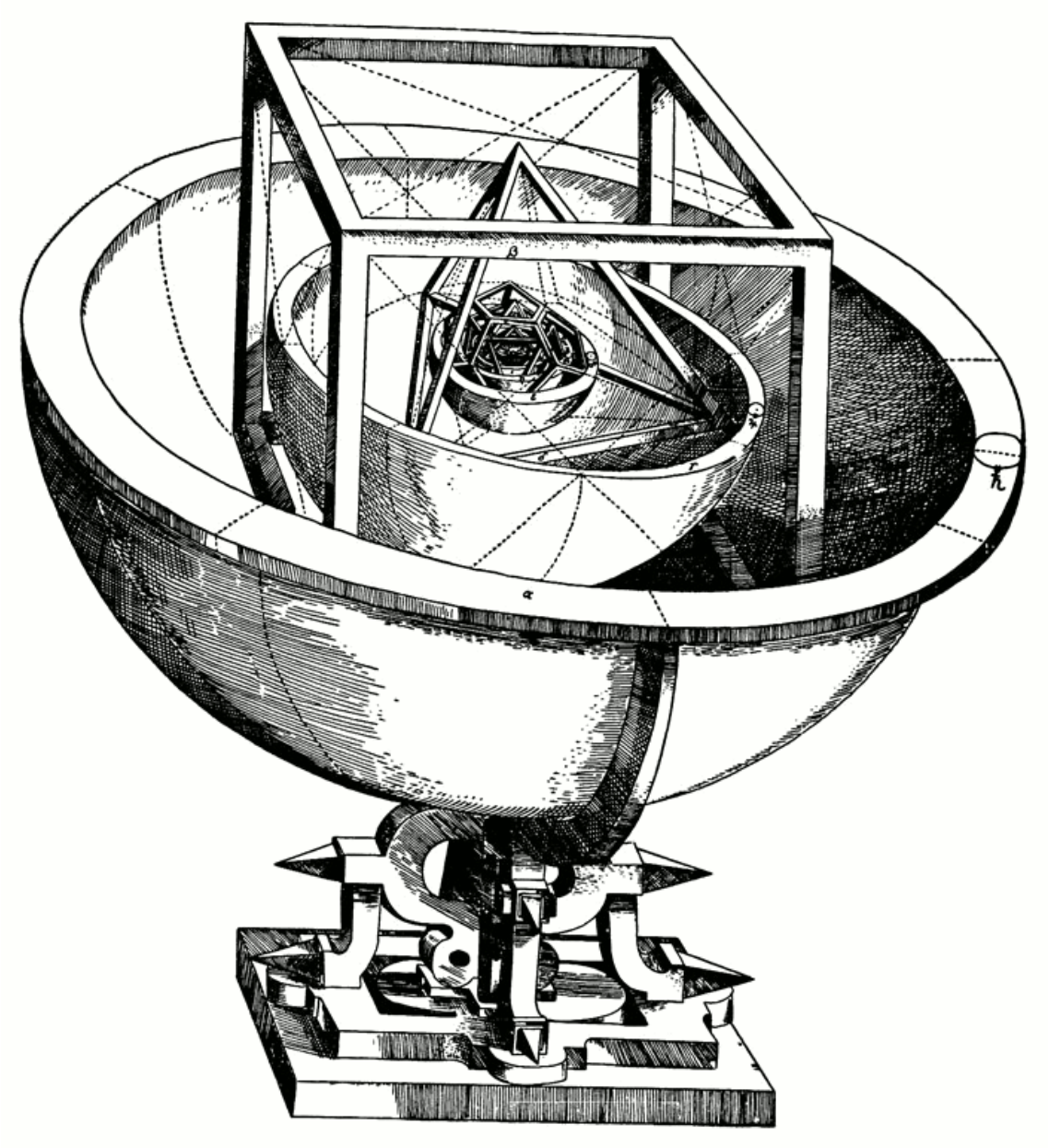

Figure 1.2. Keplers model of the solar system: the distances between the orbits of the planets could be explained by Kepler if the ratios between the successive orbits were designed to be equivalent to the spheres successively circumscribed around and inscribed within the five Platonic solids.

Chapter 4 will continue with the model independent approach of the calculation of the interaction energy by means of the critical aggregation concentration (CAC). In this chapter the effect of varying charge on the interaction energy between the single Keplerate type POMs in the POM-shell will be investigated. This will be done by measuring the dependence of the CAC on the pH of aqueous solutions for a Keplerate

type POM with a weak acidic nature. Also complications regarding this approach will be outlined.

Chapter 5 will look beyond the shell-like assemblies and places them in a broader perspective. Although the POM-shells have been commonly accepted to be thermodynamically stable, the presented results challenge that view. Results from both scattering experiments, microscopy images and sedimentation experiments will be presented in order to substantiate this claim.

Chapter 6 will address an entirely different assembly of polyoxometalates, namely an extended structure based on elementary molybdenum oxide building blocks which are linked together with the aid of urea. The resulting inorganic-organic hybrid shows an interesting molecular topology in combination with an unexpectedly high thermal stability.

Part 1

Assemblies of Keplerates

2

Shell-like Assemblies of Keplerates: Stability, Size and Interaction Energies

Abstract

We show that the equilibrium size of single-layer shells composed of polyoxometalate macro ions is inversely proportional to the relative dielectric constant of the medium in which they are dispersed. This behavior is in line with predictions made by a stabilization mechanism based on Coulomb repulsion combined with charge regulation. We estimate the cohesive energy per bond between the macro ions on the shells to be approximately -6 kT. This number is extracted from analysis based on a charge regulation model in combination with a model for defects on a sphere. This value is in agreement with the bond energy as determined by the model-independent critical aggregation concentration. Furthermore we show that there is a negligible difference in standard chemical potential of a POM in a POM-shell and a POM in the solid state.

2.1. Introduction

Polyoxometalates (POMs) are among the largest inorganic molecules known today. They can be highly symmetrical and consist of (mainly) metal oxide polyhedrals (molybdenum, tungsten, vanadium, iron, etc). The novelty of this type of inorganic molecules not only lies in their molecular structure but also in their intriguing behavior in solution. The C_{60}-like, hollow, spherical POMs known as Keplerates for instance, have been shown to spontaneously form superstructures in solution: hollow, spherical objects with an average radius in water of several tens of nanometers, and composed of more than 1000 of individual POM macro ions [**12**](Figure 2.1). Not only molybdenum-containing POMs form these type of shell-like superstructures, but also those containing tungsten and copper [**13**].

At this point, it is still an open question as to why these shell-like superstructures, or POM-shells, are stable. Due to the spherically symmetric nature of (some of) the POMs, one would expect interactions between them to be spherically symmetric as well. This would lead at most either to macroscopic phase separation or to the formation of liquid-like clusters, but certainly not the kind of hollow shells that are experimentally observed.

As of to date the driving force behind the formation of the POM-shells is still a topic of debate. In order to gain more insight into the system the problem can be broken up in to several parts and somewhat simpler questions can be asked: given the existence

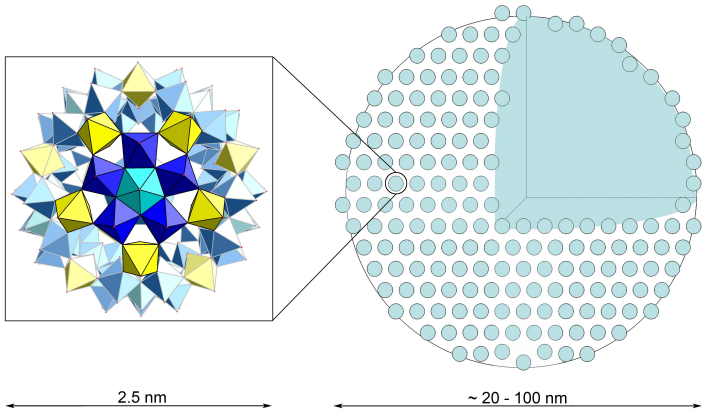

Figure 2.1. Schematic representation of a hollow spherical superstructure of polyoxometalates (POM-shells). Polyoxometalates (POMs) have been shown to spontaneously form POM-shells, which contain up to a 1000 of individual POMs and can grow up to several tens of nanometers in water. In this example the POM-shell contains the 2.5 nm large POM abbreviated as $\{Mo_{72}Fe_{30}\}$ (see section 4.2.1). Sizes of the POM-shell indicated refer to the size range in aqueous solutions.

of the POM-shells, what determines their equilibrium size? What interaction energies are involved in the formation of the shells?

In this chapter a stabilization mechanism for the POM-shells is presented based on coulomb repulsion in combination with charge regulation. The experimentally determined variation in equilibrium size of these POM-shells as a function of the dielectric constant of the solvent will be compared to predictions made by a charge regulation model. Moreover estimates will be made of the cohesive bond energies involved in the formation of the POM-shells and compared to model independent calculations.

2.2. THEORY

2.2.1. The System: $\{Mo_{72}Fe_{30}\}$

Here we study a C_{60}-like, hollow, spherically shaped, Keplerate type polyoxometalate which has the following composition in its crystalline state [**16**]:

$$Mo^{VI}_{72}Fe^{III}_{30}O_{252}(CH_3OO)_{12}\{Mo_2O_7(H_2O)\}_2\{H_2Mo_2O_8(H_2O)\}(H_2O)_{91} \bullet \text{ca.}150(H_2O)$$

This macromolecule, further referred to as $\{Mo_{72}Fe_{30}\}$, has a diameter of 2.5 nm. The detailed structure of this cluster can be visualized as a result of icosahedral disposition of 12 constituent $(Mo)Mo_5$ pentagonal building blocks along the 12 C_5 axes of the icosahedral point group. The remaining 30 'linking' C_2 sites in turn connect the 12 pentagonal units. In $\{Mo_{72}Fe_{30}\}$ the linkers are $Fe^{III}(H_2O)_2$ groups. Figure 2.2 shows the POM macro ion in both polyhedral as well as molecular representation, in which the linking Iron groups are colored yellow.

When dissolved into aqueous solution, $\{Mo_{72}Fe_{30}\}$ acts as a weak acid. Water molecules coordinated to the Iron atoms in the structure, can partially deprotonate. The number of chargeable groups is 30, however, the amount of deprotonation of the single molecules and the resulting negative charge depends on the pH of the solution [**16**].

2.2.2. Charge Regulation Mechanism

Given the existence of the shell-like superstructures, the free energy of a shell F is assumed to depend on two fluctuating and dependent variables: its aggregation number n, reflected in the radius R by means of $R = \sqrt{ns/4\pi}$ with s the area average area occupied by a monomer in the superstructure, and the effective charge Z:

$$\frac{F}{kT} = 4\pi\gamma_0 R^2 + 4\pi(2K + \bar{K}) + \frac{\lambda_B Z^2}{2R(1+\kappa R)} - \psi Z \tag{2.1}$$

In this equation, k denotes Boltzmann's constant, T the absolute temperature, $\lambda_B = \frac{e^2}{4\pi\epsilon_0\epsilon_R kT}$ the Bjerrum length (the characteristic distance over which the Coulomb interaction for singly charged ions is equal to the thermal energy) and $\kappa = (8\pi\lambda_B\rho_s)^{\frac{1}{2}}$

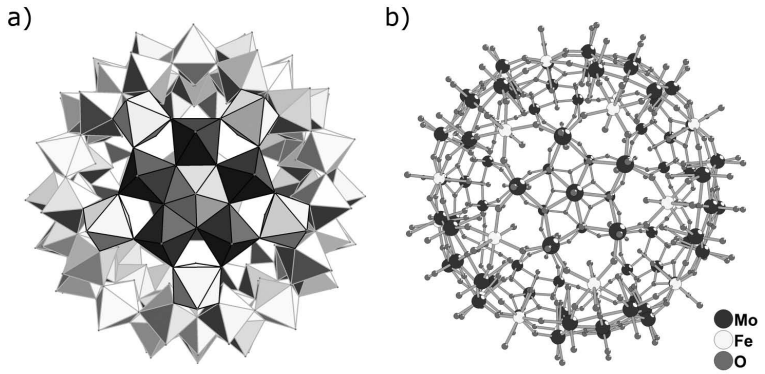

Figure 2.2. Schematic representations of the polyoxometalate (POM) $\{Mo_{72}Fe_{30}\}$. a) Polyhedral representation. b) Molecular representation. In polyhedral representation the metal atoms are located in the center and the oxygen atoms on the corners of the polyhedra. The inorganic macro ion is spherically symmetric, has a diameter of 2.5 nm and consists of 12 fivefold symmetrical units (blue and turquoise) linked by 30 Iron groups (yellow). (For the color version of this picture see the Color figures at the end of this thesis.)

the inverse Debye screening length, with e the unit charge, ϵ_0 the permittivity of vacuum, ϵ_R the relative permittivity of the medium, and ρ_s the number density of the 1:1 electrolyte.

The first term with surface tension γ_0 in Equation (2.1),which results from the creation of a surface, is extensive in the aggregation number and will not show up in the equilibrium equation, assuming the average area occupied by a POM monomer does not depend on R. The second term, with bending elastic modulus K and Gaussian modulus $\bar{K}$ is related to the curvature contribution from the Helfrich expansion of a spherical vesicle [**17**]. The third and fourth term, where Ψ denotes the zeta potential, regulate the effective charge of the aggregate. In fact, the third term arises from the screened-Coulomb interactions on a uniformly charged sphere in a background electrolyte characterized by a Debye screening length κ^{-1}, within the Debye-Hückel approximation, see [**18**]. This term is supposed to be correct as long as counter ions inside the shells can be neglected, being the case for $R \leq \kappa^{-1}$. The fourth term determines the amount of escape of ions from the narrow Gouy layer surrounding the shell. This term corresponds to a Legendre transformation from a constant charge- to a constant potential ensemble, see e.g. [**19**]. Constant potential is an appropriate condition if the majority of counter ions is confined to a narrow layer (the Gouy layer) around the surface [**18**]. In other words, the bare charge exceeds the effective charge by far. An additional condition is that the concentration of potential determining ions is constant. Potential determining ions in this case are those ions that escape from the Gouy layer leaving the surface to have a renormalized charge [**20**].

The optimum renormalized charge of a shell with fixed R follows from minimizing Equation (2.1) with respect to Z, resulting in:

$$Z = \Psi \frac{R(1+\kappa R)}{\lambda_B}. \tag{2.2}$$

This expression reduces to the cell-model result $Z = \Psi(R/\lambda_B)$ in [**20**] if $\kappa R << 1$. Reported experimental values of $\mid \Psi \mid$ are close to 6 kT for micelles, [**21**] and highly charged colloids [**22**] in aqueous media, but also smaller values have been observed depending upon (bare) charge density and ionic strength [**18, 23, 24**].

Inserting (2.2) into (2.1), the optimal cluster size is obtained by minimizing the free energy per unit area. This leads to:

$$R = \frac{16\pi\lambda_B(2K+\bar{K})}{\Psi^2}. \tag{2.3}$$

The curvature energy can in turn be related to the cohesive bond energy of the POMs on a shell. From Eulers theorem, it follows that for shells, independent of their size, at least 12 five-fold interacting monomers are required in the case that one has hexagonal packing and therefore predominantly sixfold interactions. In this case each shell misses at least 12 times the cohesive bond energy u that monomer pairs have on the shell surface. Assuming that this is the dominant contribution, in other words $\bar{K} >> K$, this translates into:

$$4\pi(2K+\bar{K}) \approx -12u \tag{2.4}$$

Inserting this into Equation (2.3), the following expression for the radius of the shells is obtained:

$$R \approx \frac{-48\lambda_B u}{\Psi^2}. \tag{2.5}$$

As $\lambda_B \approx 56/\epsilon_R$ nm, Equation (2.5) predicts that $R \propto \epsilon_R^{-1}$. It is expected that the zeta potential Ψ also depends on the dielectric constant, but only logarithmically, see reference [**18**], so that the leading behavior given by Equation (2.5) is expected.

In the above derivation of the charge regulation mechanism, careful consideration has been given to the choice of the terms of the free energy of a shell. For instance in order to illustrate the crucial role of counter ion condensation, suppose the last, charge regulating term in Equation (2.1) would be absent. The charge density on a shell would in that case be constant and the radius R in Equation (2.5) proportional to $\epsilon_R^{1/3}$.

One other remark with respect to the zeta potential Ψ has to be stated here. Ψ also depends logarithmically on the concentration of potential determining ions, which are protons in the case of $\{Mo_{72}Fe_{30}\}$ (see Section 2.2.1). Equation (2.2) implies that these concentrations vary with R, which in principle influences the value of Ψ. However, the variation of the concentration of potential determining ions caused by the variation in R in the range probed in the experiments (Figure 2.4) is less than one percent of the total concentration of these ions. These total concentrations are significantly higher

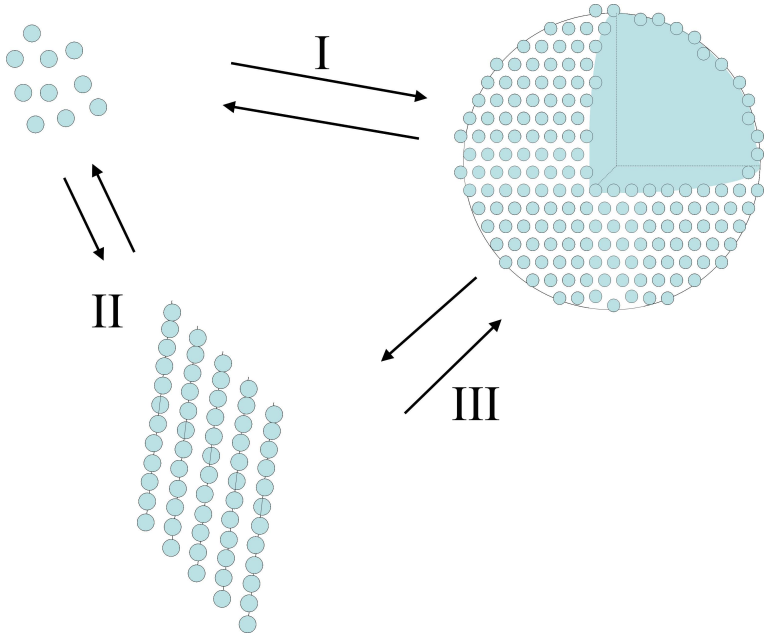

Figure 2.3. Schematic representation of the three phases present when POMs are dissolved in water beyond the maximum solubility. In this situation, three separate equilibria can be considered: **I**) Equilibrium between single POMs and POM-shells, characterized by the critical aggregation concentration (CAC). **II**) Equilibrium between single POMs and the precipitate. **III**) Equilibrium between the POM-shells and the precipitate.

than the POM concentration, as excess acetic acid or ammonium acetate is present in the POM crystals from which the samples have been prepared. It is therefore expected that the behavior predicted by Equation (2.5) will still hold.

2.2.3. Interaction Energies

The charge regulation model discussed in 2.2.2 provides insight into the cohesive bond energies of the POMs in the shell structure by means of Equation (2.5). There is also a model independent way in which these bond energies can be deduced. If one considers a solution of $\{Mo_{72}Fe_{30}\}$ in which the concentration of the POMs is gradually increased, the POMs will undergo at least two transitions. At first a critical aggregation concentration (CAC) is reached at which the POM-shells will start to form. When the concentration of POMs is increased even more and the maximum solubility is reached, macroscopic aggregates will form and precipitate out of solution. In this situation, individual POMs, shells and precipitate coexist as is schematically depicted in Figure 2.3. In this situation the chemical potentials of a POM in each state should be the same. With this in mind, the difference in standard chemical potential between each equilibrium, as a measure for the interaction energies, can be calculated.

I) Equilibrium between single POMs and POM-shells

The first equilibrium is that between the single POMs in solution and the POMs in the shells. The difference in cohesive bond energies in this case is characterized by the CAC. From the CAC mole fraction (x_{CAC}) the difference in standard chemical potential between a POM in solution and in the shell ($\Delta\mu^0$) can be calculated by means of [**25**]:

$$\Delta\mu^0 \equiv \frac{\mu_q^0 - q\mu_1^0}{(q-1)} = kT\ln x_{CAC} \tag{2.6}$$

In which μ_q^0 is the standard chemical potential of a POM-shell, μ_1^0 the standard chemical potential of a single POM in solution and q the number of POMs in a shell. The difference in standard chemical potential can be seen as the mean interaction energy of a POM in a shell relative to the monomers. It is a measure for the interaction energy between the POMs in the POM-shell. The interaction between the POMs in the shell consists of two contributions:

$$\Delta\mu^0 \cong < f_{int} > \cong n_s\epsilon_{attr} + f_{el}^s \tag{2.7}$$

an attractive part which is proportional to the average number of bonds n_s of the POM in the shell, and an electrostatic term caused by the charges on the macro ions in the shell in solution, which is in principle not pairwise additive.

II) Equilibrium between single POMs and the precipitate

At the same time the single POMs are also in equilibrium with the precipitate or crystal as depicted in Figure 2.3. By using the chemical potential of a POM in the precipitate, μ_c as a reference point, one can calculate the difference in standard chemical potential between a free POM and $\{Mo_{72}Fe_{30}\}$ in the crystal structure $\Delta\mu_c^0$ by means of:

$$\Delta\mu_c^0 \equiv \mu_1^0 - \mu_c^0 = -kT\ln x_1 \tag{2.8}$$

in which μ_c^0 is the standard chemical potential of a POM in the precipitate and x_1 the mole fraction of single POMs in solution. In the situation as given in Figure 2.3 the mole fraction of the single POMs in solution is equal to the mole fraction of the CAC. Here again the difference in chemical potential between the two different states is a measure for the mean interaction energy, only now for a POM in the crystal relative to the monomer:

$$\Delta\mu_c^0 \cong < f_{int} > \cong n_c\epsilon_{attr} + f_{el}^c \tag{2.9}$$

The attractive term is now proportional to the number of bonds in the crystal structure.

III) Equilibrium between POM-shells and the precipitate.
The third equilibrium present in this system is between the POM-shells and the precipitate. This equilibrium is characterized by the solubility. The difference in standard chemical potential of POMs in both states can be calculated directly from this concentration if the concentration of monomers can be neglected with respect to the concentration of shells. If this is the case it can be assumed that the concentration of POMs at maximum solubility is equal to the concentration of shells coexisting with the precipitate. Again using the chemical potential of a POM in the crystal, μ_c, as a reference, the difference in chemical potential of a POM in a shell containing q POMs and the precipitate $\Delta\mu_s^0$ reads:

$$\Delta\mu_s^0 \equiv \mu_q^0/q - \mu_c^0 = \frac{-kT}{q}\ln x_q \tag{2.10}$$

In which x_q is the mole fraction of the shells. A more detailed derivation of the equations given in this section can be found in the Appendix.

2.3. Experimental

Synthesis of {$Mo_{72}Fe_{30}$}. The synthesis was conducted as reported in [**26**]. In order to make {$Mo_{72}Fe_{30}$}, another POM based on molybdenum oxide was needed as a precursor. This precursor was synthesized as first published in [**14**]

Variation in Dielectric Constant. For these experiments the desired amount (usually 10-20 mg) of crystals was dissolved in 10-15 mL of the desired solvent (water, methanol, ethanol, propanol or acetone). In case of aqueous solutions, bi-distilled water was used. After dissolution of the material, which required prolonged stirring and heating to 50 °C, the solutions were filtered over a Millipore filter (0.22 μm) for samples in water, or a Fluoropore filter (0.2 μm) for other solvents. From these stock solutions the actual samples were made by dilution. These were then kept in a water bath at 50 °C until no change in the scattering behavior was observed over a period of one month.

Determination of maximum solubility. Under slight heating, solid {$Mo_{72}Fe_{30}$} was added to MillyQ water until no further dissolution was observed. After cooling of the solution to room temperature and filtration by a Millipore filter (0.22 μm), the concentration of material was measured by means of UV-Visible absorption spectroscopy. This was done for 3 different samples. From solutions of known concentrations the extinction coefficient was determined to be 15.26 ± 0.24 mL mg^{-1} cm^{-1} at 320 nm. Saturated solutions were diluted by adding 50 μL to a total volume of 10 mL of MilliQ

water. All measurements were done on a Varian Cary 1E UV-Visible spectrophotometer.

Dynamic Light Scattering. Dynamic light scattering measurements were performed on an in house setup with an Argon-ion laser (Spectra Physics) operating at a wavelength of 514.5 nm and a temperature of 298 K. The autocorrelation functions were recorded with a Malvern K7025 128-point correlator. The samples were measured in glass Danliker cuvets which were rinsed with freshly distilled acetone. Hydrodynamic radii where recorded at angles in between 35° and 120°.

2.4. Results and Discussion

2.4.1. Effect of Dielectric Constant

In section 2.2.2 an expression for the radius of the POM-shells was obtained, which states that the size of a POM-shell should be linearly dependent on the inverse of the relative dielectric constant (ϵ_R) of the solvent. This relation can be tested experimentally by measuring the hydrodynamic radii of shells in solvents with different ϵ_R with help of dynamic light scattering (DLS). Figure 2.4 shows that the POM-shells indeed follow this predicted linear behavior. In this Figure the hydrodynamic radii (extrapolated to zero angle) of the POM-shells are plotted as a function of $1/\epsilon_R$ of the solvent and a straight line can be fitted through the obtained data points.

For $\{Mo_{72}Fe_{30}\}$ it is well known that the formation of the shells is extremely slow, in particular at room temperature. Therefore the samples were heated to 50°C while the size of the structures that were formed was monitored with DLS. The samples were considered to be in equilibrium when no change in size was observed for a period of one month. However, three months after the samples were considered to be in equilibrium, the systems were double checked. In two samples corresponding to the lowest dielectric constant (propanol and acetone) the presence of shells could not be verified. This led to the conclusion that in these samples the initially formed structures are meta-stable. These structures however, do seem to follow the relationship as given in Equation (2.5). This probably is a consequence of the slow dynamics in the system, which tends to be trapped for long times in its local free energy minimum before moving to its global equilibrium state.

Additional measurements on the hydrodynamic radii of POMs shells of a slightly different POM were done by the group of Liu et al. and are included in Figure 2.4. They used mixtures of water and acetone to vary the dielectric constant of solutions of $(NH_4)_{42}[(Mo^{VI}_{72}Mo^{V}_{60}O_{372}(CH_3COO)_{30}(H_2O)_{72}]$.ca. $300H_2O$.ca.$10CH_3COONH_4$ abbreviated as $\{Mo_{132}\}$. The 2.9 nm large $\{Mo_{132}\}$ is similar to $\{Mo_{72}Fe_{30}\}$ in the sense that it also is a C_{60}-like, hollow spherical POM with icosahedral symmetry and it caries

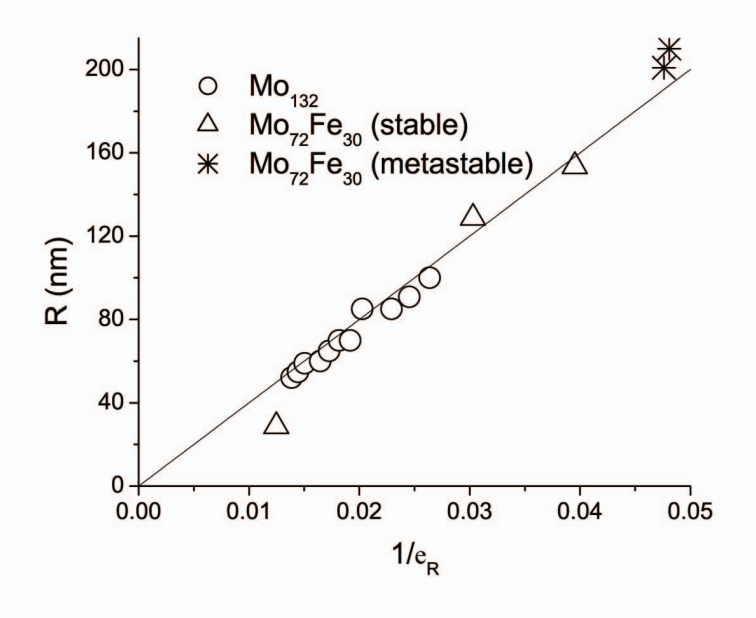

FIGURE 2.4. Shell radius as determined by dynamic light scattering as a function of the inverse relative dielectric constant of the solvent for two different POMs: $\{Mo_{72}Fe_{30}\}$ and $\{Mo_{132}\}$. The theory outlined in section 2.2.2 predicts a linear relation between the radius and the inverse of the dielectric constant. The slope of the line is given by 3824 ± 266 nm. Except for two points corresponding to $\{Mo_{72}Fe_{30}\}$ in pure propanol and acetone, the data corresponds to thermodynamically stable shells.

a negative charge in solution. It is however different in chemical nature. The major difference therein lies in the linkers that hold the pentagonal units together. In the case of $\{Mo_{132}\}$ the linkers are Mo_2 groups which are in turn stabilized by bidentate acetate ligands. The number of dissociable surface groups for this POM is 42. The aqueous $\{Mo_{132}\}$ systems with a concentration of $\sim$ 0.1-1.0 mg/mL POMs and varying acetone content (10-70 % in volume) were left in an oven at 30°C for 6-7 days, and the size of the shells was measured by DLS in a similar way as for the $\{Mo_{72}Fe_{30}\}$ systems. As can be seen in Figure 2.4, the data recorded for the two different POMs fall on the same line.

It is known from previous experiments that when packing particles on the surface of spheres, dislocations or "scars" can occur when the spheres reach a certain packing density [**27**]. The possible presence of dislocations on the POM-shells would lead to a term proportional to R in Equation (2.1) [**28**]. This, in turn, results in a sub linear or even constant relation between R and ϵ_R^{-1}. In the deduction of Equation (2.1) it is implicitly assumed that there are no dislocations present. Since the POM-shells indeed follow the behavior as predicted by Equation (2.5), it is plausible that there are indeed no dislocations or "scars" on the surface of the shells.

Table 2.1. Values of measured zeta potential (ψ), critical aggregation concentration (CAC), values of cohesive bond energies u extracted from the slope in Figure 2.4, and the interaction energy per bond $\Delta\mu^0/3$ estimated from the CAC

	$Mo_{72}Fe_{30}$	Mo_{132}
ψ (mV)	-56 (pH=4.6)	-48
CAC (mg/mL)	0.0024	-
u (kT)	-6.8	-5.4
$\Delta\mu^0/3$ (kT)	-6.6	-

2.4.2. Interaction Energies

According to Equation (2.5) the cohesive bond energies of the POMs in the shell can be deduced from the slope in Figure 2.4, if the zeta potential of the POM-shells in known. Table 2.1 lists the zeta potentials (ψ) as deduced from the mobilities of the shells measured by a commercial ZetaPals (Brookhaven Instruments, details ref.[**13**]). In the case for the shells of $\{Mo_{72}Fe_{30}\}$ in pure water, a significant pH dependence of the zeta potential was observed: $\psi = -47$ mV at pH = 4.0, while $\psi = -70$ mV at pH = 5.5. The values listen in Table 2.1 corresponds to a pH of 4.6 of a system with 0.1 mg/mL material. These are the same conditions at which the size of the $\{Mo_{72}Fe_{30}\}$-shells are measured with dynamic light scattering.

As already stated in Section 2.4.1, the measured hydrodynamic radii of both $\{Mo_{72}Fe_{30}\}$ and $\{Mo_{132}\}$ follow the same linear dependence with respect to the relative dielectric constant of the solvent. In fact the values measured fall on the same line (see Figure 2.4). Looking at the comparable values of the zeta potentials and Equation (2.5), this indicates that the cohesive bond energy u is also comparable for the two systems. From the slope in Figure 2.4 and the measured values of ψ, the cohesive bond energies can be deduced to be $u \approx -6.8kT$ for $\{Mo_{72}Fe_{30}\}$ and $u \approx -5.4kT$ for $\{Mo_{132}\}$. Considering the uncertainty of the slope in Figure 2.4 as well as the $\sim 10\%$ uncertainty in the values of Ψ, the values of u of the two POMs are not significantly different.

The interaction energy of the POMs in the shell can also be deduced by means of a model independent route as described in Section 2.2.3, by way of the critical aggregation concentration (CAC). The CAC for $\{Mo_{72}Fe_{30}\}$ was determined to be 0.0024 mg/mL as reported in [**29**] and its molecular weight is approximately 18000 g/mole. The CAC value for $\{Mo_{132}\}$ in unknown. When one assumes a predominantly hexagonal packing of the POMs on the surface of the shells the cohesive bond energy can be obtained with Equation (2.6). This results in a total cohesive energy per POM of $\Delta\mu^0 \approx -19,85kT$, corresponding to a cohesive bond energy of $u \approx \Delta\mu^0/3 \approx -6.6kT$ in the case of hexagonal packing on the surface of the POM-shell. This value is in excellent agreement

with the value of u obtained from the model, and provides additional plausibility that the finite-size POM-shells are indeed stabilized by charge regulation.

The values of the cohesive bond energy for the two POMs in Table 2.1 are consistent with hydrogen bonds [**25**] and also with the weak metal-oxygen bonds in simple complexes of Molybdenum(VI) oxide [**30**]. These values also are typical for those found in other self-assembling systems such as surfactant micelles [**25**] and virus capsids [**31**].

Using the approach outlined in Section 2.2.3 additional information about the system can be obtained. For instance the difference in chemical potential of a free POM and a POM in the precipitate can be calculated by means of Equation (2.8). Due to the equilibrium as described in Figure 2.3 in which single POMs as well as shells and crystal are present in the solution at the same time, the mole fraction of single POMs is equal to the mole faction of the CAC. Again using as the molecular weight 18000 gr/mole, the difference in standard chemical potential is $\Delta\mu_c^0 \approx -19.85\ kT$. The cohesive energies of a POM in the precipitate and a POM in a shell are by all means comparable and point to a negligible energy difference between the two states.

This can also be deduced by calculating the chemical potential difference between the two states directly from the solubility limit i.e., the concentration beyond which the POMs precipitate from solution. The maximum solubility of $\{Mo_{72}Fe_{30}\}$ has experimentally been determined to be 7.58 mg/mL by means of UV-Visible absorption spectroscopy (see section 2.3). This concentration is orders of magnitude larger then the determined CAC. Therefore one can consider this concentration to be approximately equal to the concentration of POM shells and the difference in cohesive bond energy can be calculated by using Equation (2.10). Again using a molecular weight of 18000 g/mole and taking $q = 10^3$, the mole fraction of the POM-shells is equal to $7.59 * 10^{-9}$. Using Equation (2.10) this leads to a difference in total cohesive energy between a POM in the shell and a POM in the precipitate of $\Delta\mu_s^0 = \frac{-kT}{q} \ln x_s \approx 1.87 * 10^{-2} kT$. This indeed is a very small difference and it can be concluded that the cohesive energy of a POM in a shell is equal to that in the precipitate.

Considering the definitions of the interaction energies between POMs in a shell and in the crystal as given by equations (2.7) and (2.9) the following should now hold:

$$n_s \epsilon_{attr} + f_{el}^s \cong n_c \epsilon_{attr} + f_{el}^c \tag{2.11}$$

Since the number of bonds in the compact crystal will be higher then the number of bonds in the shell structure, the total attractive energy will be higher in the crystal then in the shell, which leads to a more negative term. The electrostatic term not only accounts for the repulsion between like charges, but also for the gain in entropy by the dissociation of the counter ions. Due to this gain in entropy this term will also be negative. In order for the total interaction energy for POMs in both structures to be

equal the electrostatic term for the shell should in this case be more negative then for the crystal structure.

Given the negligible cohesive energy difference, what triggers the shells to precipitate? The volume fraction of the shells at the solubility limit of 7.58 mg/mL is $\phi_s = \frac{4}{3}\pi R^3 \rho_s \approx 0.029$, where ρ_s is the number density of shells and $R = 30\ nm$ was used. However, taking into account the electrical double layer thickness given by the Debye length, a measure of the effective volume fraction is $\phi_{eff} \approx \frac{4}{3}\pi(R + \kappa^{-1})^3 \rho_s \approx 2.08$ for an ionic strength of $10^{-5}M$. In this case the electrical double layers of the shells show considerable overlap at the solubility limit. It is therefore quite understandable that POMs would then prefer to condense into a solid precipitate if in the resulting structure this charge can be compensated by, for instance, additional bonds.

2.5. Conclusions

Finite-size shells made of POMs at low salt concentrations are stabilized by charge regulation as reflected in Equation (2.5). The variation in size of the POM-shells as a function of the dielectric constant of the solvents are in line with this charge regulation mechanism. Cohesive bond energies calculated using a charge regulation model are comparable to model independent calculations from critical aggregation concentrations. The cohesive bond energies deduces for $\{Mo_{72}Fe_{30}\}$ and $\{Mo_{132}\}$ are not significantly different and are comparable to bond energies found in other self-assembling systems. The model independent treatment of the system also showed that the cohesive energy of a POM in a shell is approximately equal to the cohesive energy of a POM in the precipitate.

Appendix: Derivation of Equations for the Interaction Energy

In the following a detailed derivation of the the equations used in section 2.2.3 will be given. This derivation is based on the equilibrium between monomers, shells and precipitate or crystal as depicted in Figure 2.3. Although all states are present in the solution at the same time, each equilibrium can be treated separately.

I) Equilibrium between single POMs and POM-shells

The equilibrium between the single POMs and the POM-shells can be treated similarly to the equilibrium as seen for, for instance, surfactant systems. The single POMs are in equilibrium with a POM-shell containing q POMs, in which q has a distinct value. The equilibrium can be written as:

$$qA \rightleftharpoons A_q \tag{2.12}$$

Equilibrium thermodynamics requires that in a system of molecules that form aggregates in solution, the chemical potential of all identical molecules in different aggregates are the same. For the above described equilibrium this can be translated into:

$$q\mu_1 = \mu_q \tag{2.13}$$

In which μ_1 is the chemical potential of a single free POM and μ_q is the chemical potential of one POM-shell containing q POMs. In the case of ideal behavior the chemical potentials can be written as:

$$q(\mu_1^0 + kTlnx_1) = \mu_q^0 + kT\ln x_q \tag{2.14}$$

In which μ_1^0 is the standard chemical potential of a single free POM, μ_q^0 the standard chemical potential of a POM-shell containing q POMs, k Boltzman's constant, T the absolute temperature, x_1 the mol fraction of single POMs and x_q the mole fraction of the POM-shells.

POM-shells, just as surfactant micelles, have a distinct size and hence are build up out of a defined number of POMs. The difference in standard chemical potentials between the two states has a peak around this value. If one would build up a shell out of the consecutive monomers, it would take $q-1$ steps in order to form the complete shell. Hence the average contribution of a monomer to the change in the standard chemical potential would then be:

$$\Delta\mu^0 \equiv \frac{(\mu_q^0 - q\mu_1^0)}{(q-1)} \tag{2.15}$$

The critical aggregation concentration (CAC) is defined as the concentration at which aggregates start to form. As long as the total concentration of POMs is lower then the CAC they will predominantly be present as single monomers in solution. Once the CAC is reached all additional POMs added to the solution will form aggregates, namely the

POM-shells. This implies that the total concentration of single POMs will not exceed the CAC concentration. It can be pro

$$x_{CAC} = e^{(\mu_q^0 - q\mu_1^0)/(q-1)kT} = e^{\Delta\mu^0/kT} \tag{2.16}$$

The difference in standard chemical potential $\Delta\mu^0$ can be seen as the mean interaction energy of a POM in a shell relative to the monomers. It is a measure for the interaction energy between the POMs in the POM-shell. The interaction between the POMs in the shell consists of two contributions:

$$\Delta\mu^0 \cong < f_{int} > \cong n_s\epsilon_{attr} + f_{el}^s \tag{2.17}$$

an attractive part which is proportional to the average number of bonds n_s of the POM in the shell, and an electrostatic term caused by the charges on the macro ions in the shell in solution, which in principle is not pairwise additive.

II) Equilibrium between single POMs and the precipitate

The second equilibrium is between the single POMs in solutions and POMs in the precipitate or crystal structure which is formed as soon as the solubility of the POMs is reached. This equilibrium can be described by:

$$A \rightleftharpoons A_c \tag{2.18}$$

Again according to equilibrium thermodynamics the following should hold:

$$\mu_1 = \mu_c \tag{2.19}$$

in which μ_c is the chemical potential of a POM in the crystal structure or precipitate. Using the chemical potential of a POM in the crystal structure as a reference point, the difference in standard chemical potential between a single free POM and a POM in the crystal $\Delta\mu_c^0$ can be deduced in the following way:

$$\mu_1 = \mu_1^0 + kT\ln x_1, \qquad \mu_c = \mu_c^0 \tag{2.20}$$

which by means of 2.19 leads to,

$$\mu_1^0 + kT\ln x_1 = \mu_c^0 \tag{2.21}$$

$$\Delta\mu_c^0 \equiv \mu_1^0 - \mu_c^0 = -kT\ln x_1 \tag{2.22}$$

in which the term $kTlnx_1$ accounts for the entropy associated with single POMs free in solution. In the situation drawn in Figure 2.3, all three states of the POMs are in equilibrium and the concentration of single POMs is equal to the critical aggregation

concentration, hence $x_1 = x_{CAC}$. Here again the difference in chemical potential between the two different states $\Delta\mu_c^0$ is a measure for the mean interaction energy, only now for a POM in the crystal relative to the monomer:

$$\Delta\mu_c^0 \cong < f_{int} > \cong n_c\epsilon_{attr} + f_{el}^c \tag{2.23}$$

The attractive term is now proportional to the number of bonds in the crystal structure.

III) Equilibrium between POM-shells and the precipitate.

At the same time the POM-shells are also in equilibrium with the precipitate, which can be described by:

$$qA_c \rightleftharpoons A_q \tag{2.24}$$

According to equilibrium thermodynamics the following should hold:

$$q\mu_c = \mu_q \tag{2.25}$$

Again using the chemical potential of a POM in the crystal μ_c as a reference point, the difference in standard chemical potential of a POM in a shell containing q POMs and the precipitate $\Delta\mu_s^0$ can be deduced as follows:

$$q\mu_c = q\mu_c^0, \qquad \mu_q = \mu_q^0 + kT\ln x_q \tag{2.26}$$

which by means of 2.25 leads to,

$$q\mu_c^0 = \mu_q^0 + kT\ln x_q \tag{2.27}$$

$$\Delta\mu_s^0 \equiv \mu_q^0/q - \mu_c^0 = \frac{-kT}{q}\ln x_q \tag{2.28}$$

In which x_q is the mole fraction of the shells at the point at which monomer, shell and crystal coexist.

This equilibrium can be characterized by the solubility. The difference in standard chemical potential of monomers in both states can be calculated directly from this concentration if the concentration of monomers can be neglected with respect to the concentration of shells. If this is the case it can be assumed that the concentration of the POMs at the maximum solubility is equal to the concentration of shells coexisting with the precipitate.

3

Structural Instability of Shell-like Assemblies of a Keplerate Type Polyoxometalate Induced by Ionic Strength

Abstract

We demonstrate a new structural instability of shell-like assemblies of polyoxometalates. Besides the colloidal instability, i.e. the formation of aggregates that consist of many single layered POM-shells, these systems also display an instability on a structural scale within the shell-like assemblies. This instability occurs at significantly lower ionic strength than the colloidal stability limit and only becomes evident after a relatively long time. For the polyoxometalate abbreviated as $\{Mo_{72}Fe_{30}\}$ it is shown that the structural stability limit of POM-shells lies between a NaCl concentration of 1.00 mM and 5.00 mM in aqueous solution.

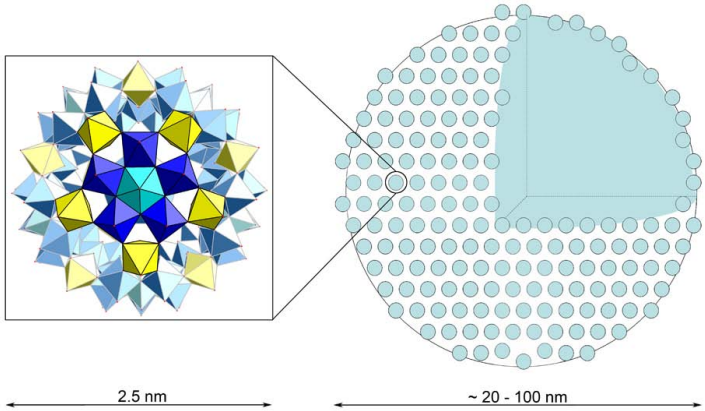

Figure 3.1. Schematic representation of a hollow spherical superstructure of polyoxometalates (POM-shells). Polyoxometalates (POMs) have been shown to spontaneously form POM-shells, which contain up to a 1000 of individual POMs and can grow up to several tens of nanometers in water. In this example the POM-shell contains the 2.5 nm large POM abbreviated as $\{Mo_{72}Fe_{30}\}$. Sizes of the POM-shell indicated refer to the size range in aqueous solutions.

3.1. Introduction

Spontaneously assembling systems are of interest in both applied as well as fundamental sciences. They are widely used for the development of complex, functional structures. Each assembled system also has its limits within which it remains in its assembled state. The limits beyond which these systems are no longer stable as well as the nature of the instability give more insight in the forces governing the assembly and are therefore just as important as the process that drives the building blocks together.

One type of system that has been shown to spontaneously assemble into large superstructures are solutions of polyoxometalates (POMs). POMs are large, highly symmetrical inorganic molecules, consisting of (mainly) metal oxide polyhedrals (molybdenum, tungsten, vanadium, iron, etc). In solution they spontaneously form hollow, spherical assemblies with an average radius in water of several tens of nanometers, and composed of a monolayer of more than 1000 of individual POM macro ions [**12**] (Figure 3.1). The formation of these intriguing shell-like assemblies or POM-shells is not limited to molybdenum-containing POMs but is also observed for POMs containing for instance tungsten or copper [**13**]. Besides the Keplerate type POMs, also wheels shaped POMs [**12**] and metal-organic nanocages containing palladium [**32**] have been shown to form these type of shell-like assemblies.

Once these POM-shells have been formed they display classical colloidal behavior in solution. The charged POMs-shells can for instance be destabilised by increasing the ionic strength. As a result the coulomb interactions between the POM-shells are screened upon which they aggregate and subsequently precipitate out of solution[**33**].

The concentration at which this aggregation is observed is dependent on the valency of the counterions, as is described by the classical Schultz-Hardy rule [**34**], see ref [**18**]. Here we demonstrate another instability in POM-shells: an instability based on a structural change in the POM-shells themselves. We here present evidence as well as a theoretical explanation of the new experimental stability limit for a system of POM-shells

3.2. THEORY

In previous research it has been shown that, given their existence, the behavior of the POM-shells can be very well described by a stabilization mechanism based on charge regulation [**35**]. This charge regulation model predicts that $R \propto \epsilon_R^{-1}$, in which R is the radius of the POM-shells and ϵ_R the dielectric constant of the solvent in which they are dispersed, which has indeed been verified experimentally. In this model the free energy is assumed to depend on two fluctuating and dependent variables: its aggregation number, reflected in the radius R, and the effective charge Z. The free energy of a POM-shell F in the limit of $\kappa^{-1} >> R$ can then be described by [**35**]:

$$\frac{F}{kT} = 4\pi\gamma_0 R^2 - 12u + \frac{\lambda_B Z^2}{2R(1+\kappa R)} - \psi Z \qquad (\kappa^{-1} >> R) \tag{3.1}$$

in which γ_0 denotes the surface tension, u the cohesive bond energy between two POMs in the POM-shell, ψ the zeta potential, $\lambda_B = \frac{e^2}{4\pi\epsilon_0\epsilon_R kT}$ the Bjerrum length and $\kappa = (8\pi\lambda_B\rho_s)^{\frac{1}{2}}$ the inverse Debye screening length, with k Boltzmann's constant, T the absolute temperature, e the unit charge, ϵ_0 the permittivity of vacuum, ϵ_R the relative permittivity of the medium, and ρ_s the number density of the 1:1 electrolyte.

The formation of the POM-shells occurs under conditions of low ionic strength. The validity of Equation (3.1) requires that counter ions inside the shell can be neglected, hence $R << \kappa^{-1}$. In this case the shell can be approximated by a charged sphere which is reflected in the third term in Equation (3.1). This term arises from the screened-Coulomb interactions on a uniformly charged sphere in a background electrolyte characterized by a Debye screening length κ^{-1}, within the Debye-Hückel approximation [**18**].

At higher salt concentrations however, counter ions inside the shell can no longer be neglected. In that case the electrostatic energy can not be described by the third term in Equation (3.1). As a limiting case the system can than be described by a charged shell with a continuous distribution of point charges [**36**]. The third term should in that case be replaced by:

$$\frac{\lambda_B Z^2}{2\kappa R^2}(1 - e^{-2\kappa R}) \qquad (\kappa^{-1} << R) \tag{3.2}$$

in the limit of $\kappa^{-1} << R$. This leads to a different behavior of the free energy with respect to the size of the system. It can be verified that including this term the free energy per unit area of the shell monotonically decreases with R for the limit that $\kappa^{-1} << R$. In this limit the shells will no longer be stable and will grow to have an infinite size. In the other limit, where the third term in Eq. (3.1) applies and in which $\kappa^{-1} >> R$, the free energy per unit area of the shell has a minimum corresponding to the optimal radius of the system.

One can also understand this result from another point of view. As soon as κ^{-1} becomes smaller than the radius of the shell, the interactions between the POMs in the shell become of shorter range than the size of the system. In this case the electrostatic interactions between the POMs are not able to prevent the system from growing and the shells can grow to have an infinite radius. In practice this means that no finite-sized shells can be stable above a certain salt concentration, leading to a limit in its structural stability.

3.3. Experimental and Results

This structural stability limit was determined experimentally for POM-shells of a C_{60}-like, hollow, spherically shaped, Keplerate type POM of 2.5 nm in diameter. It has the following composition in its crystalline state [**16**]:

$$Mo^{VI}_{72}Fe^{III}_{30}O_{252}(CH_3OO)_{12}\{Mo_2O_7(H_2O)\}_2\{H_2Mo_2O_8(H_2O)\}(H_2O)_{91} \bullet ca.150(H_2O)$$

and was prepared according to established procedures [**26**]. It will further be referred to as $\{Mo_{72}Fe_{30}\}$ (4.1). When dissolved into aqueous solution, $\{Mo_{72}Fe_{30}\}$ acts as a

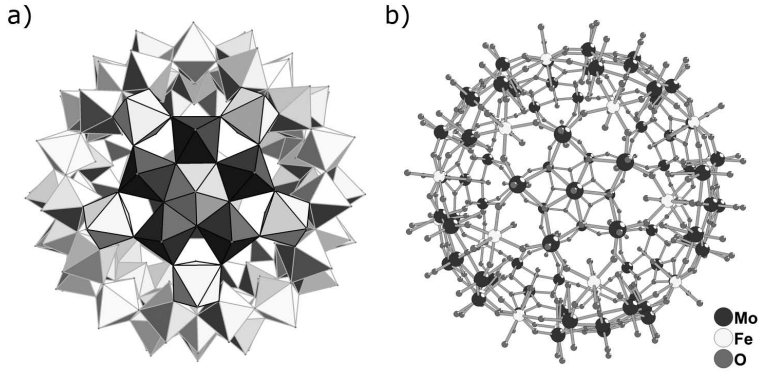

Figure 3.2. Schematic representations of the polyoxometalate (POM) $\{Mo_{72}Fe_{30}\}$. a) Polyhedral representation. b) Molecular representation. In polyhedral representation the metal atoms are located in the center and the oxygen atoms on the corners of the polyhedra. The inorganic macro ion is spherically symmetric, has a diameter of 2.5 nm and consists of 12 fivefold symmetrical units (blue and turquoise) linked by 30 Iron groups (yellow).(For the color version of this picture see the Color figures at the end of this thesis.)

weak acid. Water molecules coordinated to the Iron atoms in the structure can partially deprotonate resulting in a negative charge [**16**].

The point at which POM-shells of $\{Mo_{72}Fe_{30}\}$ are no longer stable was determined by preparing a dilution series with different concentrations of NaCl in MilliQ water. The added NaCl concentrations ranged from 0 mM to 50.0 mM. Subsequently, weighed amounts of solid $\{Mo_{72}Fe_{30}\}$ were dissolved in the different salt containing aqueous solutions so that each sample contained 0.1 mg/mL of the POM. The formation of the POM-shells in solutions of $\{Mo_{72}Fe_{30}\}$ is extremely slow, particularly at room temperature. The samples were therefore heated to 55 °C for 15 weeks.

After this period visual observation revealed that no large structures were present in samples with 5.00 mM and higher salt concentrations. A hand held laser (Helium-Neon, Hughes, model 435LF4) directed through the samples showed strong scattering in the samples with no added salt and with a concentration of 1.00 mM of NaCl (see Figure 3.3). All samples containing a higher salt concentration did not show scattering. At the same time a yellow precipitate was observed in salt concentrations higher than 1.00 mM. Where the solutions of 0 mM and 1.00 mM added NaCl had a yellow color due to the dissolution of $\{Mo_{72}Fe_{30}\}$, the solutions containing higher salt concentration were colorless. These observations were confirmed by UV-Visible spectroscopy experiments perfomed on a Cary 1E UV-Visible spectrophotometer at room temperature in quartz cuvets. $\{Mo_{72}Fe_{30}\}$ has a characteristic absorption peak at 333 nm [**26**]. Therefore the transmittance of the aqueous solutions at this wavelength was measured as a function of the concentration of added salt, the results of which are shown in Figure 3.3. For the samples containing 5.00 mM of added NaCl and higher, the samples transmitted on average 75% of the incomming light. If the loss of light in these samples is the result of absorption of single molecules of $\{Mo_{72}Fe_{30}\}$ only, the concentration of single POMs can be calculated from the extinction coefficient. The measured absorption in that case would correspond to $\{Mo_{72}Fe_{30}\}$ concentrations ranging from 0.006 mg/mL to 0.01 mg/mL. A decrease in transmittance can be the result of an increase of absorption as well as loss of light by scattering of particles in solution. The samples containing 0 mM and 1.00 mM of added salt both had a significantly lower transmittance than the other samples. This effect can be explained both by the presence of a higher concentration of single POMs and thus a higher absoption, as wel as from the los of light by scattering of the POM-shells. The difference in transmittance between 0 mM and 1.00 mM of added NaCl can be explained largely due to a higher amount of single free POMs in the sample leading to a higher contribution of the absorption.

Dynamic light scattering measurements of the samples containing 0 mM and 1.00 mM of added NaCl were done on an in house setup with an Argon-ion laser (Spectra Physics) operating at a wavelength of 514.5 nm and a temperature of 298 K. The autocorrelation functions were recorded with a multiple tau digital correlator (ALV, type 6010/160).

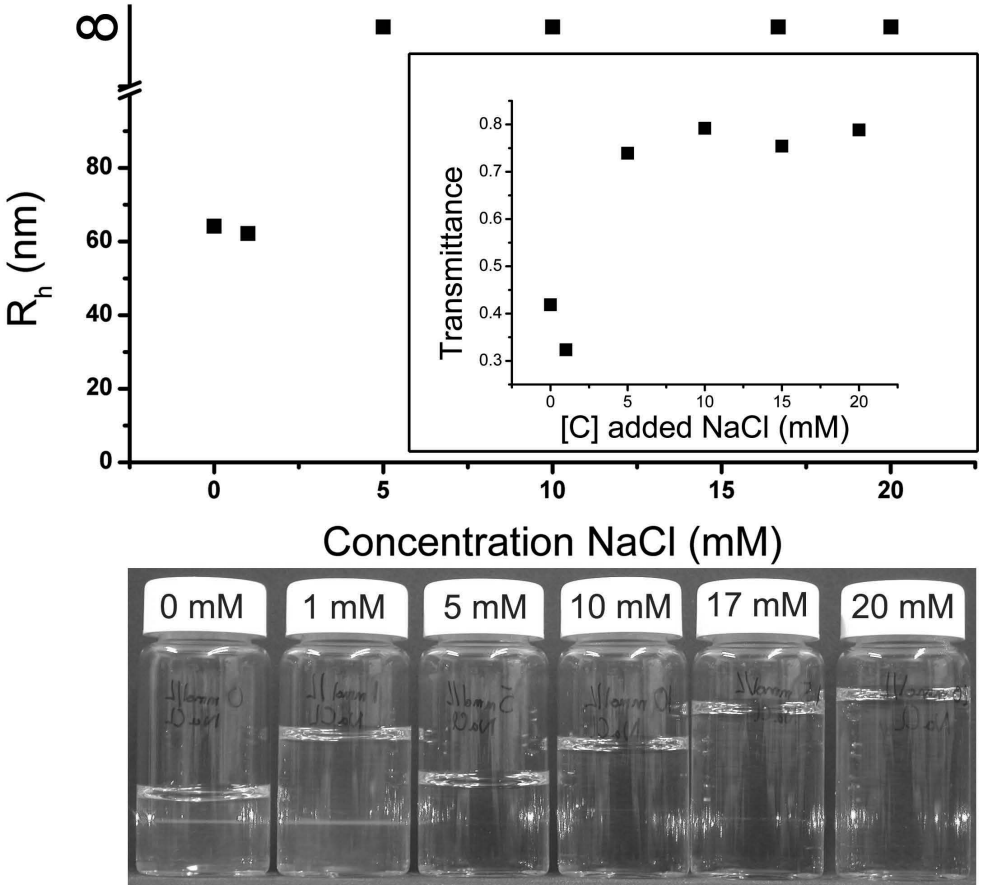

Figure 3.3. Effect of salt addition on the stability of POM-shells of $\{Mo_{72}Fe_{30}\}$. The hydrodynamic radii of the POM-shells measured with dynamic light scattering for the different salt contaning solutions are shown with underneath the graph a photograph of the different salt containing aqueous solutions of 0.1 mg/mL $\{Mo_{72}Fe_{30}\}$. A red hand held laser was directed from right to left through the glass screw cap vials. No significant scattering of the beam can be distinguished for samples with 5.00 mM NaCl and higher. Inlay: Transmittance at 333 nm of aqueous solutions of $\{Mo_{72}Fe_{30}\}$ containing different concentrations of added salt. The Transmittance of light of 333 nm is significantly lower for the samples containing 0 mM and 1.00 mM of added NaCl then for samples containing higher amounts of added salt.

The samples were cooled to room temperature and filtered with a Whatman, Schleicher and Schuell FP30/0,45 CA-S, cellulose acetate filter with pores of 450 nm mounted on a syringe. Measurements were performed in glass Danliker cuvets which were rinsed with freshly distilled acetone. Hydrodynamic radii where recorded at angles in between 35° and 120°. These measurements revealed objects with an average hydrodynamic radius of 64.17 ± 1.15 nm and 62.16 ± 0.57 nm for 0 mM and 1.00 mM of added NaCl

respectively, which is in agreement with sizes measured previously for these systems [**35**].

Althought the formation of POM-shells in aqeous solutions of $\{Mo_{72}Fe_{30}\}$ is well establised (see for instance [**29, 37, 38**]), the formation of shells in these type of solutions was verified with help of analytical ultracentrifugation. Sedimentation velocity experiments were performed on a sample containing no added salt with a concentration of 0.5 mg/mL of $\{Mo_{72}Fe_{30}\}$. Dynamic Light Scattering revealed objects with a hydrodynamic radius of $R_h = 57.70 \pm 5.00$ nm in this sample. Although the concentration of POMs in this particular sample is higher then for the samples used in the salt series, the size of the species in solution is in good agreement with what is found in both the sample with 1.00 mM added NaCl and no added salt of 0.1 mg/mL $\{Mo_{72}Fe_{30}\}$.

Sedimentation velocity experiments were performed after 2 weeks of heating at 55°C on a Beckman Coultier Optima XL-A analytical ultracentrifuge. The sample was centrifuged at a speed of 6600 rpm at a temperature of 293 K, while the sedimentation profiles were recorded at a wavelength of 405 nm with help of absorbance optics. A sedimentation coefficient distribution was deduced by means of a Van Holde-Weichet [**39**] analysis as presented in the program Ultrascan [**40**], after subtraction of the time invariant noise obtained from a two dimensional spectrum analysis.

The weight average sedimentation coefficient of the species in solution was determined to be $(6.00 \pm 2.15) * 10^{-11}$ s. Together with the measured R_h of 57.70 nm it is clear that structures in solution are not solid, in which case the sedimentation coefficient for particles with a radius of 57.70 nm would have been $182.8 * 10^{-11}$ s. If one were to assume that the species in solution in the sample consist of POM-shells with a shell thickness for which the mass is then proportional to the square of the radius, this thickness can be calculated by means of:

$$s = \frac{m_b}{f} \equiv \frac{2}{3}\frac{R_h \delta_l (\rho_l - \rho_s)}{\eta_s} \tag{3.3}$$

with $m_b \equiv 4\pi R_h^2 \delta_l (\rho_l - \rho_s)$, f the friction coefficient which for a sphere is equal to $6\pi\eta_s R_h$, δ_l the thickness of the layer, ρ_1 the density of a layer, ρ_s the density of the solvent and η_s the solvent viscosity. The weight average sedimentation coefficient is consistent with a shell of about 1 to 2 POM diameters in thickness if hexagonal packing of the POMs in the layers is assumed.

As for the salt containing aqueous solutions of $\{Mo_{72}Fe_{30}\}$, the experiments presented here indicate that the structural stability limit of POM-shells of $\{Mo_{72}Fe_{30}\}$ lies between 1.00 mM and 5.00 mM NaCl. The salt concentration of 1.00 mM corresponds to κ^{-1}=10 nm, which is the same order of magnitude as the measured 60 nm radius of the POM-shells. This result is in line with the predictions made on the basis of the charge regulation model. Previously reported stability limits of $\{Mo_{72}Fe_{30}\}$ in aqueous NaCl solutions are orders of magnitude larger then the stability limit found here ($\sim$ 51 mM in

[**33**] and 85 mM in [**34**]). At these high salt concentrations however, POM-shells display a colloidal instability as is evident, among other things, by the Schultz-Hardy rule [**18**]. Due to screening of the Coulomb interactions the POM-shells themselves aggregate and subsequently precipitate out of solution. The structure of the shells however, remains intact under those conditions. Colloidal instabilities are already apparent after approximately a day. Only close to the critical salt concentration the time scale lengthens to 30 days at most. This time scale is relatively short compared to the time scales connected to the stability limit found here. The theory summarized above describes an instability due to a structural change in the POM-shells. The activation barriers for structural changes in this system are high, as is evident from the slow formation process of the POM-shells [**38**]. Considering these slow dynamics, the structural stability limit requires significantly more time to become evident.

3.4. Conclusions

In conclusion we show here that systems of POM-shells can display two types of instabilities: colloidal instability as well as a new structural instability. Between a NaCl concentration of 1.00 mM and 5.00 mM in water POM-shells of $\{Mo_{72}Fe_{30}\}$ become unstable due to this structural instability. Above a NaCl concentration of $\sim$ 51mM the POM-shells will become unstable due to a colloidal instability. POM-shells formed by different kinds of POMs are governed by the same free energy [**35**]. It is therefore expected that these will also display a structural stability limit, pointing to a general behavior for this type of shell-forming systems [**13, 12, 32**]. The combination of both a structural and a colloidal stability limit in shell-like systems occurring at different timescales offers interesting possibilities in for instances the controlled capture and release of materials. The issue of control over the (long) time scale of the structural instability however, offers an interesting challenge.

4

The Influence of pH on the Formation of Shell-like Assemblies of the Keplerate $\{Mo_{72}Fe_{30}\}$

Abstract

Charge has been claimed to play an important role in the formation and stabilization of large hollow spherical superstructures or POM-shells formed spontaneously by Keplerate type polyoxometalates (POMs) in solution. Due to the weak acidic nature of single POMs of the Keplerate type $\{Mo_{72}Fe_{30}\}$, the charge on these POMs can be varied by changing the pH of the aqueous solutions in which they are dispersed. The effect of pH on the interaction energy between the single POMs in the POM-shell was investigated by measuring the Critical Aggregation Concentration (CAC). The results show that the interaction energy becomes more negative and hence the attraction becomes stronger when the pH of the solution increases. Increasing pH in turn, increases the charge density on the POMs. Measurements of the pH of aqueous solutions of $\{Mo_{72}Fe_{30}\}$ in time however, revealed an abundant release of additional protons. It is still an open question as to why this occurs and therefore the effect on the single POMs and the POM-shells in solution is unknown. It is therefore not possible at this point, to relate the change in interaction energy directly to a change in the level of charge on the POMs.

4.1. Introduction

The spontaneous assembly of polyoxometalates (POMs) into large hollow spherical superstructures or POM-shells raises many questions. One of the most challenging ones is why these large, predominantly hydrophilic inorganic molecules with no apparent amphiphilic nature would choose to form these hollow superstructures. Due to the spherically symmetric nature of for instance the Keplerate type POMs, one would expect interactions between them to be spherically symmetric as well. This would lead at most either to macroscopic phase separation or to the formation of liquid-like clusters, but certainly not the kind of hollow shells that are experimentally observed.

POMs consist (mainly) of metal oxide polyhedrals (molybdenum, tungsten, vanadium, iron, etc). In solution they spontaneously form hollow, spherical assemblies with an average radius in water of several tens of nanometers, and composed of a monolayer of more than 1000 of individual POM macro ions [**12**]. The formation of these intriguing shell-like assemblies or POM-shells is not limited to molybdenum-containing POMs but is also observed for POMs containing for instance tungsten or copper [**13**]. Besides the Keplerate type POMs, also wheel-shaped POMs [**12**] and metal-organic nanocages containing palladium [**32**] have been shown to form these type of shell-like assemblies.

Charge has been claimed to play an important roll in the formation and stabilization of these POM-shells. Research done previously points out that when the single POMs do not carry charge in solution the POM-shells will not form [**16, 41**]. It has also been shown that, given their existence, the behavior of the POM-shells can be very well described by a stabilization mechanism based on charge regulation [**35**] from which it has become evident that the low salt concentrations at which the POM-shells are formed and the charge that they carry play a vital role in their stability.

For several Keplerate type POMs it is possible to vary the number of chargeable groups on the single molecules in solution by for instance varying the pH of the aqueous solutions or by mixing of different solvents. This already has a significant effect on the size of the POM-shells that are formed [**16**]. Here we wish to investigate the effect of varying charge on the interaction energy between the single Keplerate type POMs in the POM-shell. This will be done by measuring the dependence of the critical aggregation concentration on the charge on the single molecules. The result of which is expected to provide more insight into the type of interactions that are involved in the formation process.

4.2. Theory

4.2.1. The System: $\{Mo_{72}Fe_{30}\}$

Here we study a C_{60}-like, hollow, spherically shaped, Keplerate type polyoxometalate which has the following composition in its crystalline state [**16**]:

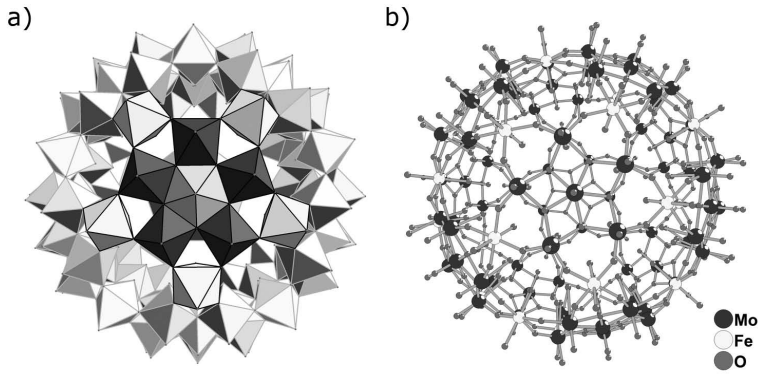

Figure 4.1. Schematic representations of the polyoxometalate (POM) $\{Mo_{72}Fe_{30}\}$. a) Polyhedral representation. b) Molecular representation. In polyhedral representation the metal atoms are located in the center and the oxygen atoms on the corners of the polyhedra. The inorganic macro ion is spherically symmetric, has a diameter of 2.5 nm and consists of 12 fivefold symmetrical units (blue and turquoise) linked by 30 Iron groups (yellow).(For the color version of this picture see the Color figures at the end of this thesis.)

$$Mo^{VI}_{72}Fe^{III}_{30}O_{252}(CH_3OO)_{12}\{Mo_2O_7(H_2O)\}_2\{H_2Mo_2O_8(H_2O)\}(H_2O)_{91} \bullet ca.150(H_2O)$$

This macromolecule, further referred to as $\{Mo_{72}Fe_{30}\}$, has a diameter of 2.5 nm. The detailed structure of this cluster can be visualized as a result of icosahedral disposition of 12 constituent $(Mo)Mo_5$ pentagonal building blocks along the 12 C_5 axes of the icosahedral point group. The remaining 30 'linking' C_2 sites in turn connect the 12 pentagonal units. In $\{Mo_{72}Fe_{30}\}$ the linkers are $Fe^{III}(H_2O)_2$ groups. Figure 4.1 shows the POM macro ion in both polyhedral as well as molecular representation, in which the linking Iron groups are colored yellow.

When dissolved into aqueous solution, $\{Mo_{72}Fe_{30}\}$ acts as a weak acid. Water molecules coordinated to the Iron atoms in the structure, can partially deprotonate. Therefore the number of chargeable groups is 30. However, the amount of deprotonation of the single molecules and the resulting negative charge depends on the pH of the solution [**16**]. By altering the pH of aqueous solutions of $\{Mo_{72}Fe_{30}\}$ one can thus influence the charge on these macroions. The general trend in this approach is that $\{Mo_{72}Fe_{30}\}$ carries less charge when the pH of the solution is more acidic [**16**].

4.2.2. CAC by Means of Static Light Scattering

The critical aggregation concentration or CAC is the concentration at which by further addition of monomers larger aggregates, in this case the POM-shells, will start to form. This concentration can be determined in several ways. One way applied in this research is by means of static light scattering (SLS).

As soon as the CAC is reached, large POM-shells will be formed. In the case of $\{Mo_{72}Fe_{30}\}$ the solution contains particles which vary up to two orders of magnitude

in size: the single POMs with a monodisperse radius of 1.25 nm and the polydisperse POM-shells with an average radius ranging from 20 nm to about 100 nm depending on the pH of the solution. The scattering intensity of these particles as a function of measurement angle can be described by the Rayleigh-Gans-Debye theory:

$$I_s = I_0 \frac{N k^4 V_p^2 \left|\bar{m} - 1\right|^2}{8\pi^2 r^2} P(q) S(q) (1 + \cos^2\theta) \tag{4.1}$$

In which I_s is the measured scattering intensity, I_0 the intensity of the incident beam, r is the distance between the sample and the detector, $k = 2\pi/\lambda$ is the length of the wave vector, V_p the volume of one particle, N the number of identical particles, $\bar{m}$ the average ratio of the refractive indices of the particle and the medium and θ the measurement angle. $P(q)$ is the form factor, which relates the angle dependence of the scattering intensity to the size and shape of the particle. $S(q)$ is the structure factor which gives information about positional ordering of the particles in the solution. When dispersions of particles are ideally diluted, as is the case for the POM systems, the particles are located at random positions and the structure factor is equal to unity.

As can be seen from (4.1) the intensity of the scattered light from a particle is dependent on the square of its volume (V_p^2). For solid spheres for which the entire particle is responsible for the scattering of the light, this means that the scattering intensity is proportional R^6 with R the radius of the particle. For hollow particles however, like the POM-shells and intrinsically the single Keplerates as well, only the outer shell scatters. In this case the volume responsible for scattering is proportional to the surface area (R^2) and hence the scattering intensity proportional to R^4.

When POM-shells are formed the radius of the scattering objects increases 1 to 2 orders of magnitude. As a result the scattering intensity of hollow particles increases 4 to 8 orders of magnitude for the same concentration of scattering particles. Therefore as soon as the CAC is reached the scattering intensity will go up drastically due to the formation of the larger POM-shells, which can be measured experimentally. The scattering intensity is also proportional to the number of particles N and hence to the concentration of particles in solution. Additional POMs added after the CAC is reached will predominantly form POM-shells. Therefore when the concentration is increased linearly, the scattering intensity should also increase linearly.

4.2.3. Effect of Charge on the Interaction Energy

Information about the interaction energy of the POMs in a POM-shell can be deduced by looking at the critical aggregation concentration (CAC) (see also Section 2.2.3). From the CAC mole fraction (x_{CAC}) the difference in standard chemical potential between a POM in solution and in the shell ($\Delta\mu^0$) can be calculated by means of

[**25**]:

$$\Delta\mu^0 \equiv \frac{\mu_q^0 - q\mu_1^0}{(q-1)} = kT\ln x_{CAC} \tag{4.2}$$

In which μ_q^0 is the standard chemical potential of a POM-shell, μ_1^0 the standard chemical potential of a single POM in solution and q the number of POMs in a shell. The difference in standard chemical potential can be seen as the mean interaction energy of a POM in a shell relative to the monomers. It is a measure for the interaction energy between the POMs in the POM-shell.

Although the nature of the interactions between the individual polyoxometalates that form the POM-shells is still a topic of debate, charge does play an important role. Therefore the interaction between the POMs in the shell can be considered to consist of two contributions:

$$\Delta\mu^0 \cong < f_{int} > \cong n_s\epsilon_{attr} + f_{el}^s \tag{4.3}$$

an attractive part which is proportional to the average number of bonds n_s of the POM in the shell (with ϵ_{attr} the energy per bond), and an electrostatic term (f_{el}^s) which is in principle not pairwise additive. The electrostatic term not only accounts for the repulsion between like charges, but also for the gain in entropy by the dissociation of counter ions.

4.3. Experimental

Synthesis of $\{Mo_{72}Fe_{30}\}$. These POMs were synthesized as reported in reference [**26**]. The original synthesis has been scaled up five times. As a precursor $\{Mo_{132}\}$ was used which was synthesized according to reference [**42**]. The original synthesis has also been scaled up five times.

Sample preparation for CAC. Samples were prepared by using 2 methods:

1. Aqueous solutions of Hydrochloric Acid were prepared with the desired pH after which the POMs were dissolved by stirring for 30 minutes to obtain a stock solution of about 0.4 mg/mL.
2. The necessary amount of $\{Mo_{72}Fe_{30}\}$ was dissolved in about 20 mL of water. Then hydrochloric acid or sodium hydroxide was added until the desired pH was reached. To reach the final concentration for the stock solution (about 0.4 mg/mL) the solution was diluted with a solution of hydrochloric acid with the required pH.

The stock solutions were diluted to the required concentrations (between 0.001 mg/mL and 0.02 mg/mL), with solutions of hydrochloric acid with the same pH as the stock. The pH of all solutions was measured with a Hanna Instruments pH210 Microprocessor pH meter equipped with a glass electrode. After preparation the samples were kept in

an oven at 55 °C in sealed plastic or glass vials. The resulting solutions were considered to be in equilibrium when no significant change in scattering intensity was observed after a minimum period of 2 weeks.

CAC determination by means of static light scattering. The critical aggregation concentration (CAC) was determined by making use of an in house automated static light scattering setup, equipped with a water cooled high pressure 200 W Hg arc lamp (USH200DP, Oriel 6283). The samples were irradiated with light from a spectral line from the Hg-lamp with a wavelength of 546.1 nm by use of a filter. The scattered intensity of all samples was measured with a Hamamatsu Photo Multiplier Tube (H5784-06) at all angles between 30° and 120°. The measurements were performed at a temperature of 298 K. During the measurement the samples were immersed in a cylindrical container filled with toluene.

In order to be able to compare the scattering intensity of the different samples all measurements were done in the same, with freshly distilled acetone rinsed glass Danliker cuvet, placed in the same position in the toluene bath. All samples were centrifuged at 2000 rpm for 5 minutes in a Hettich Universal 16A table centrifuge to remove possible dust particles.

A standard was used to compare measurements done at different times. The standard solution was prepared by diluting 0.3 grams of Ludox HS-40 to 1000 mL with water. After filtration through a 0.22 μm Millipore filter it was kept in a closed glass Danliker cuvet. A sample containing only MilliQ water was measured as a background.

UV-Visible Absorption. UV-Visible absorption measurements were carried out on a Varian Cary 1E UV-Visible spectrophotometer at room temperature. The absorption was recorded at all wavelengths between 200 and 700 nm. Samples were measured in quartz cuvets with an optical path length of 1 cm.

Dynamic Light Scattering. Dynamic light scattering measurements were performed on an in house setup with an Argon-ion laser (Spectra Physics) operating at a wavelength of 514.5 nm and a temperature of 298 K. The autocorrelation functions were recorded with a multiple tau digital correlator (ALV, type 6010/160). The samples were measured in glass Danliker cuvets which were rinsed with freshly distilled acetone. Hydrodynamic radii where recorded at angles in between 35° and 120°.

pH change over time. Weighed amounts of solid $\{Mo_{72}Fe_{30}\}$ were dissolved into MilliQ water in glass vials. The resulting solutions where kept in an over at 55 °C. The same synthesis batch of $\{Mo_{72}Fe_{30}\}$ was used for all samples. The pH of the solutions was measured at room temperature with a Hanna Instruments pH210 Microprocessor

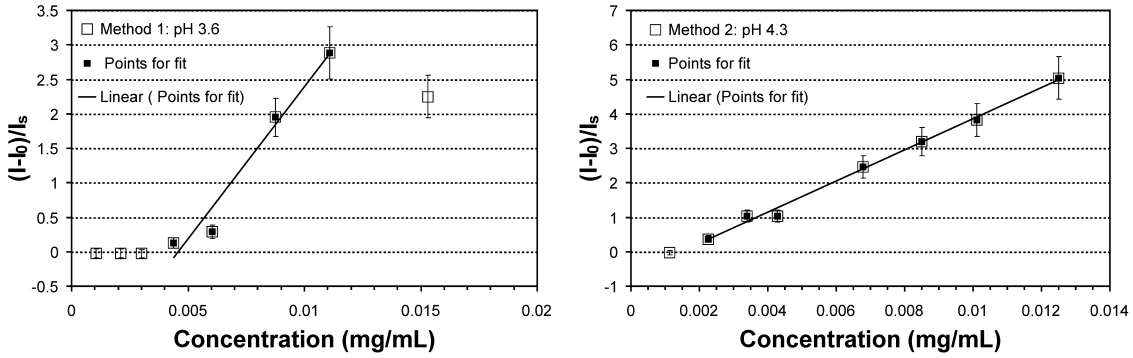

Figure 4.2. Typical results for the scattering intensity as a function of $\{Mo_{72}Fe_{30}\}$ concentration. Method 1: By adjusting the pH of the aqueous solution before addition of $\{Mo_{72}Fe_{30}\}$, Method 2: By adjusting the pH after the addition of $\{Mo_{72}Fe_{30}\}$.

pH meter equipped with a glass electrode. Scattering experiments were performed on the in house static light scattering setup as described under the CAC determination by means of static light scattering.

4.4. Results and Discussion

4.4.1. Critical Aggregation Concentration

With help of static light scattering (SLS) and the procedure described in the experimental section, the scattering intensity of samples with varying concentrations of $\{Mo_{72}Fe_{30}\}$ at different pH could be determined. From the scattered intensity of the samples at 90° the scattering of pure MilliQ water at 90° was subtracted. The resulting intensity was divided by the scattered intensity of the standard at 90° to filter out any variations in scattering due to variations in the experimental set-up (see Section 4.3). From the scattering experiments it followed that the scattered intensity of the low concentrated samples which contained only single POMs was negligible compared to the scattering of the POM-shells. Therefore a linear fit was made through the measurement points with a scattered intensity above zero. The CAC was then defined as the intersection of this fit at zero intensity. Typical result for the scattering intensity as a function of the concentration of $\{Mo_{72}Fe_{30}\}$ for both sample preparation methods can be found in Figure 4.2. The CAC-values calculated from these SLS-measurements are represented in Figure 4.3.

Method 1: Adjusting pH before addition of $\{Mo_{72}Fe_{30}\}$.

The scattering intensity as a function of the concentration of POMs as illustrated in the left graph in Figure 4.2 is typical for the scattering behavior seen for this series

of measurements. At low concentrations no significant scattering was observed until the CAC was reached, after which the scattering intensity increases linearly with the concentration of POM-shells. At a certain point however, the scattering intensity decreases even though the concentration of $\{Mo_{72}Fe_{30}\}$ increases, thereby deviating from the linear behavior. This effect was more or less pronounced depending on the pH of the series, however no direct correlation with the pH of the series was seen. A possible explanation could be that it is due to an effect of variations in the size distribution of the vesicles in the samples within one series. The concentrations at which this occurred were not included in the linear fit for the determination of the CAC.

As can be seen from Figure 4.3, the CAC values measured for solutions with pH of 3.6, 4.8 and 5.6 before the addition of $\{Mo_{72}Fe_{30}\}$ can be considered equal within the measurement error. Only the CAC value for the samples with a starting pH of 3.3 is significantly different. However, as already stated in the theory in Section 4.2.1 $\{Mo_{72}Fe_{30}\}$, acts as a weak acid in solution. In fact a solution of 0.5 mg/mL of this POM in MilliQ water already results in a pH of 3.9 [**16**]. Although the concentrations of $\{Mo_{72}Fe_{30}\}$ in the samples used for the determination of the CAC are orders of magnitude lower, the acidifying effect of the POMs can not be ignored. By adding $\{Mo_{72}Fe_{30}\}$ to the adjusted solutions the final pH at which the POMs are left to equilibrate is lowered, thereby shifting the resulting CAC value to a slightly lower pH.

This in itself would not pose a problem, since the final pH of the solutions could simple be measured after the addition of the POMs. However, since the POMs act as weak acids there is also an effect of concentration: more POMs result in a lower pH. This results in an even larger deviation in the sense that the pH at which the POMs are left to equilibrate is no longer constant throughout the same series. Measurements performed just after preparation of the solutions showed that the change in H^+ concentration was linearly dependent on the concentration of $\{Mo_{72}Fe_{30}\}$.

From this dependency the charge on the individual POMs could also be estimated which for $\{Mo_{72}Fe_{30}\}$ macro ions in aqueous acidified solutions of pH 4.8 and 5.6 resulted in a charge of between 4- and 5- per single POM for both series. This value is in agreement with calculations done based on charge regulation as presented in [**35**], which under the given experimental conditions predicts a charge that cannot much exceed 4-.

It is known that the ionic strength of the solution in which the POMs are dispersed can have a pronounced effect on the stability of the POM-shells (see Chapter 3). In adjusting the acidity of the solutions, one introduces additional ions in the system. It was previously shown that by the addition of 5.00 mM of NaCl to an aqueous solution of $\{Mo_{72}Fe_{30}\}$, the POM-shells will become structurally unstable. However, as shown in Table 4.1 the ions introduced in the system estimated by means of the pH value as measured after the addition of the POMs do not reach these concentrations and one

can safely assume that they will not affect the stability of the POM-shells.

Method 2: Adjusting pH after addition of $\{Mo_{72}Fe_{30}\}$.

With this method of preparation the pH could now be kept constant throughout a concentration series. An estimate of the ionic strength of these solutions can again be made from the pH of the solutions right after preparation. As can be seen in Table 4.1 the ionic strength is of the same order of magnitude as for the two highest pH series made by method 1 and should not have any significant influence on the stability of the POM-shells.

For all series the scattering intensity of the samples did not change over a period of 1 month. Therefore it was assumed that the solutions were in equilibrium. The CAC values as shown in Figure 4.3 show a decreasing trend with increasing pH. It can be stated however that the last two values are again the same within the measurement error.

The formation of POM-shells of $\{Mo_{72}Fe_{30}\}$ is a slow process, even when heating is applied. The dynamics of the system can also be increased by increasing the concentration of the samples. Therefore the equilibration of the system is faster at higher concentrations. In the series with pH 4.9 and 5.9 the scattering intensity as a function of $\{Mo_{72}Fe_{30}\}$ concentration showed a deviation from the linear behavior at lower concentration. This resulted in somewhat large errors in the CAC determined by the above mentioned fitting procedure. The deviation of the scattering intensity of these samples could be due to the fact that as a result of the low concentration of particles, the samples had not reached equilibrium yet. Even though the scattering intensity has not changed significantly in the course of one month.

4.4.2. Interaction Energies.

From the measured values for the CAC and taking 18000 g/mol as the molar weight of a single molecule of $\{Mo_{72}Fe_{30}\}$, the interaction energy between two POMs in a POM-shell ($\Delta\mu^0$) was calculated by means of Equation (4.2). Figure 4.4 shows the calculated interaction energies as a function of the pH of the solution. The results show

Table 4.1. Estimated values for the ionic strength by the addition of acid as calculated from the measured pH for series prepared by method 1 and 2.

pH Method 1	Ionic Strength (mM)	pH Method 2	Ionic Strength (mM)
3.3	0.6	4.0	0.9
3.6	0.3	4.6	0.3
4.8	0.02	5.0	0.3
5.6	0.002 - 0.005	5.6	0.3

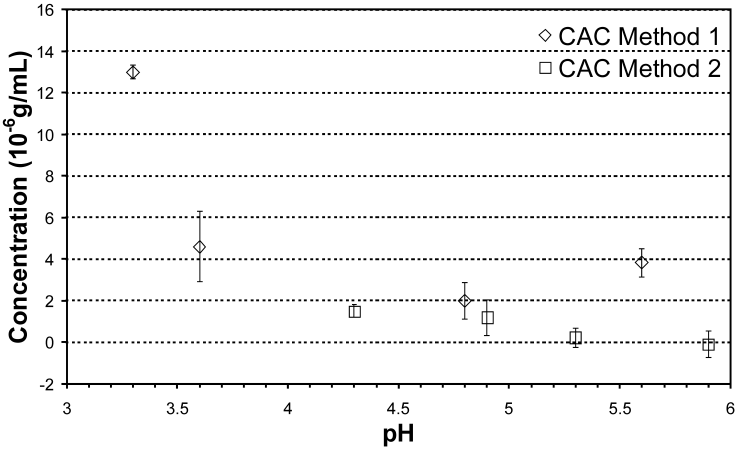

Figure 4.3. Critical Aggregation Concentration for the formation of POM-shells of $\{Mo_{72}Fe_{30}\}$ in aqueous solution as a function of the pH. The pH of the solution was adjusted before (Method 1) or after (Method 2) the addition of $\{Mo_{72}Fe_{30}\}$. By increasing the pH, and thus the charge on the single macro ions in solution, the POM-shells will start to form at lower concentrations of $\{Mo_{72}Fe_{30}\}$

that the total interaction energy becomes more negative when the pH of the solution increases. The interaction energy calculated for the series with pH 5.6 as prepared by method 1 however, deviates from this trend. This could be explained by the effect that the pH of the samples is influenced by the addition of the POMs. The pH after addition of the POMs in this series ranged from 5.6 to 5.1, depending on the concentration of $\{Mo_{72}Fe_{30}\}$.

For the series of pH 5.9 as prepared by adjusting the pH after addition of $\{Mo_{72}Fe_{30}\}$, the CAC as calculated from the measurement cannot be distinguished from zero. By extrapolation of the trend seen in the interaction energy as a function of pH, the interaction energy at a pH of 5.9 was estimated to be -22.5 kT which corresponds to a CAC of $8 * 10^{-5}$ mg/mL. This value is simply too low to determine with the applied scattering techniques.

When hexagonal packing of the single POMs on the surface of the POM-shell is presumed, the order of magnitude of the bond energy would range from approximately -6 kT to -7 kT. These values are consistent with hydrogen bonds [**25**] and also with the weak metal-oxygen bonds in simple complexes of Molybdenum(VI) oxide [**30**].

The results show that the total interaction energy becomes more negative and hence the attraction becomes stronger when the pH of the solution increases. The charge on a single $\{Mo_{72}Fe_{30}\}$ POM is also expected to increase with pH [**16**]. However, it will be shown in section 4.4.4 that the pH of the solutions does not remain stable in time. An additional decrease in the pH of the solutions revealed the release of a large number

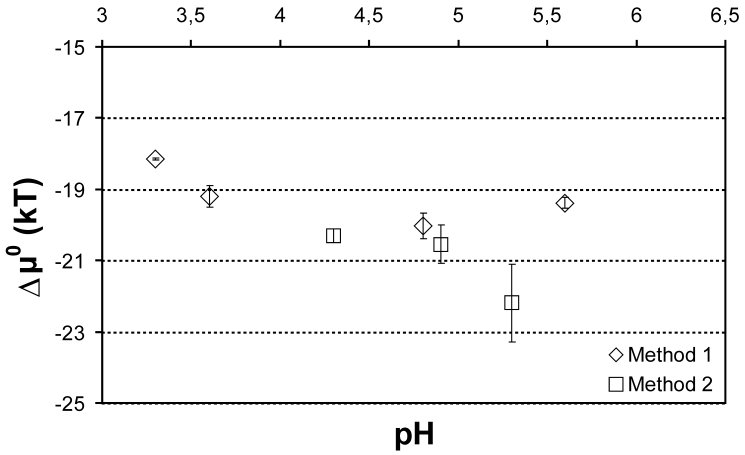

Figure 4.4. Difference in standard chemical potential between $\{Mo_{72}Fe_{30}\}$ in solution and in the shell ($\Delta\mu^0$) as a function of the pH of the solution. The difference in standard chemical potential can be seen as the mean interaction energy of a POM in a shell relative to the monomers. It is a measure for the interaction energy between the POMs in the POM-shell. The results show that the interaction energy between the POMs in the POM-shell becomes more negative when the pH of the solution, and hence the charge on the single POMs, increases.

of protons. A release which could not be explained. It is therefore not possible at this point to relate the change in interaction energy directly to the change in charge on the POMs in solution.

4.4.3. Vesicle Size

POM-shells have a rather broad size distribution, therefore it is difficult to get an accurate radius of gyration from a single static light scattering measurement. However, according to Equation 4.1 the total scattering intensity is linearly proportional to the concentration and to the scattering volume. It is assumed that all other possible variables are the same for all the measured systems. In this case, if the size of the POM-shells is known for one pH series, the sizes of the POM-shells in the other series can be estimated from the slope of the scattering intensity versus the concentration. This approach is valid as long as the size distribution of the POM-shells does not vary with pH. The radii of the POM-shells as a function of the pH of the solution estimated in this manner can be seen in Figure 4.5. The hydrodynamic radius of the POM-shells for the series of pH 4.3 prepared by method 2 as measured by dynamic light scattering was used as a reference (Hydrodynamic radius $\approx$ 51 nm). The results show that the size of the POM-shells increases with increasing acidity, which is consistent with what has been found in [**16**].

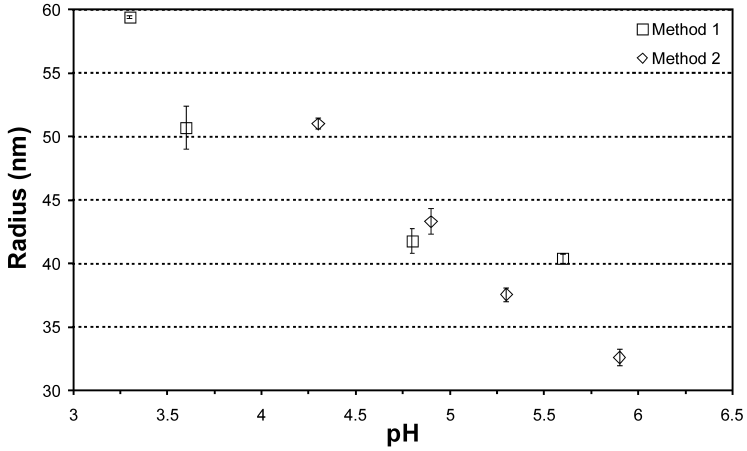

Figure 4.5. Hydrodynamic radius of POM-shells of $\{Mo_{72}Fe_{30}\}$ as a function of the pH of the solution. The radii are estimated from the dependence of the scattering intensity on the concentration of $\{Mo_{72}Fe_{30}\}$. The hydrodynamic radius of POM-shells of the concentration series at pH 4.3 ($\approx$ 51 nm) as measured by dynamic light scattering was taken as a reference from which the radii of the other pH series could be estimated.

4.4.4. Change in pH over Time

During the measurements of the CAC values for the different series, it was noticed that after the initial adjustment of the pH it did not remain stable in time. In fact for both method 1 and 2 a drop in the pH was observed in the coarse of approximately 56 days, corresponding to the release of additional protons in solution as can be seen in Figure 4.6. These are in addition to the ones already released by the $\{Mo_{72}Fe_{30}\}$ POMs themselves as a result of their weak acid nature. Additional measurements done on solutions with varying $\{Mo_{72}Fe_{30}\}$ concentration in non-acidified MilliQ water show that the drop in pH occurs within a few days after preparation of the solutions. After this drop the pH level remains constant. From the measured pH the additional release of protons per POM in solution could be calculated. As can be seen from Figure 4.6, the number of protons released per POM increases as the total concentration of POMs decreases.

There are several possibilities that could explain these results. For instance the presence of impurities in the form of unreacted Iron in the crystals of the POMs used for these experiments. If the crystals are not properly cleaned after synthesis residual Iron present can take up OH^- from the solution and form the highly insoluble $Fe(OH)_3$. By taking up hydroxide the pH of the solution drops. If this was however the case simple determination of the Fe content provides an estimate in the drop in pH which could then be observed. Elemental analysis of solid material used for a solution of 0.01 mg/mL revealed an excess of 2.5 atoms of Iron per POM which could theoretically account for

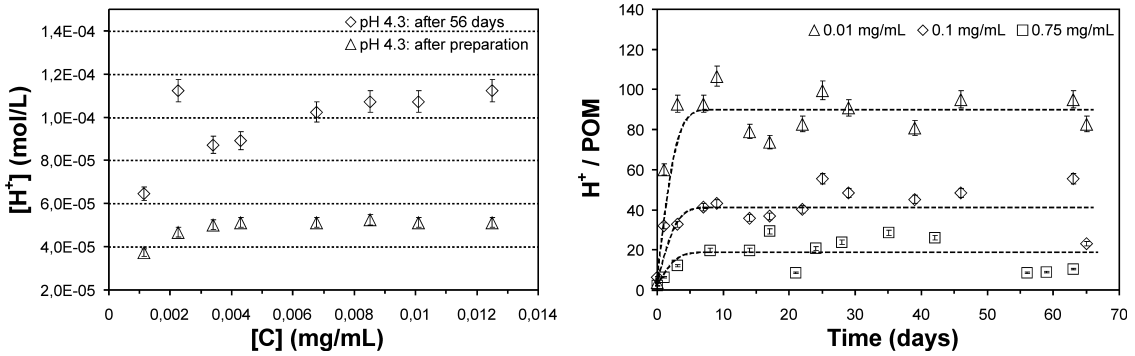

Figure 4.6. Change in pH of aqueous solutions of $\{Mo_{72}Fe_{30}\}$ over time. Left: The total proton concentration as calculated from the pH of the solution right after preparation of the series and after 56 days. The data presented is for the concentration series adjusted to a pH of 4.3 after the addition of $\{Mo_{72}Fe_{30}\}$. The results show a significant increase in proton concentration after 56 days. Right: The number of protons per $\{Mo_{72}Fe_{30}\}$ POM as calculated from the pH of the aqueous solutions as a function of time for three different total concentrations of POMs. The increase in proton concentration occurs after roughly 3 days after preparation. The number of additional protons per POM released increases for decreasing total concentrations of $\{Mo_{72}Fe_{30}\}$.

the additional release of 7.5 H^+. This is however not enough to explain the drop in pH which is experimentally observed for this solution. For example if one assumes a charge on the single POMs in solution of 5-, which corresponds to the release of five protons, the solution of 0.75 mg/mL would need 5 additional Fe atoms to be present per POM to account for the average drop in pH. For a solution of 0.01 mg/mL this should be as much as an additional 28 Iron atoms per POM originating from impurities. Also, if the drop in pH was caused by the presence of impurities, it seems more likely that the number of protons released per POM would remain constant as a function of total POM concentration since for the results shown in Figure 4.6 solid material of $\{Mo_{72}Fe_{30}\}$ from the same synthesis was used for all solutions. In addition, multiple samples with a concentration of 0.01 mg/mL prepared with solid material from the same synthesis showed roughly the same number of additional protons released per POM. This also the case for samples prepared from different synthesis batches.

Another possibility is that part of the POMs decompose. It is well known that in very dilute solution as the ones used for determining the CAC, small quantities of OH^- can lead to decomposition of the cluster and the precipitation of the brown/yellow $Fe(OH)_3$. If however the fraction of POMs that would have to decompose in order to account for the additional release of H^+ is calculated for, for instance the solution containing 0.01 mg/mL, the drop in pH would indicate a loss of 94% of the material. Considering the fact that this concentration is commonly used in order to characterize the POM-shell

structures, this would be very unlikely. Moreover, the decomposition of $\{Mo_{72}Fe_{30}\}$ occurs predominantly at pH $\geq$6.6. The MilliQ water used in the experiments is in itself slightly acidic (pH $\approx$5.5) which only increases the stability of the single POMs and makes it less likely that $\{Mo_{72}Fe_{30}\}$ will decompose.

During the formation of the POM-shells the solutions are heated. In order to check the influence of heating and the stability of the solvent a blank of pure MilliQ water was measured. There was however no significant change in pH of the water.

There is also the possibility that the release of the additional protons is correlated to the formation of the POM-shells. In order to investigate this possibility not only the scattering intensity of a sample containing 0.1 mg/mL of $\{Mo_{72}Fe_{30}\}$ was monitored in time, but at the same time the pH was monitored as well. The results show that large objects form in the course of 10 days after which the scattering intensity increased only very slightly, while the change in pH had already stabilized in roughly 3 days. The increase in proton concentration and the formation of the POM-shells occur on different time scales and are therefore not correlated. This can be seen even more clearly in Figure 4.7 in which the scattering intensity and proton content are plotted in the same graph.

During sedimentation experiments of $\{Mo_{72}Fe_{30}\}$, it was observed that small molecules were present in aqueous solutions of $\{Mo_{72}Fe_{30}\}$ that did not correspond to the POM-shells nor the single POMs [**43**]. It was suggested that ligands in the form of acetic acid, $Mo_2O_7(H_2O)$ and $H_2Mo_2O_8(H_2O)$ could be released by the POMs. These ligands could also be responsible for the change in proton content. However, since acetic acid is a weak acid and is present in its unprotonated state in the molecule, it is far more likely that it would take up protons from solution. As for the other ligands, their effect on pH is unknown.

None of the possibilities mentioned above are able to explain the measured change in pH. The effect of impurities and decomposition of the POMs however, can not be ruled out yet. If a presence of an additional 7.5 protons per POM due to Iron impurities in the crystals is taken into account, the percentage of decomposition of POMs needed to account for the change in pH can be recalculated. When both effects are taken into account for a solution of 0.75 mg/mL of $\{Mo_{72}Fe_{30}\}$, a total amount of 22% of the POMs will have to decompose in order to account for the additional protons present. For a solution of 0.01 mg/mL this would be as much as 86%. Therefore, even when the presence of impurities in the solid material is taken into account, the loss of material needed in order to explain the additional drop in pH is still considerable and hence very unlikely to occur.

In fact, none of the options mentioned can even explain the increase in number of protons per POM for decreasing total POM concentration. This thus leaves us with an open question as to why this occurs. The change in pH of these solutions also poses a

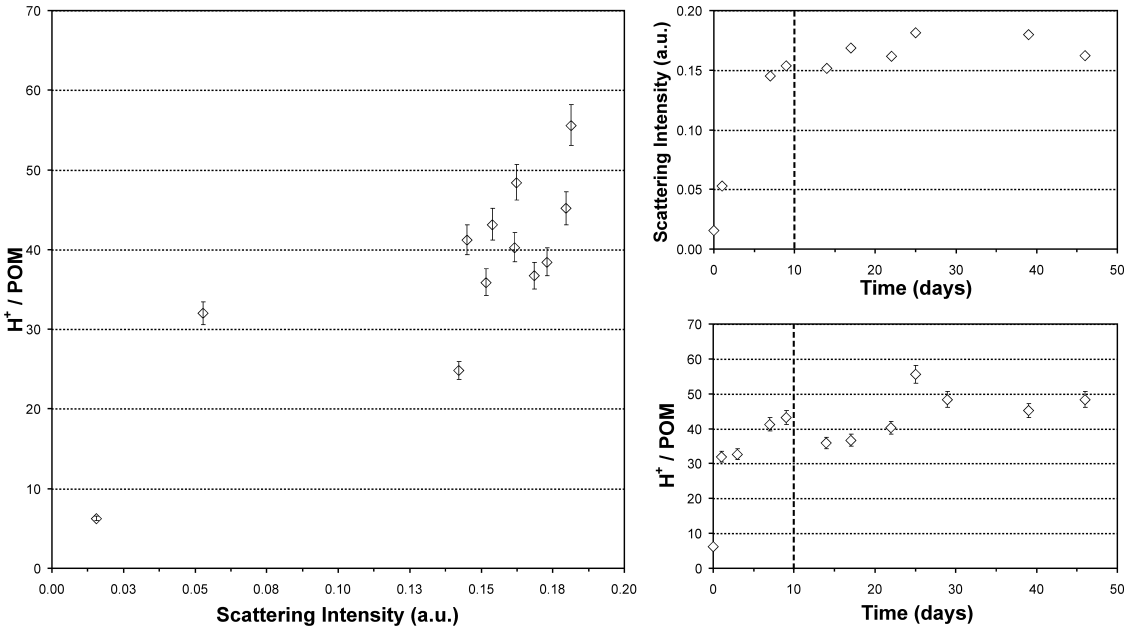

Figure 4.7. Correlation between the formation of POM-shells of $\{Mo_{72}Fe_{30}\}$ and the change in pH of the aqueous solutions. Right top: The formation of the POM-shells can be monitored by measuring the increase in scattering intensity at 90° in time. Right bottom: At the same time the change in pH of the solution was monitered and the number of protons per POM released in time could be calculated. Left: Scattering Intensity as a function of the number of protons per POM in solution. From the scattering and pH measurements no clear correlation between the formation of the POM-shells and the release of additional protons in the system could be deduced. The increase in proton concentration occurs within the first 3 days after preparation of the sample, while the shell-formation continuese even after this time period as is evident from the continuing increes in scattering intensity.

problem when interpreting the measured CAC values as a function of the initial pH of the solutions. Because it is not known what causes this change, the effect on the single POMs and the POM-shells in solution is also not known. It is therefore not possible at this point to relate the change in interaction energy directly to a change in charge on the POMs.

4.4.5. Absorption Change in Time

Besides the change in pH of the solutions, it was also observed that the absorption spectrum of the solutions changed in time. The single $\{Mo_{72}Fe_{30}\}$ POMs have a characteristic absorption peak at approximately 333 nm which is caused by a charge transfer between the Iron and Molybdenum in the molecule. During the formation process of the POM-shells it was noticed that the absorption of this characteristic peak decreased in time. Figure 4.8 shows the absorption curves at different times for aqueous solutions

containing 0.00728 mg/mL of $\{Mo_{72}Fe_{30}\}$ which were kept at 20 °C, 55 °C and 80 °C respectively.

The rate at which the absorption of the characteristic peak decreases is also dependent on the temperature. In the inlay in Figure 4.8 this rate is represented as the disappearance of $\{Mo_{72}Fe_{30}\}$ in time. The concentration of single POMs was calculated using the extinction coefficient of 13.50 ± 1.25 OD mL mg^{-1} cm^{-1} at 333 nm determined by measuring the absorption at 333 nm of fresh solutions of $\{Mo_{72}Fe_{30}\}$ in MilliQ water with known concentrations. The rate at which the absorption initially decreases at 55 °C is approximately 5 times faster than at 20 °C. This rate is even higher for samples kept at 80 °C (approximately 180 times faster then at 20 °C). However, after 141 days a precipitate appeared pointing to the formation of large aggregates. This was not observed for the samples kept at 20 °C and 55 °C.

The timescale in which the characteristic absorption peak for the $\{Mo_{72}Fe_{30}\}$ monomers decreases is comparable to the measured increase in scattering intensity contributed to the formation of the POM-shells. Therefore the disappearance of the characteristic absorption peak could be linked to the formation of POM-shells. Perhaps during the formation of the POM-shells the characteristic absorption is quenched.

Apart from the gradual decrease of the characteristic absorption of the monomers, an additional peak appears at 230 nm which does not change over time. This can be seen most clearly in the absorption spectra measured for the solution at 20 °C. The spectrum taken after 5 days shows the appearance of an additional peak which does not change in absorbance even though the characteristic peak at 333 nm keeps decreasing. For the sample kept at 55 °C a third peak became visible at 260 nanometer after a period of 141 days. This was also observed for the pH series used for the determinating of the CAC, but not in the samples kept at 20 °C and 80 °C. It is unknown what causes this peak to appear, but it could indicate that a second slower process occurs.

4.5. Conclusions

The interaction energy between $\{Mo_{72}Fe_{30}\}$ POMs in a POM-shell as calculated from measured critical aggregation concentrations becomes more negative and hence the attraction becomes stronger when the pH of the solution is increased. Increasing pH in turn, increases the charge density on the POMs. Over the course of the formation of the POM-shells it is observed that the characteristic absorption peak for the $\{Mo_{72}Fe_{30}\}$ monomers gradually decreases. On a shorter timescale than the formation of the POM-shells the pH of solutions of $\{Mo_{72}Fe_{30}\}$ decreases and an absorption peak at 230 nm appears. This additional decrease in the pH of the solutions revealed an abundant release of additional protons. It is unknown why this occurs. This poses a problem when interpreting the measured CAC values as a function of the pH of the solutions. Since it is not known what causes this change, the effect on the single POMs and the

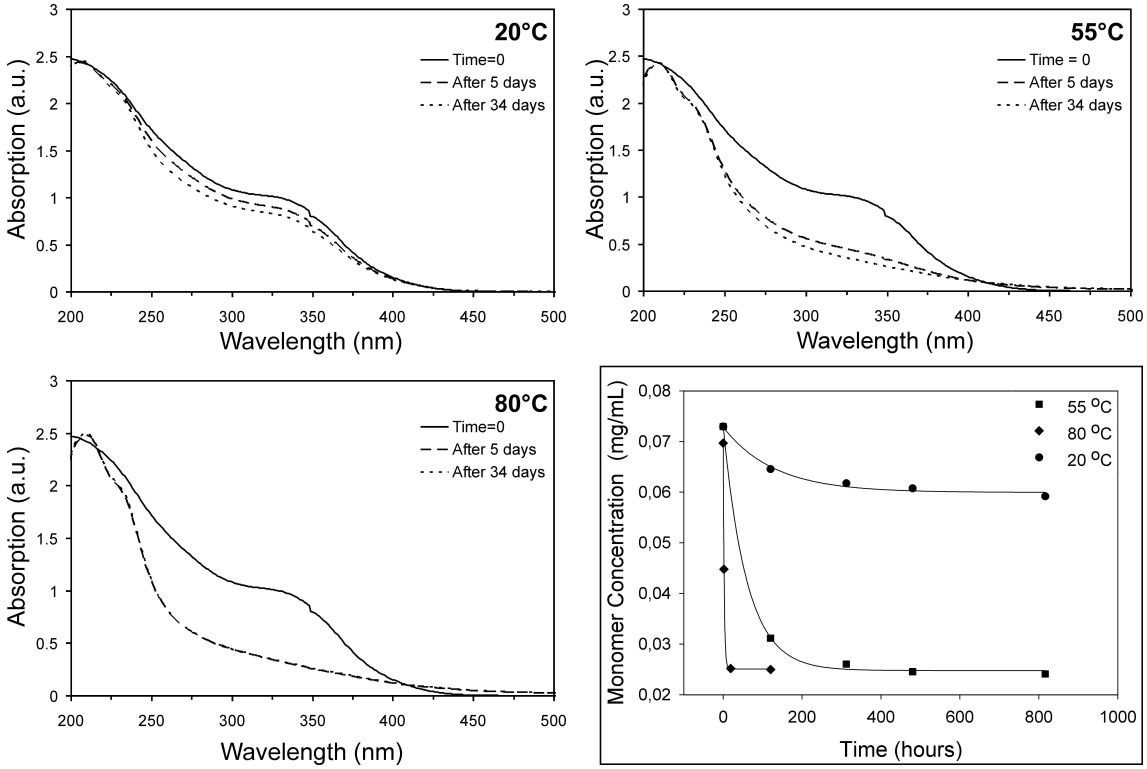

Figure 4.8. Change in UV-Visible absorption in time for aqueous solutions containing 0.00728 mg/mL of $\{Mo_{72}Fe_{30}\}$ which were kept at 20 °C, 55 °C and 80 °C respectively. The characteristic aborption peak of $\{Mo_{72}Fe_{30}\}$ at 333 nm decreases in time while an additional peak appears at a wavelength of 230 nm. Inlay: Decrease in $\{Mo_{72}Fe_{30}\}$ concentration in time as calculated from the absorption at 333 nm measured at different temperatures.

POM-shells in solution is also unknown. It is therefore not possible at this point, to relate the change in interaction energy directly to a change in charge on the POMs.

Acknowledgements

Marieke Bode is thanked for the large amount of work done on the determination of the CAC's. Karel Planken is thanked for his help with UV-VIS spectroscopy measurement. Bonny Kuipers and Emile Bakelaar are thanked for their help with the light scattering measurements and interpretation of the data.

5

Shape Transformation in Solutions of a Keplerate Type Polyoxometalate: From Shells to Needles

Abstract

Inorganic macromolecules known as polyoxometalates (POMs) can spontaneously organize themselves into large hollow spherical superstructures or 'POM-shells' in solution. These POM-shells consist of a monolayer of over 1000 of individual POMs and can have diameters ranging from 20-100 nm in water. These POM-shells have been considered to be thermodynamically stable. We show here that POM-shells do change over time and that the preparation route of solutions of POMs has an effect on the resulting species in solution. Moreover, in concentrated samples we observe a transition from spherical objects to elongated agglomerates. The elongated objects subsequently grow into large, crystalline, needle-like structures. From these observations we conclude that POMs follow an unusual nucleation route in which the POM-shells are in fact metastable intermediates.

5.1. Introduction

Polyoxometalates, or POMs for short, come in a variety of shapes and sizes. Some of them are among the largest inorganic molecules known today. These POMs can be highly symmetrical and are composed of up to hundreds of (mainly) metal oxide polyhedrals (molybdenum, tungsten, vanadium, iron, etc.) by sharing of the oxygen atoms. The novelty of this type of inorganic molecules not only lies in their molecular structure but also in their extraordinary behavior in solution.

POMs have been shown to spontaneously form large, hollow, spherical assemblies in solution containing a monolayer of over 1000 of individual POM macro-ions [**12**]. The formation of these intriguing assemblies or POM-shells is not limited to molybdenum-containing POMs but is also observed for POMs containing for instance tungsten or copper [**13**]. Very recently it was shown that metal-organic nanocages containing palladium also form this type of structures in solution [**32**].

Traditionally, POM-shells are prepared by dissolving the necessary amount of POMs in crystalline form in a solvent and allowing the solutions to equilibrate. The resulting single layered POM-shells remain stable and apparently unchanged in solution for months and were therefore considered to be thermodynamically stable. In contrast, we provide evidence that these shell-like assemblies are not a thermodynamically stable state. We show here that for a Keplerate type POM these POM-shells are in fact an unusual intermediate in a crystallization process towards needle shapes crystals.

5.2. Theory

5.2.1. The System: $\{Mo_{72}Fe_{30}\}$

Here we study a C_{60}-like, hollow, spherically shaped, Keplerate type polyoxometalate which has the following composition in its crystalline state [**16**]:

$$Mo^{VI}_{72}Fe^{III}_{30}O_{252}(CH_3OO)_{12}\{Mo_2O_7(H_2O)\}_2\{H_2Mo_2O_8(H_2O)\}(H_2O)_{91} \bullet \text{ca.}150(H_2O)$$

This macromolecule, further referred to as $\{Mo_{72}Fe_{30}\}$, has a diameter of 2.5 nm. The detailed structure of this cluster can be visualized as a result of icosahedral disposition of 12 constituent $(Mo)Mo_5$ pentagonal building blocks along the 12 C_5 axes of the icosahedral point group. The remaining 30 'linking' C_2 sites in turn connect the 12 pentagonal units. In $\{Mo_{72}Fe_{30}\}$ the linkers are $Fe^{III}(H_2O)_2$ groups. Figure 5.1 shows the POM macro ion in both polyhedral as well as molecular representation, in which the linking Iron groups are colored yellow.

When dissolved into aqueous solution, $\{Mo_{72}Fe_{30}\}$ acts as a weak acid. Water molecules coordinated to the Iron atoms in the structure, can partially deprotonate. The number of chargeable groups is 30, however, the amount of deprotonation of the single molecules and the resulting negative charge depends on the pH of the solution [**16**].

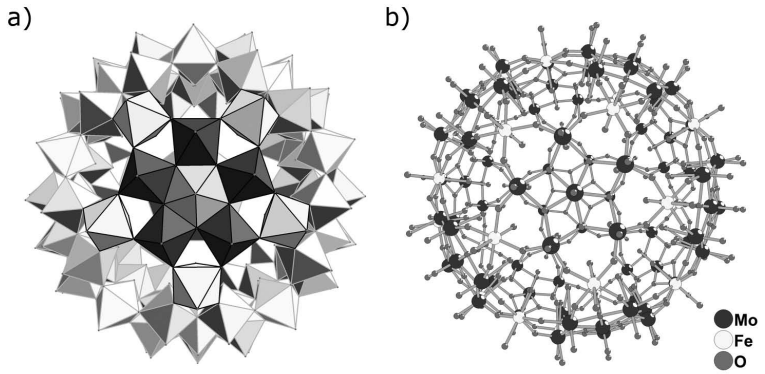

Figure 5.1. Schematic representations of the polyoxometalate (POM) $\{Mo_{72}Fe_{30}\}$. a) Polyhedral representation. b) Molecular representation. In polyhedral representation the metal atoms are located in the center and the oxygen atoms on the corners of the polyhedra. The inorganic macro ion is spherically symmetric, has a diameter of 2.5 nm and consists of 12 fivefold symmetrical units (blue and turquoise) linked by 30 Iron groups (yellow).(For the color version of this picture see the Color figures at the end of this thesis.)

5.3. Experimental

Synthesis of $\{Mo_{72}Fe_{30}\}$. The synthesis was conducted as reported in [**26**]. For the synthesis of $\{Mo_{72}Fe_{30}\}$, a precursor based on molybdenum oxide was needed. This precursor was synthesized as reported in [**14**]

Sample preparation. Dilution method: An aqueous solution (MilliQ water) at maximum solubility ($\sim$ 16 mg/mL) was kept at 55°C for two weeks to ensure complete dissolution of the crystals. After cooling of the solution to room temperature and subsequent filtration (Millipore filter, 1.2 μm pore size), a dilution series was made which was again placed at 55°C for two weeks. All measurement done afterwards where performed at room temperature.

Direct Dissolution method: As a comparison additional samples were made by direct dissolution of the desired amount of material in MilliQ water which were also placed at 55°C for a minimum of 2 weeks.

Small Angle X-ray Scattering. Small angle x-ray scattering measurements of the aqueous $\{Mo_{72}Fe_{30}\}$ solutions were done at the ID02 beam line at the European Synchrotron Radiation Facility in Grenoble, France. For details of the setup see reference [**44**].

Dynamic Light Scattering. Dynamic light scattering measurements were performed on an in house setup with an Argon-ion laser (Spectra Physics) operating at

a wavelength of 514.5 nm and a temperature of 298 K. The autocorrelation functions were recorded with a multiple tau digital correlator (ALV, type 6010/160). The samples were measured in small 5 mL glass screw cap vials (Chromacol). Hydrodynamic radii where recorded at angles in between 35° and 120°.

Cryogenic Electron Microscopy. The samples were prepared using an automated vitrification robot (FEI Vitrobot Mark III) with which samples are automatically blotted and plunged into liquid ethane. Blotting was done at 100 % humidity which resulted in a frozen layer of about 100 nm. The transmission electron microscopy grids used (R2/2 Quantifoil Jena) were purchased from Aurion and were surface plasma treated using a Cressington 208 carbon coater operating at 5 mA for 40 seconds before the vitrification procedure.

Transmission Electron Microscopy. TEM images were recorded on a Philips Tecnai12 microscope using formvar-coated copper grids on which a droplet of undiluted sample was placed and dried in air.

Analytical Ultracentrifugation. Sedimentation velocity experiments were performed on a Beckman Coultier Optima XL-A analytical ultracentrifuge. Sedimentation profiles were recorded with help of absorbance optics. Two samples containing 0.5 mg/mL $\{Mo_{72}Fe_{30}\}$ were measured directly after 2 weeks of heating at 55 °C. One sample was prepared by direct dissolution of the required material in MilliQ water. The other sample was made by dilution of a saturated solution of $\sim$ 20 mg/mL which had already been kept at 55 °C for a period of 2 weeks. Both samples were centrifuged at a speed of 6600 rpm while the sedimentation profiles were recorded at wavelength of 405 nm and 412 nm for the direct dissolution sample and dilution sample respectively. Sedimentation coefficient distributions were deduced by means of a Van Holde-Weichet [**39**] analysis as presented in the program Ultrascan [**40**], after subtraction of the time invariant noise by means of a two dimensional spectrum analysis.

5.4. Results and Discussion

5.4.1. POM-shells

If the POM-shells are indeed thermodynamically stable, the equilibrium state will only depend on the composition of the sample (at fixed temperature and pressure). In other words, the method of preparation of the samples should not affect the resulting species in solution. In order to test this two samples with a concentration of 0.5 mg/mL of $\{Mo_{72}Fe_{30}\}$ in water were prepared in two distinctly different ways, namely by direct dissolution and by first creating a saturated solution from which a dilution was made (see Section 5.3). After 2 weeks of heating at 55 °C, the hydrodynamic radii of the

species in solution were determined by dynamic light scattering (DLS). The sample prepared by means of direct dissolution contained objects with a hydrodynamic radius (R_h) of 57.70 ±5.00 nm, while the sample made by the dilution method contained objects of 31.53 ±1.73 nm in radius. Although the concentration of $\{Mo_{72}Fe_{30}\}$ in both samples is the same, the radius of the POM-shells is roughly twice as large for the direct dissolution method as compared to the dilution method. This is already a significant difference between the two methods of sample preparation.

Analytical ultracentrifugation (AUC) was used to measure the sedimentation velocity of the large species in solution. For both samples a distribution of sedimentation coefficients was obtained. The weight average sedimentation coefficients for the dilution and direct dissolution method were $(6.00 \pm 2.15) * 10^{-11}$ s and $(21.44 \pm 3.97) * 10^{-11}$ s respectively. This result together with the measured hydrodynamic radius for both systems ($R_h = 57.70 \pm 5.00$ nm for direct dissolution and $R_h = 31.53 \pm 1.73$ nm for the dilution method) shows that the species in solution are not solid. In that case the sedimentation coefficients for particles with a radius of 31.53 nm and 57.70 nm would have been $54.60 * 10^{-11}$ s and $182.8 * 10^{-11}$ s, respectively.

If one were to assume that the species in solution in both samples consist of POM-shells with a shell thickness for which the mass is then proportional to the square of the radius, this thickness can be calculated by means of:

$$s = \frac{2}{3}\frac{R_h n_l \delta_l (\rho_l - \rho_s)}{\eta_s} \tag{5.1}$$

as reported in [**43**], with n_l the number of layers, δ_l the thickness of one layer which in this case is approximately equal to the diameter of one $\{Mo_{72}Fe_{30}\}$ POM, ρ_1 the density of a layer, ρ_s the density of the solvent and η_s the solvent viscosity. The weight average sedimentation coefficient indicates that the solution prepared by the direct dissolution method is consistent with shells with two layers of $\{Mo_{72}Fe_{30}\}$ when hexagonal packing of the POMs in the layers is assumed. The same calculation for the dilution method indicates POM-shells with only one layer. For cubic packing instead of hexagonal packing the number of layers for the direct dissolution method can even go up to three when a bond distance of 2 Å is taken into account. This distance would be consistent with hydrogen bonding between the POMs in the shell.

Since the AUC measurements reveal a large distribution in sedimentation coefficients for both samples, it is conceivable that the shells present in solution do not all contain the same number of layers. However, without additional measurements it is impossible to tell whether or not this is the case. What can be concluded however, is that the species in solution obtained by the direct dissolution method have a higher density then the species obtained by the dilution method.

Recent results also show that for the POM abbreviates as $\{Mo_{72}Fe_{30}\}$ the POM-shells do change over time. Although light scattering techniques show that the size

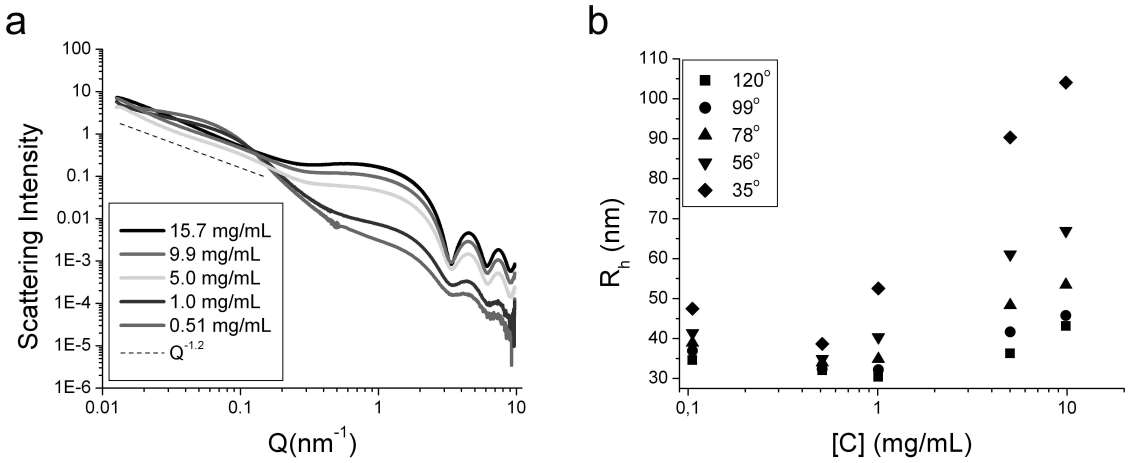

Figure 5.2. SAXS data (a) and DLS (b) measurements. a, In the low q-regime of the measured scattering curves, a change in the slope of the curve is observed. Between 1.0 mg/mL and 5.0 mg/mL the slope changes towards a $q^{-1.2}$ dependence for the higher concentrated samples. This indicates the presence of elongated agglomerates. b, The graph shows the measured hydrodynamic radius at different scattering angles as a function of the concentration of $\{Mo_{72}Fe_{30}\}$.(For the color version of this picture see the Color figures at the end of this thesis.)

of POM-shells of $\{Mo_{72}Fe_{30}\}$ in an aqueous solution of 80 μg/mL does not change significantly over the course of three years, they do become heavier. Sedimentation velocity measurements showed a doubling of the molar weight of these POM-shells [**43**].

This slow but significant change in the single layer POM-shells obtained by direct dissolution of $\{Mo_{72}Fe_{30}\}$ as well as the difference in the species in solution created by different preparation methods show that these shell-like assemblies are not thermodynamically stable. However, when there are only single layered POM-shells present in solution, the system may find itself trapped in a local free energy minimum due to the high activation barriers associated with structural changes [**38**]. Since in this case the system is in a meta-stable equilibrium it can still be accurately described by making use of equilibrium thermodynamics [**35**].

5.4.2. Needles

Even more interesting is what is observed at even higher concentrations prepared by the dilution method. Scattering curves from small angle x-ray scattering (SAXS) of a series of aqueous solutions with a concentration range from 0.5 mg/mL to 16 mg/mL were measured almost directly after preparation and are shown in Figure 5.2. In this figure the scattering intensity is given as a function of the angle in the form of the wave vector $q = (4\pi/\lambda)sin(\theta/2)$, in which λ is the wavelength of the radiation used and θ

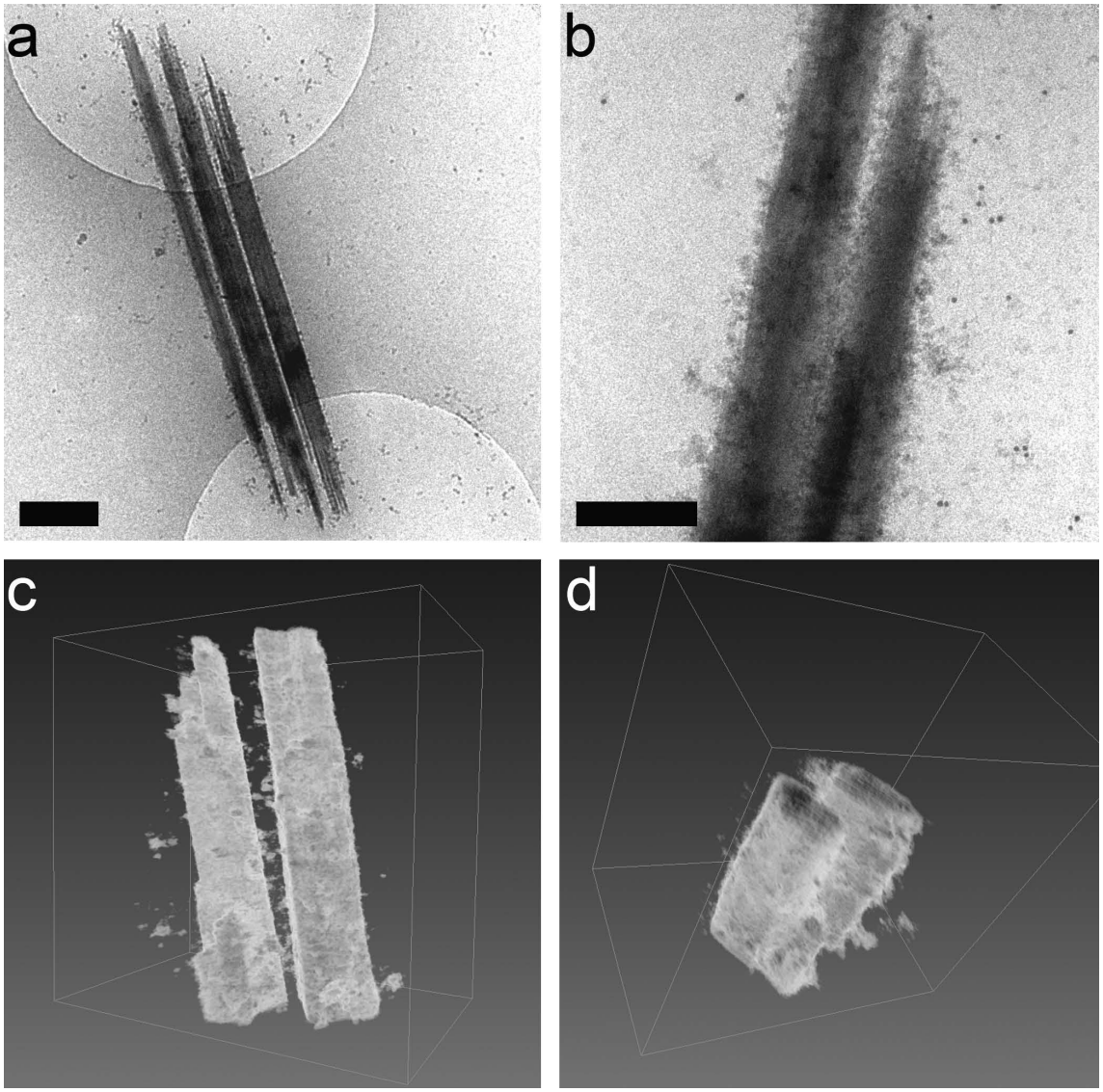

Figure 5.3. Cryogenic Transmission Electron Microscopy (Cryo-TEM) pictures of the needle-like structures. a, Three needles lying parallel to each other, demonstrating the dimensions and fine structure of the objects. Scale bar, 0.5 μm. b, Close up of two needles. The black dots on the background are gold particles needed in order to reconstruct the three dimensional image from images obtained by tilting the sample. Scale bar, 200 nm. c, d, Computer-aided visualization of the tomograms recorded from the needles in b. In d a cut is made through the needles from which can be seen that the needles are solid.(For the color version of this picture see the Color figures at the end of this thesis.)

is the angle between the incident beam and the detector. At large q values the curves represented in Figure 5.2 originate from the scattering by the single POMs, which is comparable for all concentrations. At low q values however, the scattering behavior is

different for different concentrations. Going from low to high POM concentration there is a change in slope of the scattering curves. For the three highest concentration the q dependence at the low q regime shifts towards a $q^{-1.2}$ dependence which indicates the presence of elongated structures (for comparison the q dependence of pure rod-like particles is q^{-1} [**45**]). Going from low to high POM concentration, there is thus a transition from spherical to more elongated agglomerates. The average radius of gyration (R_g) of the structures shifts from 40 nm (at 0.10 mg/mL) to 65 nm (at 1.0 mg/mL) to about 90 nm at the three highest concentrations.

Dynamic light-scattering (DLS) measurements performed 4 months after preparation of the samples reveal the same transition in hydrodynamic radius (R_h): from about 47.02 ±1.59 nm at 0.10 mg/mL to increasingly higher radii at the highest concentrations (see Figure 5.2b). For spherical particles it is known that there is at most a weak dependence of R_h on the scattering angle. The appearance of a large spread in the measured hydrodynamic radii as a function of scattering angle is also indicative of the presence of larger objects in solution. This is in agreement with what is found with SAXS experiments.

When results from both scattering techniques are compared in Table 5.1, it shows that for the samples which contained spherical objects (0.1-1.0 mg/mL), the R_h obtained by extrapolation to zero angle is roughly equal to the measured R_g. If the fraction of the total mass of a spherical object distributed at the surface increases, the ratio R_g/R_h increases. When it approaches a value of 1 the corresponding spherical object has all its mass on its surface as is the case for hollow shells [**46**]. As a comparison the R_g/R_h

Table 5.1. Measured radii and length scales for the objects in aqueous solutions of $\{Mo_{72}Fe_{30}\}$ at different concentrations from both small angle x-ray scattering (SAXS) and dynamic light scattering (DLS). When the concentration of the samples increases from 1.0 to 5.0 mg/mL a transition from spherical to elongated objects was observed. For low concentrated samples with spherical objects the hydrodynamic radius R_h could be measured by means of dynamic light scattering. For the samples containing elongated objects the diffusion coefficients measured at an angle of 35° are listed. The radii of gyration R_g given are obtained from the small angle x-ray scattering measurements.

Concentration (mg/mL)	R_h (nm)	D (35°) ($\mu m^2/s$)	R_g (nm)	R_g/R_h (nm)	Thin rods l (nm)
15.7	-	2.15	80	-	277
9.9	-	2.35	90	-	312
5.0	-	2.71	95	-	329
1.0	50.50 ± 3.82	-	65	1.29	-
0.51	38.03 ± 1.15	-	45	1.18	-
0.10	47.02 ± 1.59	-	40	0.85	-

ratio for solid spherical particles is equal to 0.77. The ratios as presented in Table 5.1 show a large variation. The values calculated are all larger then 0.77 suggesting that the particles become more dense towards the surface. This is consistent with results from sedimentation experiments of the solution containing 0.5 mg/mL $\{Mo_{72}Fe_{30}\}$. The sedimentation coefficient of the large objects present as presented in Section 5.4.1 points out that these objects are not solid.

The hydrodynamic radii as presented in Figure 5.2 are calculated from the measured diffusion coefficients by assuming a spherical conformation. SAXS however indicates that the highest concentrated samples contain elongated agglomerates. From the measured radii of gyration (R_g) for these samples, an estimate can be made of the length of the objects. For a thin rod R_g is equal to $L/\sqrt{12}$ which results in lengths of the elongated agglomerates of the order of 300 nm (see Table 5.1). If polydispersity in size, shape and refractive index of the particles is neglected and the rotational and translational diffusion are considered to be decoupled, the diffusion coefficients for rod-like particles as measured by DLS can be described by [**47**]:

$$D_{0,||} = \frac{kT[log(l/d) - 0.207 + 0.98(d/l) - 0.133(d/l)^2]}{2\pi\eta l} \tag{5.2}$$

$$D_{0,\perp} = \frac{kT[log(l/d) + 0.839 + 0.185(d/l) + 0.233(d/l)^2 2]}{4\pi\eta l} \tag{5.3}$$

where $D_{0,||}$ and $D_{0,\perp}$ are the translational diffusion coefficients parallel and perpendicular to the long axis, respectively, k is the Boltzmann constant, l the length and d the diameter of the rod and η is the viscosity of the solvent, which in this case is takes as the viscosity of water. The translation diffusion coefficients can be related to the weighted-average translation diffusion coefficient as measured by DLS by way of:

$$\langle D \rangle = 1/3 D_{0,||} + 2/3 D_{0,\perp} \tag{5.4}$$

From the measured diffusion coefficients for the concentration of 15.7 to 5.0 mg/mL measured at a scattering angle of 35°, an estimate can be made of the diameter of the objects. When a length of 300 nm is assumed (as was calculated from R_g) the diameter of the rods would be 27 nm. If one would assume length scales of the elongated objects that are $\leq$ 200 nm, no diameter can be found corresponding to a rod-like particle that would result in a diffusion coefficient of 2.3 $\mu m^2/s$ as measured by DLS. When the length of the rods is $\geq$ 600 nm, the resulting diameter of the rod would be smaller then the diameter of a single $\{Mo_{72}Fe_{30}\}$ POM. Therefore the length of the elongated agglomerates as determined by both dynamic light scattering and small angle x-ray scattering are in good agreement.

At this point it is not clear whether the elongated structures are the result of crystallization of the individual POMs or of a shape transition. In the case of crystallization,

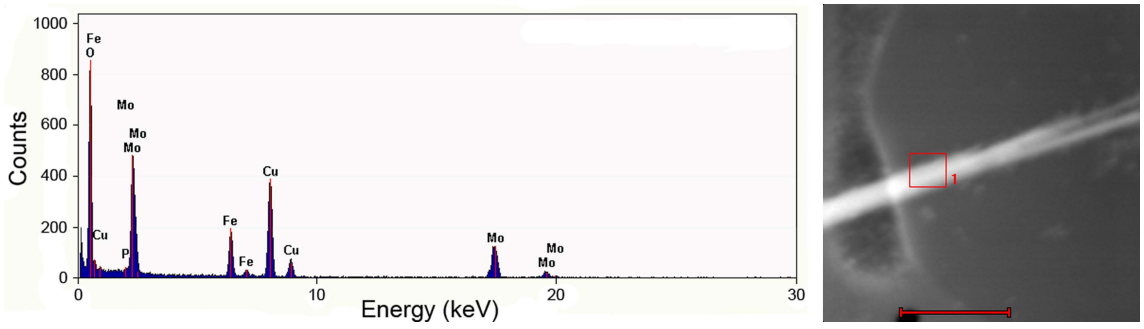

Figure 5.4. Electron Dispersive X-ray spectroscopy of the needles during Cryo-STEM (cryo scanning-transmission electron microscopy) confirms the presence of both Molybdenum and Iron in the structure. In the Cryo-STEM image on the left a single needles is depicted. The scale bar is 500 nm. In this imaging method the contrast is given according to the density of the material and to the atomic number Z (contrast $\propto Z^{1.7}$), hence the white color of the needle. The square in the image indicates the measurement position of the EDX spectrum given on the right.

the resulting elongated structures should be solid and crystalline. The POMs could in theory also display a shape transition from the shell-like assemblies towards cylindrical assemblies, similar as for surfactant systems. Since the POM-shells carry charge in solution and they are formed under conditions of low ionic strength, the electrical double layers of the shells will overlap if the concentration of POM-shells becomes too high. When this occurs the repulsion between the assemblies can be reduced if they assume a different conformation, for instance hollow cylinders.

In order to distinguish between the two possible scenarios, more insight had to be obtained in the structure of the elongated agglomerates. Cryogenic Transmission Electron Microscopy (Cryo-TEM) in this case offers a direct view of the objects as they appear in solution. A solution of 16 mg/mL $\{Mo_{72}Fe_{30}\}$ was investigated by means of Cryo-TEM and revealed the presence of large needle-like structures of several micrometers in length and approximately 100 nm in width as can be seen in Figure 5.3. Closer examination revealed that there are no POM-shells present in this sample; the needles do not coexist with the shell-like structures. In fact, only individual POMs could be detected evenly spread throughout the frozen film.

Electron-dispersive X-ray spectroscopy (EDX) of the needles during Cryo scanning-transmission electron microscopy (Cryo-STEM) confirmed the presence of both Molybdenum and Iron in the structure (see Figure 5.4). This confirms that the long needle-like structures indeed contain $\{Mo_{72}Fe_{30}\}$ and that these objects are not the result of decomposition of the inorganic molecules. A three-dimensional reconstruction of the needles could be made with help of Cryo-tomography (Figure 5.3c and d). Images of a sample

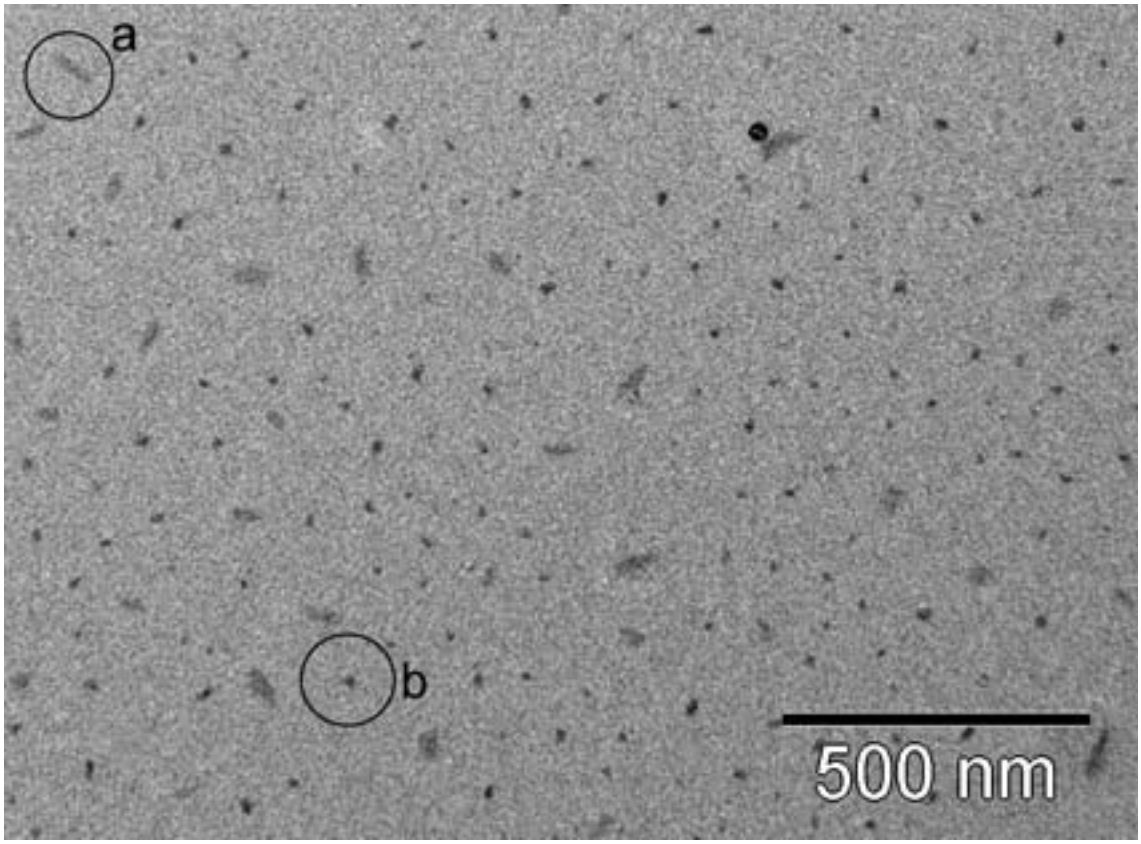

Figure 5.5. Transmission Electron Microscopy image of an aqueous solution of 0.5 mg/mL $\{Mo_{72}Fe_{30}\}$ taken 7 months after sample preparation. Small angle x-ray scattering performed directly after sample preparation revealed only spherical object in solution. After 7 months however, both elongated (a) as well as spherical (b) objects can be found in the same sample.

were recorded at tilting angles from -65° to +65° at 1.5° intervals. A cut made through the needles as shown in Figure 5.3 reveals that they are solid.

5.4.3. Crystallization

The solid composition of the needles, as well as the observation that the needles do not coexist with the shell-like assemblies both indicate that the elongated structures are a result of crystallization of the POMs. Although the presence of needles could be detected by scattering techniques immediately after preparation, needles with the dimensions as shown by microscopy only become visible after 10 weeks. This change in time of the species in solution for the dilution series was also seen at lower concentrations of $\{Mo_{72}Fe_{30}\}$. A solution of 0.5 mg/mL of $\{Mo_{72}Fe_{30}\}$ measured immediately after preparation showed only the presence of spherical objects in SAXS as can be seen from Figure 5.2a. When the same sample was investigated with electron microscopy 7 months after preparation, it contained both spherical and elongated species as can be seen in Figure 5.5.

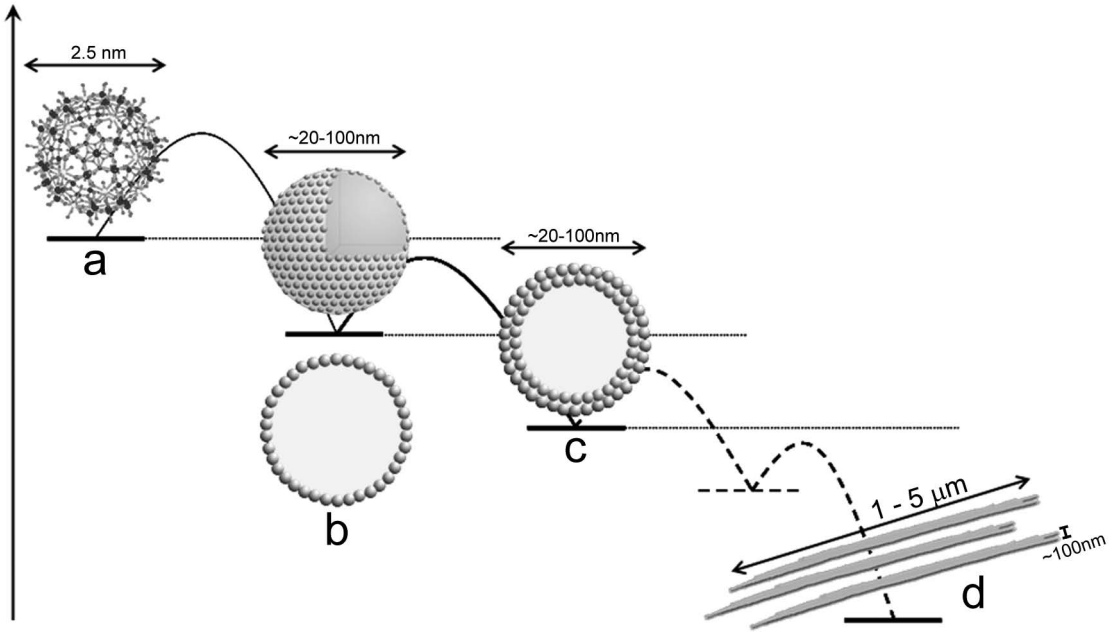

Figure 5.6. Crystallization of $\{Mo_{72}Fe_{30}\}$. The POM abbreviated as $\{Mo_{72}Fe_{30}\}$ (a) can crystallize into needles shaped crystals (d) by means of a shell-like intermediate. The POM-shells initially have only one layer of POMs (b) but may develop multiple layers over time (c).(For the color version of this picture see the Color figures at the end of this thesis.)

The change over time of the POM-shells together with the gradual change from spherical objects to more elongated structures indicates that the POM-shells are an intermediate in the crystallization process towards needle-like crystals. Although the exact pathway of crystallization and the resulting species in solution may depend on the preparation and concentration of the samples we suggest that $\{Mo_{72}Fe_{30}\}$ follows the crystallization route as depicted in Figure 5.6.

The fact that this crystallization process has not been observed before is most probably due to the long timescale over which changes in the assemblies take place. The formation of the POM-shells in itself is already a very slow process due to the high activation barrier involved for this transition [**38**]. By increasing the concentration of POMs one essentially increases the supersaturation of the solution. This effect decreases the activation barrier for the formation of nuclei and increases the rate of crystallization [**48**]. The timescale at which the needles are formed therefore depends on the concentration of the solution. It is even conceivable that by first creating a supersaturated solution and then diluting, the monolayer shell state is skipped and the species formed immediately go towards a more dense state.

This then raises the question as to why this system forms shell-like intermediates. The formation of in essence two dimensional objects contradicts with the systems preference to form a more dense state in the form of the crystalline needles. By forming shells the

POMs have a smaller number of possible bonds with neighbors then they would have in the crystal. The attraction between the POMs is however opposed by the charges that are present on the macro-ions. The addition of another layer of POMs on top of the first would not only result in more bonds but also in an increase in the electrostatic repulsion. There is thus a high energy barrier associated with the addition of a second layer.

5.5. Conclusions

In conclusion we have shown that POM-shells are meta-stable rather then thermodynamically stable and that they are an intermediate in the crystallization into needle shaped crystal structures. Since more POM systems form shell-like assemblies in a similar fashion as $\{Mo_{72}Fe_{30}\}$ [**35**] it is expected that they too will follow this route towards crystallization, suggesting a general behavior for this type of shell-forming systems. It is generally assumed that it is unlikely that significant levels of complexity can emerge for single-component systems [**49**]. Although at first glance solutions of $\{Mo_{72}Fe_{30}\}$ appear to be a simple single-component system, the occurrence of such complex behavior in solution might indicate otherwise. An experimental indication for this is presented in Chapter 4.

Acknowledgements

With this I would like to acknowledge ID02 for in-house beam time allocation and Theyencheri Narayanan for the use of his setup. I would also like to thank Nico Sommerdijk for his support and the opportunity to make use of his Cryo-TEM facility. Fabio Nudelman is thanked for the Cryo-TEM work on the needle-shaped structures.

Part 2

Assemblies of Polyoxomolybdates

6

Extended Structure Design with Simple Molybdenum Oxide Building Blocks and Urea As a Directing Agent

Abstract

We report here a simple one-pot directed synthesis of an oxomolybdate urea composite in which elementary molybdenum oxide building blocks are linked together with the aid of urea. This type of directed material design resulted in large rod-like crystals of an inorganic-organic hybrid extended structure of $\{MoO_3(NH_2 - CO - NH_2)\}_\infty$ consisting of right- and left-handed helical units. In the crystal structure urea acts both as glue that links the inorganic molybdenum units into a helix, as well as a supramolecular linker for the stabilization of the crystal structure as a whole. This type of molecular topology resulted in an unexpectedly high thermal stability.

6.1. Introduction

The directed synthesis of extended structures is a challenge in several fields of chemistry and materials sciences. Of special interest in this field are the polyoxometalates (POMs), since they combine high stability with extensive structural diversity [**50**]. In the syntheses of these types of extended structures, literature reports several design principles. One of these is based on links between isolated large molecular moieties. In this approach organic molecules are used to direct the growth of polyoxometalates. Examples include the use of Keggins, Dawson-Wells POMs and the dimeric $\{Mo_6\}_2$ cluster as the POM-building blocks for these types of structures [**51, 52, 53, 54**]. Another example is the use of the large wheel-shaped molybdenum oxide based POM $\{Mo_{154}\}$ as a building block, which can form a larger framework with the use of urea as a structure directing agent [**55, 56**]. It was shown there that urea can act as linker, holding the larger molybdenum oxide POMs together.

A second design principle based on template-directed self-assembly in hydrothermal synthesis resulted in the creation of a wide range of inorganic-organic hybrid extended structures [**57**] of which some examples contain helices [**58, 59, 60, 61, 62, 63, 64**]. Here the use of polyoxometalates and organic structure-directing agents resulted in the creation of crystal structures containing single and double stranded helices [**53, 64, 65**].

Both design principles mentioned above use POMs as the building units for the extended structures and an organic molecule as the directing agent. However, these syntheses use relatively large POMs which already have their own structural architecture. The use of more simple molybdenum oxide building blocks would allow more freedom in directing and creating extended structures with interesting structural architectures. This work makes use of much smaller and simpler building blocks for the creation of an inorganic extended structure. Moreover, the synthesis of extended structures containing helical characteristics requires high temperatures, high pressure and often several synthesis steps. Here we report of a simple one-pot directed synthesis of an oxomolybdate urea composite in which simple molybdenumoxide building blocks are linked together with the aid of urea leading to the creation of an inorganic-organic hybrid framework consisting of helical units.

6.2. Experimental

Synthesis. 5.0 g of ammonium heptamolybdate (VI) tetrahydrate (Lancaster) was dissolved in 40 mL of Millipore water. To this 4.2 g of urea (cryst. extra pure, Acros) was added together with 30 mL of 1 M HCl solution. The resulting solution was kept at a constant temperature of 20 °C. After one day the large white crystals obtained were filtered and dried under a nitrogen flow. Yield: 4.67 g, 78.7 %, based on Mo content.

Crystal data. $MoO_3(NH_2 - CO - NH_2)$, $CH_4N_2O_4Mo$, M = 204.00 g/mol, monoclinic, space group P2/c, a = 7.57090(11), b = 7.35570(10), c = 12.99040(18) Å, β = 91.6093(12)°, V = 723.141(18) Å^3, Z = 6, ρ_c = 2.811 g/cm^3, μ = 2.64 mm^{-1}, T = 100 K, R_{int} = 0.0644. R_1 = 0.0366 and wR_2 = 0.0943 for 1352 independent reflections with $I > 2\sigma(I)$; R_1 = 0.0414 and wR_2 = 0.0976 for all 1451 independent reflections, 103 refined parameters, GoF = 1.175, max/min = 0.86/-1.00 e/Å^3. The structure contains two independent formulae units (Z' = 2), one in a special and the other in the general position. Therefore, the symmetry has been verified with ADDSYM routine in PLATON [**66**]. No higher metric or crystallographic symmetry has been detected.

A single crystal of about 40 μm in width has been selected from the bulk sample and measured at the Swiss-Norwegian Beam Lines (SNBL) at the European Synchrotron Radiation Facility (ESRF). Diffraction data were collected at 100K using the MAR345 Image Plate detector, at the wavelength 0.72906 Å and the crystal-to-detector distance of 110 mm. 359 frames have been collected with 30 to 60 sec exposure time (fixed dose mode). Diffraction spots were indexed in a monoclinic unit cell, and 9925 diffraction intensities were integrated using CrysAlis software [**67**], and scaled with SADABS [**68**]. The structure was solved and refined using SHELX [**69**], H(N) atoms were modelled in the riding model.

Elemental analysis. C, 5.69 Wt % (found), 5.89 Wt % (calc.); N, 13.2 Wt % (found), 13.7 Wt % (calc.); H, 2.31 Wt % (found), 1.98 Wt % (calc.); Mo, 45 Wt % (found), 47 Wt % (calc.).

Thermo Gravimetric Analysis (TGA). For the TGA 55.316 mg of the material was heated from 293 K to 773 K with a rate of 5.00 K/min, under an oxygen flow of 10.00 mL/min.

Spectroscopic data. IR: ν/cm^{-1} (KBr disk) Characteristic bands: ca. 1405w, ca. 1546(sh), 1128w, ca. 1030w, ca. 956(sh), ca. 914(sh), ca. 895(sh), ca. 770(sh)

N-H	Distance [Å] (N-H)	Distance [Å] (H..A)	Angle N-H-A	Distance [Å] (N..A)	A	Symmetry code for A
N1-H11	0.880	2.294	120.08	2.839	O5	x, y-1, z
N1-H12	0.880	2.158	154.84	2.979	O4	-x+1, -y, -z
N2-H21	0.880	2.413	117.57	2.926	O1	-x+1, -y+1, -z
N2-H22	0.880	2.361	145.97	3.129	O4	-x+1, -y, -z
N3-H31	0.880	2.221	133.46	2.897	O3	-x+2, -y+1, -z
N3-H32	0.880	2.356	151.13	3.155	O2	x, y+1, z
N3-H32	0.880	2.574	127.50	3.187	O4	x, y+1, z

Table 6.1. Hydrogen bonds found in compound **1** and their characteristics. The table lists the different urea -NH_2 groups and the bond lengths measured between the hydrogen atoms and the oxygen atoms of a neighboring helical backbone. A graphical representation of the hydrogen bonds can be found in Figure 6.2

6.3. Results and Discussion

The one-pot synthesis consists of the addition of a 2.5-fold excess of urea with respect to molybdenum to an acidified aqueous solution of $Mo_7O_{24}^{-6}$. After one day this resulted in the precipitation of rod-like single crystals of approximately 0.5 mm in length of $\{MoO_3(NH_2 - CO - NH_2)\}_\infty$ **1** at room temperature. These long rod-like crystals displayed birefringence. In order to ensure a good crystal quality, the synthesis was repeated at a lower concentration of the starting materials. These small (about 40 microns in size) crystals were subsequently characterized by elemental analysis, thermo gravimetric analysis (TGA), IR spectroscopy and single crystal X-ray structure analysis.

These characterizations show that the asymmetric unit of the structure consists of two independent Mo-centered octahedra and two urea units. The carbonyl oxygen of the urea acts as a μ-2-ligand between two molybdenum centres of the two adjacent edge-shared octahedra. The fixation of the metal oxide in the highest oxidation state by urea is quite unique, not only for Mo but for all other metals. A somewhat similar case was found for Dioxoneptunium(VI) chromate(VI) complex with urea, $(NpO_2)(CrO_4)(CO(NH_2)_2)$ [**70**], where the highest oxidation state of Neptunium is stabilized by coordinated urea molecules. In this case, however, urea is coordinated only with one Neptunium atom.

As the molybdenum atoms in the structure **1** are bridged by the urea molecules, helical chains form along the crystallographic *a*-axis (Figure 6.1-A). Each turn in the helix consists of three units of $\{MoO_3(NH_2 - CO - NH_2)\}$ in which the NH_2 groups

of urea point outward, as can be seen in the in-depth view of the helix in Figure 6.1-B. The backbone of the helix contains the two Mo-centered octahedra Mo1 and Mo2 which alternate in the sequence $(\mathrm{Mo1}-\mathrm{Mo2}-\mathrm{Mo2})_\mathrm{n}$. The helical structure of the chain becomes even more evident when only the connections between the carbon atoms of the urea parts are shown (Figure 6.1-C). This clearly illustrates the spiral formed by the urea molecules. In Figure 6.1-A one turn in the helix has been boxed, emphasizing the tweezer-type configuration of the turn in the helix.

The crystal lattice of **1** contains left- and right-handed helices, which are mirror images of each other. The birefringence of the crystal results from the packing of the helices, which align themselves along one crystallographic axis. Figure 6.1 shows the crystal structure of **1** as seen along the three crystallographic axes, the different handedness is represented by two different colors (orange and green). Pseudo -3_1 symmetry of the chain favors efficient packing where the helices can be placed in close proximity to each other. This is particularly evident when the crystal is viewed along the crystallographic *b*-axis. The hydrogen atoms of the alternating urea branches form strong hydrogen bridges with the oxygen atoms of the molybdate backbone, in this way stabilizing the structure as a whole. One hydrogen atom from the urea NH_2 group even forms two hydrogen bonds with two oxygen atoms from the neighboring backbone (for the hydrogen bonds present in **1** and their characteristics see Table 6.1 and Figure 6.2). Urea's part in the formation of the extended structure is thus a dual one. It not only links the molybdenum oxide units into a helix, but also connects the helices to form an extended structure.

The only other example, to our knowledge, of a crystal containing both left- and right-handed single stranded helices of molybdenum oxide is $[NH_3(CH_2)_2NH_3(CH_2)_2NH_3]_2$-$[Mo_9O_{30}]$ (**2**) reported by Xu et al. [**64**]. Their goal was also to use a simple molybdate as a building block for complex extended structures. MoO_4 was used together with an organic polyamine in the hydrothermal synthesis, resulting in a structure made of Mo-based helical chains of linked $\{MoO_6\}$-octahedra, charge compensated by the protonated amine located between the helices. In this way structure **2** differs from structure **1**, as in the former case the organic template is not incorporated into the resulting crystal structure. Moreover, the helices in compound **2** are build up of $[Mo_9O_{30}]^{6-}$ subunits, which are much larger then the simple MoO_6 octahedra that form the backbone in structure **1** by edge sharing. Structure **2**, as stated earlier, was synthesized by a hydrothermal reaction. Hydrothermal reactions often result in formation of phases which are metastable at ambient conditions. Structure **1** on the other hand, was synthesized at room-temperature in a simple one-pot reaction, making it a thermodynamically stable phase at ambient conditions.

In order to determine the thermal stability of the crystal structure we carried out thermo-gravimetrical analysis (TGA). A TGA of **1** was recorded up to a temperature of

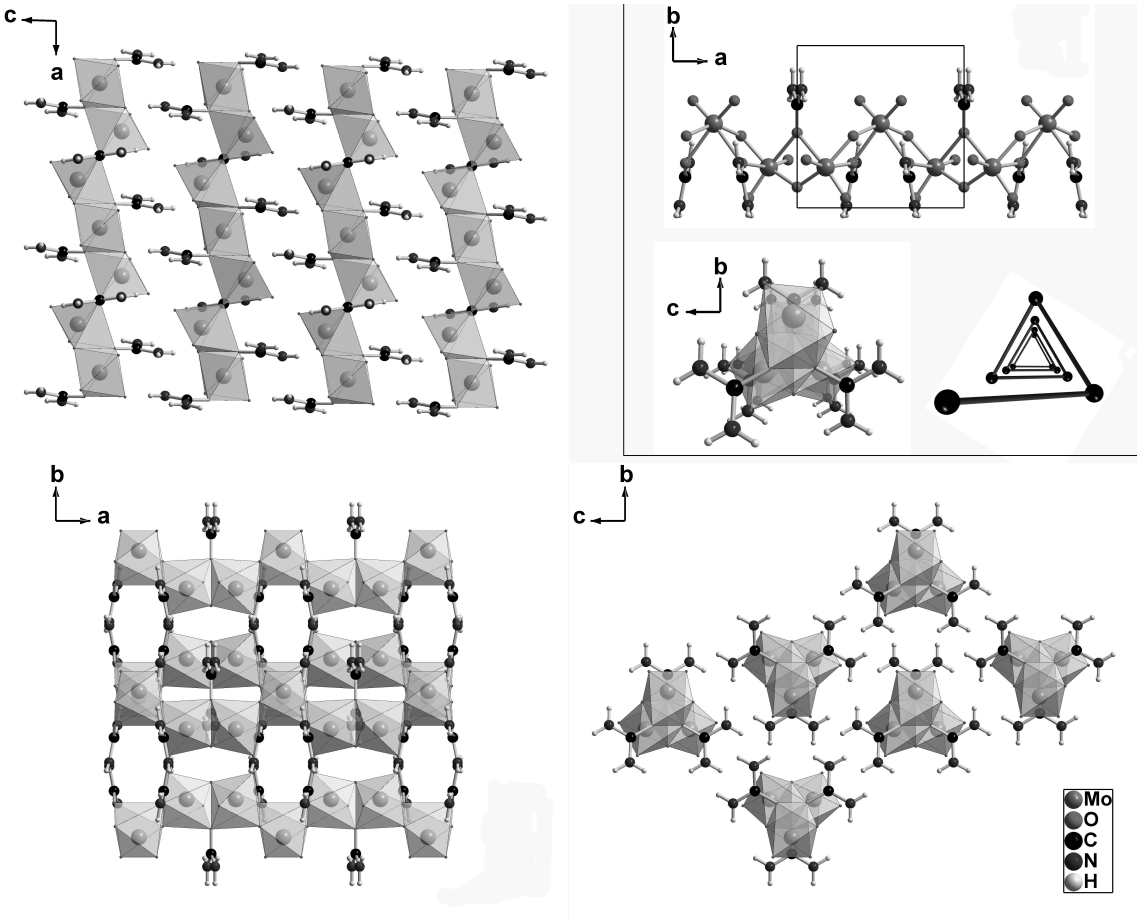

Figure 6.1. Crystal structure of **1** viewed along the three different crystallographic axes. The molybdenum backbone is given in polyhedral representation. The left- and right-handed helices present in the crystal are shown in two colors: green and orange. Inlay: (A) One helical chain with one helical turn boxed along the crystallographic *a*-axis. The turn consists of three $\{MoO_3(NH_2 - CO - NH_2)\}$ units. The tweezer-type configuration of the repetitive building unit together with the hyperconectivity of the oxygen of urea is clearly visible. (B) In-depth view of one helical chain as seen along the crystallographic *a*-axis. (C) In-depth view of one helical chain as seen along the crystallographic *a*-axis, in which only the carbon atoms of the urea molecules have been connected. The spiral emphasizes the helicity of the chain.(For the color version of this picture see the Color figures at the end of this thesis.)

773 K under a constant oxygen flow at a heating rate of 5 degrees per minute. Already at the start of the heating procedure a slight loss of weight was observed. When a temperature of about 500 K was reached, the rate of weight loss increased to the total of 31.2 % at 548 K. This amount is equivalent to the total amount of urea in the structure **1** (Figure 6.3). With the help of IR spectroscopy during heating the change

in the lattice structure was investigated. IR spectra at several stages during heating show that indeed urea is removed from the crystal after reaching a temperature of 548 K (as is indicated by the disappearance of the characteristic urea vibrations at 1548 cm^{-1}, 1128 cm^{-1} and 1030 cm^{-1}) but that the structure stays intact up to this point. However, beyond 548 K other modes appear especially at the lower wavenumbers due to the reduction of the crystal symmetry (Figure 6.3). Solid urea itself decomposes at a temperature of 402 K, which is significantly lower than the temperature at which the crystal of **1** loses its urea. The crystal structure is clearly retained up to 548 K, revealing its unexpectedly high thermal stability which renders it attractive for potential catalytic applications.

6.4. Conclusions

A simple directed material design with urea and an elementary molybdenum oxide as building blocks results in large rod-like single crystals of an inorganic-organic hybrid extended structure consisting of helical units. The structure of **1** has an interesting molecular architecture where urea links the inorganic molybdenum units in a helix and acts as a supramolecular linker for the stabilization of the crystal structure as a whole. In addition, the high thermal stability makes it an attractive agent for various materials science applications. Employing urea-based organic structure-directing agents

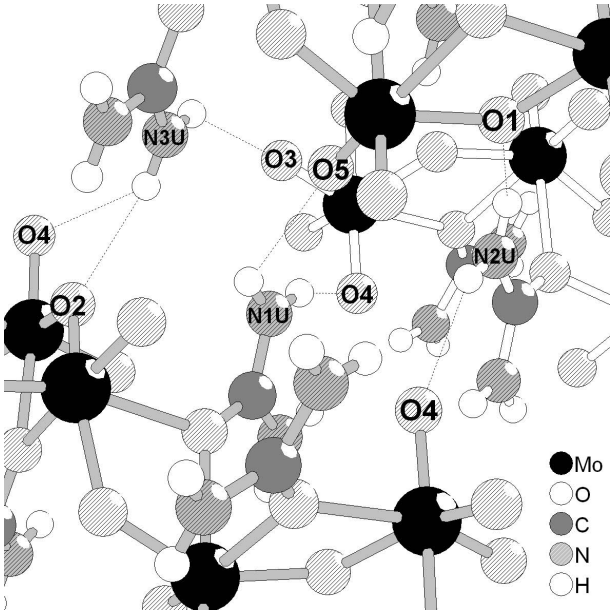

Figure 6.2. Graphical representation of the hydrogen bonds found in **1**. The different urea -NH_2 groups interconnect three helical chains. The atomic labels correspond to the labels given in Table 6.1. The hydrogen bonds are represented by the dotted lines.

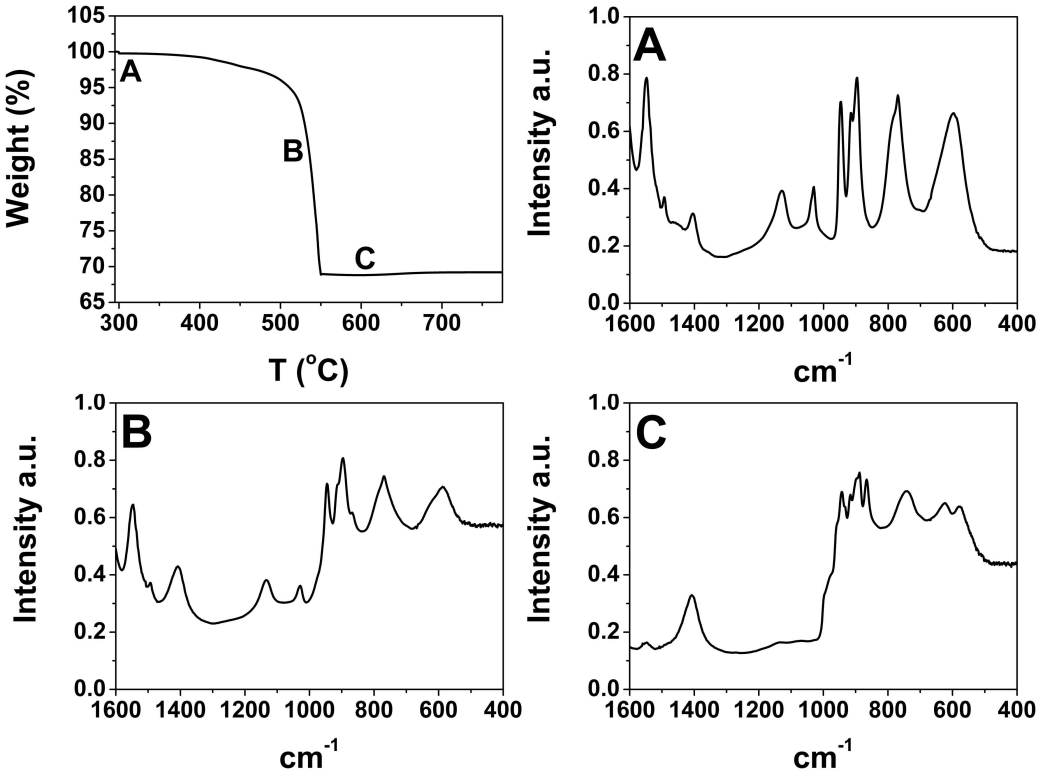

Figure 6.3. TGA of **1** and infrared spectra taken from **1** at (A) 298 K, (B) 538 K and (C) 594 K. The TGA shows a weight drop at 548 K. The disappearance of the characteristic urea vibrations at 1548 cm^{-1}, 1128 cm^{-1} and 1030 cm^{-1} in spectrum (C) shows that urea is removed from the crystal. An increase of the number of peaks in the skeletal region of the spectrum (< 1000 cm^{-1}) suggests a symmetry reduction upon decomposition.

with various alkyl spacers in a simple synthetic route reported here opens a possibility to engineer highly thermo-stable materials with interesting structural architectures.

Acknowledgements

This work was done in collaboration with Dmitry Chernyshov and Yaroslav Filinchuk (SNBL at ESRF, France), Soumyajit Roy, Andrei V. Petukhov and Willem K. Kegel. Essential work on the stability and initial structure characterization was done in collaboration with Tom Visser, Fouad Soulimani, Fred Broersma and Marjan Versluijs-Helder from Inorganic Chemistry and Catalysis at Utrecht University. With this I would also like to acknowledge SNBL for in-house beam time allocation and Vladimir Dmitriev for his kind support of this work.

Bibliography

[1] L. Gmelin. *Gmelin Handbuch der Anorganischen Chemie.* Molybdän. Springer-Verslag, Berlin - Heidelberg - New York, 8th edition, 1935.

[2] T. Liu, A. Diemann, and A. Müller. Hydrophilic inorganic macro-ions in solution: Unprecedented self-assembly emerging from historical blue waters. *J. Chem. Educ.*, 84(3):527, 2007.

[3] J. J. Berzelius. Beitrag zur näheren kenntniss des molybdäns. *Poggend. Ann. Phys. Chem.*, 6:369, 1826.

[4] A. Müller, E. Krickemeyer, J. Meyer, H. Bögge, F. Peters, W. Plass, E. Diemann, S. Dillinger, F. Nonnenbruch, M. Randerath, and C. Menke. $[Mo_{154}(NO)_{14}O_{420}(OH)_{28}(H_2O)_{70}]^{(25\pm5)-}$: A water-soluble big wheel with more than 700 atoms and a relative molecular mass of about 24000. *Angew. Chem. Int. Ed.*, 34:2122, 1995.

[5] A. Müller and C. Serain. Soluble molybdenum blue-"des pudels kern". *Acc. Chem. Res.*, 33:2, 2000.

[6] E. Coronado and C. J. Gómez-García. Polyoxometalate-based molecular materials. *Chem. Rev.*, 98:273–296, 1998.

[7] M. Vazylev, D. Sloboda-Rozner, A. Haimov, G. Maayen, and R. Neumann. Strategies for oxidation catalyzed by polyoxometalates at the interface of homogeneous and heterogeneous catalysis. *Topics in Catalysis*, 34:93–99, 2005.

[8] M. K. Harrup and C. L. Hill. Thermal multi-electron transfer catalysis by polyoxometalates. application to the practical problem of sustained, selective oxidation of hydrogen sulfide to sulfur. *J. Mol. Catalysis A*, 106:57–66, 1996.

[9] J. T. Rhule, C. L. Hill, and D. A. Judd. Polyoxometalates in medicine. *Chem. Rev.*, 98:327–357, 1998.

[10] J. F. Keggin. The structure and formula of 12-phosphotungstic acid. *Proceedings of the Royal Society of London. Series A, Containing Papers of a Mathematical and Physical Character*, 144:75–100, 1934.

[11] A. Müller, A. Diemann, C. Kuhlmann, W. Eimer, C. Serain, T. Tak, A. Knöchel, and P.K. Pranzas. Hierarchic patterning: architectures beyond 'giant molecular wheels'. *Chem. Commun.*, page 1928, 2001.

[12] T. Liu, E. Diemann, H. Li, A.W.M. Dress, and A. Müller. Self-assembly in aqueous solution of wheel-shaped Mo_{154} oxide clusters into vesicles. *Nature*, 426:59–62, 2003.

[13] G. Liu, T. Liu, S.S. Mal, and U. Kortz. Wheels-shaped polyoxotungstate $[Cu_{20}Cl(OH)_{24}(H_2O)_{12}(P_8W_{48}O_{184})]^{25-}$ macroanions from supramolecular "blackberry"structure in aqueous solution. *J. Am. Chem. Soc.*, 128:10103–10110, 2006.

[14] A. Müller, E. Krickemeyer, H. Bögge, M. Schmidtmann, and F. Peters. Organizational forms of matter: An inorganic super fullerene and keplerate based on molybdenum oxide. *Angew. Chem. Int. Ed.*, 37(24):3360–3363, 1998.

[15] J. Kepler. *Mysterium Cosmographicum.* 1569.

[16] T. Liu, B. Imber, E. Diemann, G. Liu, K. Cokleski, H. Li, Z. Chen, and A. Müller. Deprotonation and charges of well-defined $\{Mo_{72}Fe_{30}\}$ nano-acids simply stepwise tuned by ph allow control/variation of related self-assembly processes. *J. Am. Chem. Soc.*, 128:15914–15920, 2006.

[17] W. Helfrich. *Z. Naturforch.*, 28c:693, 1973.

[18] R. J. Hunter. *Foundations of Colloid Science*. Oxford University Press, New York, 2nd edition, 2001.

[19] R. P. Feynman, R. B. Leighton, and M. L. Sands. *The Feynman Lectures on Physics - Commemorative Issue*, volume II. Addison-Wesley, Redwood CA, 1989.

[20] S. Alexander, P. M. Chaikin, P. Grant, G. J. Morales, P. Pincus, and D. Hone. Charge renormalization , osmotic pressure, and bulk modulus of colloidal crystals: Theory. *J. Chem. Phys.*, 80(11):5776–5781, 1984.

[21] S. Bucci and C. Fagotti. Small-angle neutron-scattering study of ionic-nonionic mixed micelles. *Langmuir*, 7:824–826, 1991.

[22] J. C. Crocker and D. G. Grier. When like charges attract: The effects of geometrical confinement on long-range colloidal interactions. *Phys. Rev. Lett.*, 77(9):1897–1900, 1996.

[23] E. Aicart, P. del Burgo, O. Llorca, and E. Junquera. Electrochemical, microscopic, and spectroscopic characterization of prevesicle nanostructures and vesicles on mixed cationic surfactant systems. *Langmuir*, 22:4027–4036, 2006.

[24] F. Bordi, Cametti C., Sennato S., Paoli B., and Marianecci C. Charge renormalization in planar and sperical charged lipidic aqueous interfaces. *J. Phys. Chem. B*, 110:4808–4814, 2006.

[25] J.N. Israelachvili. *Intermolecular and Surface forces*. Academic Press, san Diego, 2nd edition, 1992.

[26] A. Müller, S. Sarkar, S.Q.N. Shah, H. Bögge, M. Schmidtmann, S. Sarkar, P. Kögerler, B. Hauptfleisch, A.X. Trautwein, and V. Schünemann. Archimedian synthesis and magic numbers: "sizing" giant molybdenum-oxide-based molecular spheres of the keplerate type. *Angew. Chem. Int. Ed.*, 38(21):3238–3241, 1999.

[27] A.R. Bausch, M.J. Bowick, A. Cacuito, A.D. Dinsmore, M.F. Hsu, D.R. Nelson, M.G. Nikolaides, A. Travesset, and D.A. Weitz. Grain boundary scars and spherical crystallography. *Science*, 299:1716–1718, 2003.

[28] M.J. Bowick, D.R. Nelson, and A. Travesset. Interacting topological defects on frozen topographies. *Phys. Rev. B*, 62(13):8738–8750, 2000.

[29] G. Liu and T. Liu. Strong attraction among the fully hydrophillic $\{Mo_{72}Fe_{30}\}$ macroanions. *J. Am. Chem. Soc.*, 127:6942–6943, 2005.

[30] I.Lj. Validzic, G. Hooijdonk, S. Oosterhout, and W.K. Kegel. Thermodynamic stability of clusers of molybdenum oxide. *Langmuir*, 20:3435–3440, 2004.

[31] W.K. Kegel and P. van der Schoot. Competing hydrophobic and screened-coulomb interactions in hepatitis b virus capsid assembly. *Biophysical Journal*, 86:3905–3913, 2004.

[32] D. Li, J. Zhang, K. Landskron, and T. Liu. Spontaneous self-assembly of metal-organic cationic nanocages to form monodisperse hollow vesicles in dilute solutions. *J. Am. Chem. Soc.*, 130:4226–4227, 2008.

[33] G. Liu, Y. Cai, and T. Liu. Automatic and subsequent dissolution and precipitation process in inorganic macroionic solutions. *J. Am. Chem. Soc.*, 126:16690–16691, 2004.

[34] G. Liu, M Cons, and T. Liu. The ionic effect on supramolecular associations in polyoxomolybdate solutioin. *J. Mol. Liquids*, 118:27–29, 2005.

[35] A. A. Verhoeff, M. L. Kistler, A. Bhat, J Pigga, J. Groenewold, M. Klokkenburg, S. J. Veen, S. Roy, T. Liu, and W. K. Kegel. Charge regulation as a stabilization mechanism for shell-like assemblies of polyoxometalates. *Phys. Rev. Lett.*, 99:066104, 2007.

[36] S. V. Lyulin, L. J. Evers, P. Van der Schoot, A. A. Darinskii, A. V. Lyulin, and M. A. J. Michels. Efect of solvent quality and electrostatic interactions on size and structure of dendrimers. brownian dynamics simulation and mean-field theory. *Macromolecules*, 37:3049–3063, 2004.

[37] G. Liu and T. Liu. Thermodynamic properties of the unique self-assembly of Mo72Fe30 inorganic macro-ions in salt-free and salt-containing aqueous solutions. *Langmuir*, 21:2713–2720, 2005.

[38] T. Liu. An unusually slow self-assembly if inorganic ions in dilute aqueous solution. *J. Am. Chem. Soc.*, 125:312–313, 2003.

[39] B. Demeler and K. E. van Holde. Sedimentation velocity analysis of highly heterogeneous systems. *Anal. Biochem.*, 335(2):279–288, 2004.

[40] B. Demeler. Ultrascan 9.9; a comprehensive data analysis software package for analytical ultracentrifugation experiments, The University of Texas Health Science Center at San Antonio, Department of Biochemistry.

[41] M. L. Kistler, A. Bhat, G. Liu, D. Casa, and T. Liu. A complete macroion-blackberry assembly-macroion transition with continuously adjustable assembly sizes in $\{mo_{132}\}$ water/acetone systems. *J. Am. Chem. Soc.*, 129:6453–6460, 2007.

[42] A. Müller, S.K. Das, E. Krickemeyer, and C. Kuhlmann. Polyoxomolybdate clusters: giant wheels and balls. In *Inorganic Syntheses*, pages 191–200. 2004.

[43] K. L. Planken. *Analytical Ultracentrifugation of Inorganic Colloids*. PhD thesis, Universiteit Utrecht, 2008.

[44] T. Narayanan. Chapter 5: Synchrotron small-angle x-ray scattering. In *Soft Matter: Scattering, Imaging, and Manipulation*.

[45] O. Glatter and O. Kratky. *Small Angle X-ray Scattering*. Academic Press, San Diego, San Francisco, New York, Boston, London, Sydney, Tokyo, 1982.

[46] S. Zhou, C. Burger, B. Chu, M. Sawamura, N. Nagahama, M. Toganoh, U. E. Hackler, H. Isobe, and E. Nakamura. Spherical bilayer vesicles of fullerene-based surfactants in water: A laser light scattering study. *Science*, 291:1944–1947, 2001.

[47] J.K.G. Dhont. Chapter 3, light scattering. In D. Mbius and R. Miller, editors, *An Introduction to Dynamics of Colloids*. Elsevier, 1996.

[48] J. Lyklema. volume IV of *Fundamentals of Interface and Colloid Science*. Academic Press, San Diego, San Francisco, New York, Boston, London, Sydney, Tokyo, 2000.

[49] H Cölfen and S Mann. Higher-order organization by mesoscale self-assembly and transformation of hybrid nanostructures. *Angew. Chem. Int. Ed.*, 42:2350–2365, 2003.

[50] M.T. Pope. *Heteropoly and Isopoly Oxometalates*. Springer-Verlag, New York, Tokyo, Berlin, Heidelberg, 1983.

[51] C.L. Hill, T.M. Anderson, and X. Fang. Enantiomerically pure polytungstates: Chirality transfer through zirconium coordination centers to nanosized inorganic clusters. *Angew. Chem. Int. Ed.*, 44:3540 3544, 2005.

[52] M.T. Pope, M.H. Dickman, and M. Sadakane. Chiral polyoxotungstates. 1. stereoselective interaction of amino acids with enantiomers of $[Ce^{III}(\alpha_1 - P_2W_{17}O_{61})(H_2O)_x]^{7-}$. the structure of $DL - [Ce_2(H_2O)_8(P_2W_{17}O_{61})_2]^{14-}$. *Inorg. Chem.*, 40:2715–2719, 2001.

[53] H.Y. An, E.B. Wang, D.R. Xiao, Y.G. Li, Z.M. Su, and L. Xu. Chiral 3d architectures with helical channels constructed from polyoxometalate clusters and copperamino acid complexes. *Angew. Chem. Int. Ed.*, 45:904 908, 2006.

[54] C. Streb, D.L. Long, and L. Cronin. Engeneering porosity in a chiral heteropolyoxometalate-based framework: the supramolecular effect of benzenetricarboxylic acid. *Chem. Commun.*, pages 471–473, 2007.

[55] A. Müller, S. Roy, M. Schmidtmann, and H. Bögge. Urea as 'deus ex machina' in giant molybdenum blue type cluster synthesis: an unusual hybrid compound with perspectives for related nano, supramolecular and extended structures. *Chem. Commun.*, pages 2000–2002, 2002.

[56] S. Roy. *Giant polyoxomolybdates: Syntheses, structure and stability studies.* Phd-thesis, University of Bielefeld, 2005.

[57] P. J. Hagrman, D. Hagrman, and J. Zubieta. Organic-inorganic hybrid materials: From "simple" coordination polymers to organodiamine-templated molybdenum oxides. *Angew. Chem., Int. Ed.*, 38:2638–2684, 1999.

[58] V. Soghomonian, Q. Chen, R. C. Haushalter, J. Zubieta, and C. J. O'Conner. An inorganic double helix: Hydrothermal synthesis, structure, and magnetism of chiral $[(CH_3)_2NH_2]K_4[V_{10}O_{10}(H_2O)_2(OH)_4(PO_4)_7] * 4H_2O$. *Science*, 259:1596–1599, 1993.

[59] T. E. Gier, X. Bu, P. Feng, and G. D. Stucky. Synthesis and organization of zeolite-likematerials with three-dimensional helical pores. *Nature*, 395:154–157, 1998.

[60] S. Neeraj, S. Natarajan, and C.N.R. Rao. A novel open-framework zinc phosphate with intersecting helical channels. *Chem. Commun.*, pages 165–166, 1999.

[61] A. Yilmaz, X. Bu, M. Kizilyalli, and G. D. Stucky. $Fe(H_2O)_2BP_2O_8 * H_2O$, a first zeotype ferriborophosphate with chiral tetrahedral framework topology. *Chem. Mater.*, 12:3243–3245, 2000.

[62] J. Liang, Y. Wang, J. Yu, Y. Li, and R. Xu. Synthesis and structure of a new layered zinc phosphite $(C_5H_6N_2)Zn(HPO_3)$ containing helical chains. *Chem. Commun.*, pages 882–883, 2003.

[63] Y. Wang, J. Yu, M. Guo, and R. Xu. $[Zn_2(HPO_4)_4Co(dien)_2] * H_3O$: A zinc phosphate with multidirectional intersecting helical channels. *Angew. Chem. Int. Ed.*, 42:4089, 2003.

[64] L. Xu, C. Qin, X. Wang, Y. Wei, and E. Wang. Hydrothermal synthesis and structure of a new helical chain constructed from only molybdenum-oxide building blocks. *Inorg. Chem.*, 42:7342–7344, 2003.

[65] D. Xiao, H. An, E. Wang, and L. Xu. Syntheses and structures of two novel inorganicorganic hybrid octamolybdates: $[H_2enMe]_2[Mo_8O_{26}] * 2H_2O$ and $[Ni(2,2' - bpy)_3]_2[\delta - Mo_8O_{26}]$. *J. Mol. Struct.*, 738:217–225, 2005.

[66] A.L. Spek. Platon, 2006.

[67] OxfordDiffraction. Crysalis software package, 2006.

[68] G.M. Sheldrick. Shelxs97 and shelxl97 software package, 1997.

[69] G.M. Sheldrick. Sadabs software package, 1997.

[70] G.B. Andreev, M.Y. Antipin, A.M. Fedoseev, and N.A. Budantseva. Synthesis and crystal structure of bis(carbamide)chromatoneptunyl $NpO_2CrO_4 * 2[OC(NH_2)_2]$. *Kristallografiya*, 46:433–434, 2001.

Summary

This thesis deals with assemblies of polyoxometalates. Polyoxometalates, or POMs for short, come in a variety of shapes and sizes. Some of them are among the largest inorganic molecules known today. These molecules can be highly symmetrical and, as the name already implies, consist of (mainly) metal (molybdenum, tungsten, vanadium, iron, etc) and oxygen atoms in the form of metal oxide polyhedrons. The POMs that are in the center of this thesis are mostly polyoxomolybdates, meaning that the metal is mostly molybdenum.

The first part of this thesis addresses assemblies of a subclass of POMs known as Keplerates. Keplerates are highly symmetric, hollow, spherically shaped POMs. They consist of 12 five-fold building blocks or pentagons which are linked together to form a sphere in much the same way as a soccer ball. In solution these POMs spontaneously form large, hollow, spherical superstructures or POM-shells with an average radius in water of several tens of nanometers, composed of a monolayer of more than 1000 of individual POMs. In the first chapters an attempt is made to understand this curious phenomenon: In Chapter 2 it is shown that the equilibrium size of POM-shells of Keplerate type POMs is inversely proportional to the relative dielectric constant of the medium in which they are dispersed. This behavior is in line with predictions made by a stabilization mechanism based on Coulomb repulsion combined with charge regulation. The cohesive energy per bond between the POMs on the shells is estimated to be approximately -6 kT. This number is extracted from analysis based on a charge regulation model in combination with a model for defects on a sphere. This value is in agreement with the bond energy as determined by the model-independent critical aggregation concentration. Furthermore it is shown that there is a negligible difference in interaction energy of a POM in a POM-shell and a POM in the solid state.

The charge regulation model can also be used to explain a new structural instability of POM-shells. In Chapter 3 it is shown that besides the colloidal instability, i.e. the formation of aggregates that consist of many shells, these systems also display an instability on a structural scale within the shell-like assemblies. This instability occurs at significantly lower ionic strength than the colloidal stability limit and only becomes evident after a relatively long time. For the polyoxometalate abbreviated as $\{Mo_{72}Fe_{30}\}$ it is shown that the structural stability limit of POM-shells lies between a NaCl concentration of 1.00 mM and 5.00 mM in aqueous solution.

Not only the ionic strength influences the properties of POM-shells in solution. It has been claimed that the number of charges on the POMs themselves plays an important roll in their formation and stabilization as well. Due to the weak acid nature of single POMs of the Keplerate type $\{Mo_{72}Fe_{30}\}$, the charge on these POMs can easily be varied by changing the pH of the aqueous solutions in which they are dispersed. The effect of pH on the interaction energy between the single POMs in the POM-shell was investigated by measuring the Critical Aggregation Concentration (CAC). The results show that the interaction energy becomes stronger when the pH of the solution increases. Increasing pH in turn, increases the charge density on the POMs. Measurements of the pH of aqueous solutions of $\{Mo_{72}Fe_{30}\}$ in time however, revealed an abundant release of additional protons. It is still an open question as to why this occurs and therefore the effect on the charge of the single POMs and the POM-shells in solution remains unclear. It is therefore not possible at this point, to relate the change in interaction energy directly to a change in charge on the POMs.

Up till now the POM-shells have been considered thermodynamically stable. Experimental evidence presented in Chapter 5 challenges this view. It is shown that POM-shells change over time and that the preparation route of solutions of POMs affects the resulting species in solution. Moreover, in concentrated samples, a transition from spherical objects to elongated agglomerates was observed. The elongated objects subsequently grow into large, crystalline, needle-like structures. From these observations we conclude that POMs follow an unusual nucleation route in which the POM-shells are in fact metastable intermediates.

In the second part of this thesis, the term assembly is taken a step further. Here polyoxomolybdates are used in order to create extended structures. Chapter 6 reports of a simple one-pot directed synthesis of an oxomolybdate urea composite in which elementary molybdenum oxide building blocks are linked together with the aid of urea. This type of directed material design resulted in large rod-like crystals of an inorganic-organic hybrid extended structure consisting of right- and left-handed helical units. In the crystal structure urea acts both as glue that links the inorganic molybdenum units into a helix, as well as a supramolecular linker for the stabilization of the crystal structure as a whole. This type of molecular topology resulted in an unexpectedly high thermal stability.

Samenvatting voor Iedereen

Wat zijn Polyoxometalaten?

Polyoxometalaten, afgekort als POMs, zijn anorganische moleculen die voornamelijk bestaan uit metaal- (molybdeen, wolfraam, vanadium, ijzer enzovoorts) en zuurstofatomen. Deze moleculen worden opgebouwd uit polyhedra: een enkel metaalatoom omgeven door zuurstofatomen (zie Figuur 1). Het voorvoegsel "poly-"geeft aan dat zo'n molecuul een veelvoud van deze polyhedra kan bevatten. Deze moleculen zijn er dan ook in diverse maten en vormen. Van bolvormig tot wielvormig, van lange ketens tot aan deeltjes waarvan de vorm het beste beschreven kan worden als lijkende op een citroen.

Kepleraten

In het eerste deel van het proefschrift staat een speciaal soort POM centraal, namelijk de Kepleraten. Kepleraten zijn zeer symmetrische, holle, bolvormige POMs. Ze zijn opgebouwd uit 12 vijfvlakken die verbonden zijn tot een bol op eenzelfde manier als wel te zien is in een voetbal. Op de kaft van dit proefschrift staat een model van zo'n deeltje. In oplossing organiseren deze POMs zich spontaan tot grotere superstructuren die er uitzien als holle bollen en die zijn opgebouwd uit een enkele schil van meer dan 1000 van deze deeltjes.

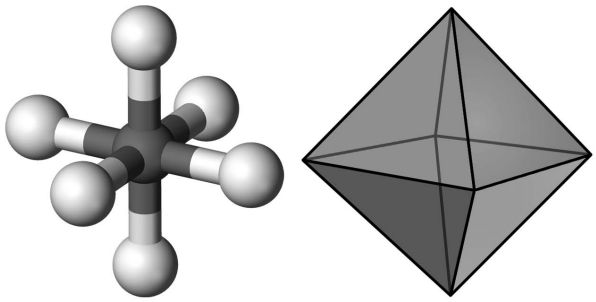

Figuur 1. Polyhedra: In de structuur links worden de atomen weergegeven door bollen. De middelste donkere bol is het metaalatoom en de witte bollen die er aan verbonden zijn geven de zuurstofatomen weer. Een andere manier van weergeven van deze structuren is door niet de bindingen tussen de atomen weer te geven, maar denkbeeldige lijnen te trekken tussen de zuurstofatomen. Het resultaat hiervan is een polyhedron en is te zien in de rechter figuur.

Dat moleculen spontaan grotere structuren kunnen vormen is niet nieuw. Een veel voorkomend voorbeeld is het ontstaan van structuren van zeep. Zeepmoleculen hebben een kop die graag in contact wil zijn met water (hydrofiel) en een staart die dat absoluut niet wil (hydrofoob). In water zullen zeepmoleculen dan ook de staarten bij elkaar steken om zoveel mogelijk het contact met water te vermijden terwijl de koppen zich naar het water toekeren. De op deze manier gevormde superstructuren heten micellen. Het ontstaan van deze superstructuren komt doordat zeep twee verschillende kanten heeft met ieder een eigen voorkeur. Het bijzondere aan de POMs is dat deze moleculen dat juist niet hebben. Ze zijn perfect symmetrisch en zijn volledig hydrofiel waardoor ze goed oplossen in water. Toch vormen ze ook grote holle superstructuren (zie Figuur 2).

Superstructuren van Kepleraten

De vraag die dan ook centraal staat in het eerste deel van dit proefschrift is waarom de POMs grote superstructuren vormen. Wat tot nu toe bekend is van deze deeltjes is dat ze geladen zijn in oplossing. Naast een aantrekkende kracht die voelbaar wordt als de POMs dicht bij elkaar komen, stoten deze deeltjes elkaar hierdoor ook over lange afstand af. Om dicht genoeg bij elkaar te kunnen komen om aan elkaar te plakken moeten de POMs daarom eerst de afstotende kracht overwinnen. Omdat deze erg sterk is, duurt het erg lang voordat de structuren in oplossing gevormd worden. Welke kracht of binding nu echt voor de aantrekking zorgt is nog niet bekend. Daarom kan de vraag 'waarom' ook nog niet beantwoord worden.

Wat we wel kunnen doen is, uitgaande van het feit dat de structuren nu eenmaal bestaan, voorspellen hoe groot deze structuren worden als de POMs worden opgelost in verschillende oplosmiddelen. Daar gaat Hoofdstuk 2 over. Daarin wordt een theorie beschreven die voorspelt dat de bolvormige superstructuren groter worden, naarmate het oplosmiddel een lagere diëlectrische constante heeft. De diëlectrische constante van een oplosmiddel beschrijft het effect dat het oplosmiddel heeft op de sterkte van interacties tussen ladingen in de oplossing. Daarbij geldt dat oplosmiddelen met een lagere diëlectrische constante zorgen voor een minder sterke interactie.

Experimenteel is vast gesteld dat deze voorspelling ook klopt voor twee soorten Kepleraten namelijk twee POMs afgekort met de formule $\{Mo_{72}Fe_{30}\}$ en $\{Mo_{132}\}$. Als we verder aannemen dat de enkele POMs in een specifiek patroon in de schil geordend zijn, kunnen we ook iets zeggen over de sterkte van de interacties tussen de POMs. De sterkte van deze interactie blijkt vergelijkbaar te zijn met wat ook gemeten wordt tussen moleculen in superstructuren van zeep die eerder al genoemd werden. Het heeft ook dezelfde orde grootte als waterstofbruggen die gevormd kunnen worden tussen de zuurstof- en de waterstofatomen in het molecuul.

De invloed van lading

Door middel van de theorie uit Hoofdstuk 2 kunnen we ook laten zien dat de holle superstructuren structureel niet meer stabiel zijn als de zoutconcentratie in waterige oplossingen te hoog wordt. De afstand waarover ladingen elkaar kunnen voelen wordt o.a. bepaald door de hoeveelheid ionen in de oplossing. Als er veel ionen in de oplossing zitten dan kunnen deze de lading op de POMs afschermen waardoor individuele POMs dichter bij elkaar kunnen komen zonder dat ze elkaar afstoten. Vanuit de theorie kunnen we afleiden dat de superstructuren structureel stabiel blijven zolang de afstand waarover ladingen afgeschermd worden (de Debye-lengte) even groot of groter is dan de straal van de superstructuur. Deze stelling is ook experimenteel bewezen, door zout toe te voegen aan waterige oplossingen van de POMs afgekort als $\{Mo_{72}Fe_{30}\}$. Het punt waarop na 15 weken er geen superstructuren meer aanwezig waren bleek overeen te komen met wat er door de theorie voorspeld was.

De POM afgekort als $\{Mo_{72}Fe_{30}\}$ heeft ook de eigenschap dat de hoeveelheid lading op het oppervlak van deze deeltjes beïnvloed kan worden door de zuurgraad van de oplossing. De hoeveelheid lading op de POMs wordt namelijk groter naarmate de oplossing minder zuur is. In Hoofdstuk 4 wordt gekeken wat de invloed van de zuurgraad is op de sterkte van de interacties tussen de POMs in de superstructuren. Experimenten wijzen uit dat de aantrekking sterker wordt als de oplossing minder zuur is en dus de lading op de deeltjes groter is. De metingen laten echter ook zien dat de zuurgraad van de oplossing aanzienlijk verandert in de loop van de tijd. Het is nog onduidelijk wat hier de oorzaak van is. Het is daardoor ook onduidelijk wat het precieze effect van de verandering in zuurgraad zal zijn op de enkele deeltjes en de superstructuren in oplossing. Daarom is het niet mogelijk de verandering in de interactiesterkte direct te koppelen aan een verandering van de lading op de enkele POMs in oplossing.

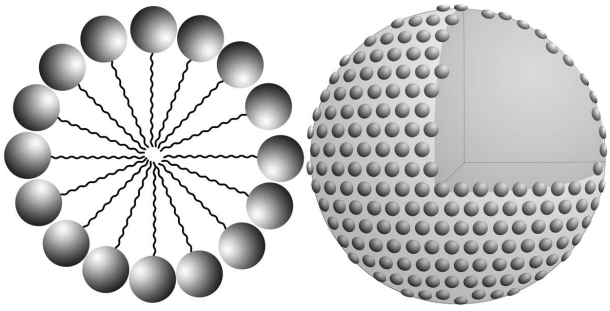

Figuur 2. Superstructuren: Zeepmoleculen kunnen in water micellen (links) vormen. Hun hydrofobe staarten groeperen bij elkaar om zoveel mogelijk het contact met water te vermijden, terwijl de hydrofiele koppen van de moleculen naar het water toe keren. POMs hebben dit tweeledige karakter niet, ze zijn volledig hydrofiel. Toch vormen ook zij holle, bolvormige superstructuren in water (rechts).

SUPERSTRUCTUREN ALS ONDERDEEL VAN KRISTALLISATIE

Omdat de holle superstructuren van de POMs erg lang in oplossing blijven bestaan, werd er altijd aangenomen dat dit de meest stabiele vorm is die de POMs kunnen aannemen. Dit zou betekenen dat het niet uit zou mogen maken hoe je de oplossingen maakt. Zolang ze dezelfde concentratie aan bestanddelen hebben en bij dezelfde temperatuur en druk bewaard zouden worden dan zouden er altijd precies dezelfde superstructuren in oplossing moeten zitten. In Hoofdstuk 5 laten we echter zien dat dit niet het geval is. De superstructuren kunnen maanden tot aan jaren in oplossing blijven. Op het eerste gezicht lijkt er niets te veranderen, maar als er goed gekeken wordt dan blijkt dat na drie jaar de superstructuren ineens twee keer zo zwaar zijn. Verder blijkt ook dat als oplossingen van deze deeltjes op verschillende manieren bereid worden, de superstructuren in oplossing niet hetzelfde zijn. Ook al is de concentratie gelijk en zijn de monsters even oud.

Vaak worden de superstructuren bestudeerd in oplossingen met een lage concentratie die gemaakt worden door direct de juiste hoeveelheid vaste stof op te lossen in water. Als de concentratie tien of honderd keer zo hoog wordt in oplossingen die gemaakt worden door een zeer hoog geconcentreerd monster te verdunnen, dan zien we dat er langwerpige superstructuren gevormd worden in plaats van bolvormige. Deze langwerpige superstructuren blijven groeien en vormen uiteindelijk naald-achtige kristallen. Ook werd gezien dat in een monster waarin eerst bolvormige superstructuren zaten, er langzaamaan ook langwerpige superstructuren ontstonden. Deze resultaten laten zien dat de superstructuren niet de meest stabiele vorm van de POMs zijn, maar dat ze een tussenfase zijn in een kristallisatie proces waarbij uiteindelijk naaldvormige kristallen worden gevormd.

ORGANISATIE VAN POLYOXOMOLYBDATEN

In het tweede deel van het proefschrift doen we een klein stapje terug. We nemen bouwstenen die veel simpeler zijn dan de deeltjes die hierboven beschreven staan. We nemen in feite maar één polyhedron en plakken deze aan elkaar met ureum. Ureum is een molecuul bestaande uit koolstof, stikstof, waterstof en zuurstof. Dit platte molecuul heeft als het ware drie armen. Eén van deze armen bevat een zuurstofatoom en de andere twee stikstof- met elk twee waterstofatomen. Als we deze twee simpele bouwstenen bij elkaar voegen in zure waterige oplossing vormen zich spontaan kristallen, opgebouwd uit lange ketens van polyhedra aan elkaar gelinkt door middel van de ureum. Dit gebeurt op een speciale manier. De in deze synthese gebruikte polyhedra bestaan uit molybdeen die omgeven is door zuurstof. In het kristal is één van de zuurstofatomen die het metaal omgeeft afkomstig van het ureum. Dit zuurstofatoom is in deze vorm verbonden met niet één maar twee molybdeen centra. Op deze manier plakt het de polyhedra aan elkaar

tot lange spiraalvormige ketens oftewel helixen. Deze ketens worden onderling bij elkaar gehouden door de twee andere armen van het ureum. De twee stikstofuiteinden kunnen met hun waterstofatomen zogenoemde waterstofbruggen vormen met de zuurstofatomen van aangrenzende helixen. Op deze manier weven de ketens zich samen tot een kristal. Het kristal is erg stabiel en kan tot hoge temperaturen verhit worden zonder dat het uit elkaar valt. Dit is belangrijk voor mogelijke toepassingen van het materiaal in bijvoorbeeld de katalyse. Een katalysator kan reacties versnellen zonder dat het daarbij verbruikt wordt. Dit soort reacties vinden vaak plaats bij hoge temperaturen.

Wat ook zeer speciaal is aan deze manier van synthetiseren is dat er moleculen zijn die erg veel op ureum lijken: met drie armen waarvan er één zuurstof heeft en twee stikstof- met elk twee waterstofatomen. De lengte van de armen en bijvoorbeeld de flexibiliteit kunnen per molecuul variëren, maar doordat ze wel in staat zijn de polyhedra aan elkaar te linken kunnen ze zo mogelijk verschillende structuren en kristallen vormen. Andere structuren zouden dan weer andere soorten reacties kunnen versnellen in katalyse.

Color figures

- **Schematic representations of the polyoxometalate (POM)** $\{Mo_{72}Fe_{30}\}$

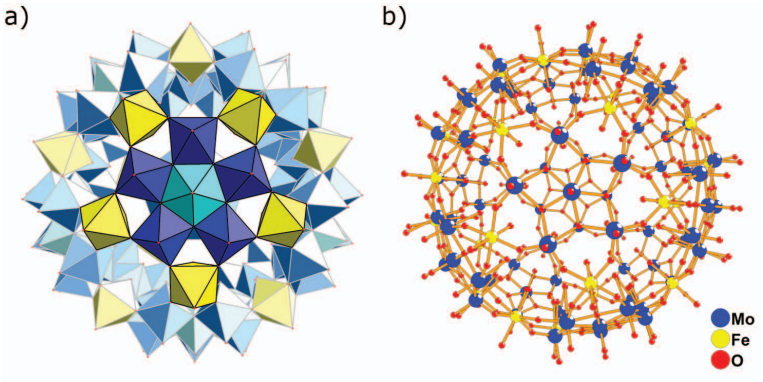

- **Figure 5.2: SAXS (a) data and DLS (b) measurements.**

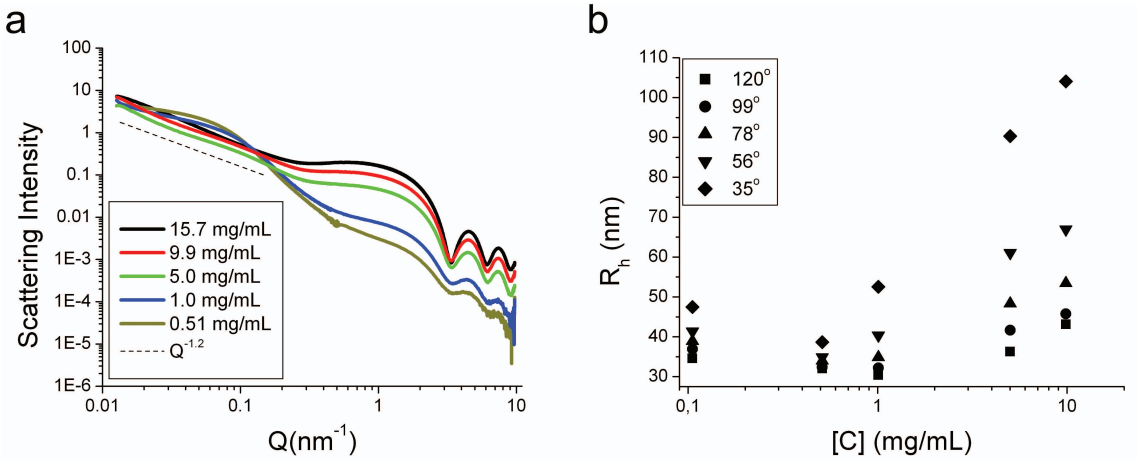

- **Figure 5.3: Cryogenic Transmission Electron Microscopy (Cryo-TEM) pictures of the needle-like structures.**

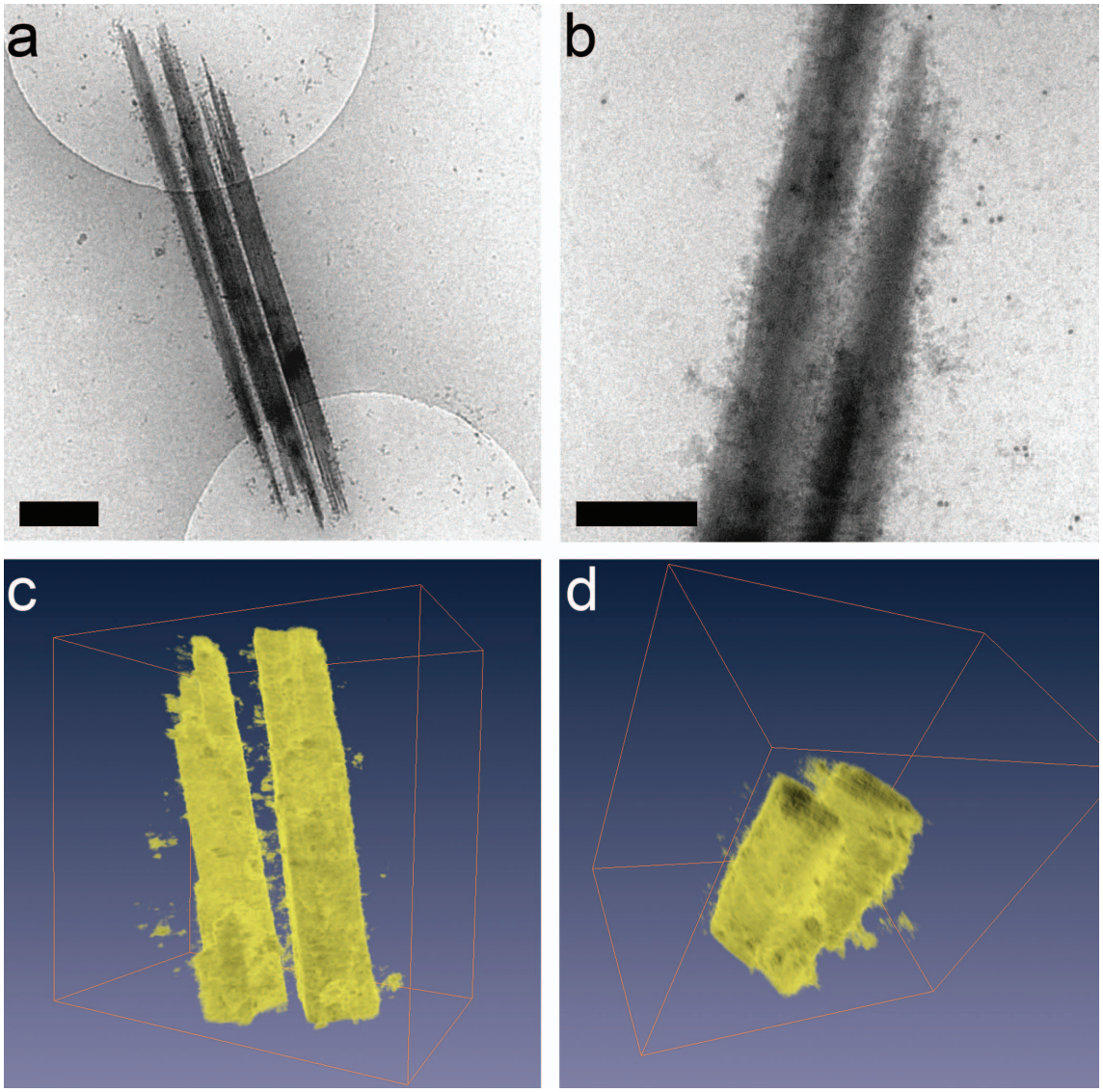

Acknowledgements

"It was the best of times, it was the worst of times.... "
From "A Tale of Two Cities"
Charles Dickens

During a PhD one not only learns how to do research, but besides one's self one also gets to know many people. In the last four years many individuals crossed my path and walked along it for a shorter or longer while. The person who started me on this path in the first place is of course my supervisor Willem Kegel. After mentioning to Bonny Kuipers that I wanted to do a PhD at the Van 't Hoff Laboratory, I suddenly received an e-mail that you might have a position available. As soon as I read the Vici proposal I immediately got excited about the project. So as they say in Dutch: "Willem, je wordt bedankt". But seriously, I thank you for giving me this opportunity and the many lessons learned. I also would like to extend my thanks to Marianne, your kind character and uplifting words meant a lot to me.

And then there are of course my two lovely paranimfs Esther (van den Pol) and Daniela (Kraft). Thank you for listening to me rattle on and on at times when I would walk into your offices and would start blabbing my frustrations. I can't think of any other two people that I would have wanted to have by my side as my backup during my defense. Thanks for your support and for the fun in the lab and during shopping.

During my four years as a PhD student, I had the privilege of residing in an office with a legendary history and reputation. I would like to thank my roommates in past and present: Soumyajit, Karel, Dima and Dzina for making my stay there not only educational but also an interesting one.

Every Friday afternoon we would have a brainstorm session in Willem's office. Up until the point that his group got too big to fit in there. I have always enjoyed these brainstorm sessions because you would always learn something new and see the exciting results of projects done by other people. In this respect I would also like to extend my thanks to Tian Hui Zhang, Raja Mani, Jan Groenewold (thanks for signing the cookbooks, too) and all the students that shared their knowledge and results during these sessions.

The Van 't Hoff Laboratory for Physical and Colloid Chemistry was and still is a great place to work. With kind and helpful colleagues and an organized and clean lab. In general I would like to thank all the people from the lab for making me feel at home. I would like to thank Bonny Kuipers and Emile (Eb) Bakelaar for their help and skillful

knowledge. Dominique Thies-Weesie I would like to thank for ensuring that everyone keeps the lab clean and organized and for many helpful discussions when we were both trying to figure out AUC. I would also like to thank Andrei Petukhov for introducing me into the world of SAXS and Kees de Kruif for his interest in the "Pommetjes horlepiep". During my stay in the lab there were of course many enthusiastic other PhD-students that started and finished their work. Thanks to all for all the good times. Of them Lia Verhoeff also did her master project at FCC which was the first work on POMs done is this lab. I would like to thank her for the work and exchange of experience which helped me to start up my project. Maurice (Mourad), thank you for extending your deadline for a while so that we could defend on the same day. Figuring things out together is much less stressful.

Part of the research could not have been done without the help of people from other groups. I am very grateful for the help from Tom Visser, Fouad Soulimani, Marjan Versluijs, Fred Broersma and Bert Weckhuysen from Inorganic Chemistry and Catalysis for helping me out with a large part of the inorganic chemistry that one comes in contact with through the POMs. I would also like to extend my gratitude to Hans Meeldijk for his help and patience with the TEM. I would also like to thank our collaborators outside of Utrecht University namely: Vladimir Dmitriev, Dimitri Chernyshov, Yaroslav Filinchuk (SNBL) and Theyencheri Narayanan (ID02) from the ESRF in France; Peter Frederik, Nico Sommerdijk and Fabio Nudelman (Eindhoven University of Technology) for their enthusiasm and the wonderful work on Cryo-TEM; Gijs Wuite and Wouter Roos (Vrije Universiteit Amsterdam) for using their incredible AFM. I would also like to thank prof. Tianbo Liu for giving me the opportunity to visit his lab and prof. Achim Müller for many helpfull discussions.

During a PhD it is expected that PhD-students help out with teaching. It is because of this that I met several enthusiastic students to help me with my research: Marieke, Lydia, Jeroen, Thijs, Nitesh, Daan en Sander. Thank you for a lot of fun. Nina, as a master student of Willem we had a lot of nice and helpful discussions. And of course all the other master and bachelor students with whom I spend some good evenings full of gaming.

Promoveren vergt veel tijd en aandacht. Daardoor wil je nog wel eens vergeten dat je buiten je werk ook nog bestaat. Gelukkig zijn er daar dan de mensen van KoH die me er aan hielpen herinneren dat er belangrijkere dingen in het leven zijn. Mensen: For the KoH! Pap, mam, bedankt dat jullie me altijd gesteund hebben in alles wat ik deed. Sven, mijn kleine broertje die al lang niet zo klein meer is. Marcel, je kent me beter dan ik mezelf ken, bedankt dat je me altijd weer tot de orde wist te roepen als ik me weer eens veel te veel liep druk te maken, bedankt voor je geduld en je steun, mijn lieverd.

List of publications

This thesis is based on the following publications:

- Alletta A. Verhoeff, Melissa L. Kistler, Joe Pigga, Jan Groenewold, Mark Klokkenburg, Sandra J. Veen, Soumyajit Roy, Tianbo Liu and Willem K. Kegel, *Charge Regulation as a Stabilization Mechanism for Shell-Like Assemblies of Polyoxometalates*, Physical Review Letters, 99(6), 066104 (2007). (Chapter 2)
- Sandra J. Veen, Soumyajit Roy, Yaroslav Filinchuk, Dmitry Chernyshov, Andrei V. Petukhov, Marjan Versluijs-Helder, Alfred Broersma, Fouad Soulimani, Tom Visser and Willem K. Kegel, *Extended Structure Design with Simple Molybdenum Oxide Building Blocks and Urea as a Directing Agent*, Inorganic Chemistry, 47, 6863-6866 (2008). (Chapter 7)
- Sandra J. Veen and Willem K. Kegel, *Structural Instability of Shell-like Assemblies of a Keplerate Type Polyoxometalate Induced by Ionic Strength*, submitted. (Chapter 3)
- Sandra J. Veen, Dmytro Byelov, Andrei V. Petukhov, Theyencheri Narayanan, Fabio Nudelmann, Nico Sommerdijk and Willem K. Kegel, *Shape Transformation in Solutions of a Keplerate Type Polyoxometalate: From Shells to Needles*, to be submitted. (Chapter 5)

Other papers by the author:

- Lambert K. van Vugt, Sandra J. Veen, Erik P. A. M. Bakkers, Aarnoud L. Roest, and Danil Vanmaekelbergh, *Increase of the Photoluminescence Intensity of InP Nanowires by Photoassisted Surface Passivation*, J. Am. Chem. Soc., 127, 12357-12362 (2005).
- Cornelis A. van Walree, Veronica E. M. Kaats-Richters, Sandra J. Veen, Birgit Wieczorek, Johanna H. van der Wiel, and Bas C. van der Wiel, C*harge-Transfer Interactions in 4-Donor 4'-Acceptor Substituted 1,1-Diphenylethenes*, Eur. J. Org. Chem., 3046-3056 (2004).
- Hana Robson Marsden, Alexander V. Korobko, Ellen N. M. van Leeuwen, Emilie M. Pouget, Sandra J. Veen, Nico A. J. M. Sommerdijk and Alexander Kros, *Noncovalent Triblock Copolymers Based on a Coiled-Coil Peptide Motif*, J. Am. Chem. Soc., 130(29), 9386-9393 (2008).

Curriculum Vitae

Sandra Joyce Veen was born on the 2^{nd} of October, 1981 in Vianen, The Netherlands. In 1999 she graduated from the Christelijke Scholengemeenschap Oosterlicht College in Nieuwegein. From 1999 until 2005 she studied Chemistry at Utrecht University. During the college year of 2001-2002 she was a member of the Utrecht Chemistry Student Association Proton in which she held the position of Secretary. As part of the Master Chemistry and Physics, she performed her master research at the group of Condensed Matter and Interfaces under supervision of Drs. L. K. van Vught and Prof. dr. Daniel A. M. Vanmaekelbergh on Indium Phosphide Nanowires: Single wire Luminescence and Photoetching. Also as part of her masters she performed a short research project at Akzo Nobel Coatings Research in Arnhem under supervision of Dr. Bart Reuvers and Dr. Willem K. Kegel on the Film Formation of Waterborn Paints. In 2005 she graduated with distinction as a Master of Science at Utrecht University. In the same year she started a PhD research at the Van 't Hoff Laboratory under supervision of Prof. dr. Willem K. Kegel. Her research on the assembly of polyoxometalates is described in this thesis.

- **Figure 5.6: Crystallization of** $\{Mo_{72}Fe_{30}\}$

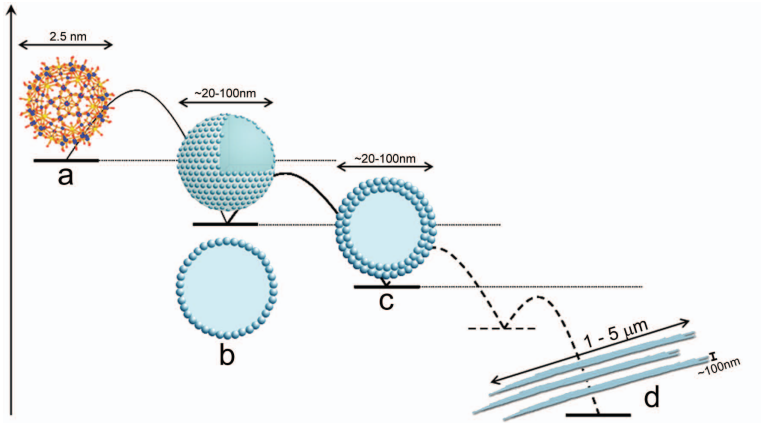

- **Figure 6.1: Crystal structure of 1 viewed along the three different crystallographic axes.**